VHF-UHF PHASED ARRAY TECHNIQUES

PART II: MUTUAL EFFECTS IN FINITE ARRAYS OF SLOTS

Mohamed A. Hidayet
John A. M. Lyon
Charles B. Loftis, Jr.

4970-2-T = RL-2121

FOREWORD

This report, AFAL-TR-73-399, Part II, was prepared by the Radiation Laboratory of The University of Michigan, Department of Electrical and Computer Engineering, 2216 Space Research Building, 2455 Hayward Street, Ann Arbor, MI. 48105 under the direction of Professor Ralph E. Hiatt and Professor John A.M. Lyon on Air Force Contract F33615-71-C-1495, Task 05 of Project 6099, "VHF-UHF Phased Array Techniques". The research covered in Part II of this report was performed during the period 1 September 1972 through 31 August 1973 exclusive of the time devoted to preparation of the report. The work was administered under the direction of the Air Force Avionics Laboratory, Wright-Patterson Air Force Base, Ohio 45433. The Program Monitor was Mr. Harold E. Weber, AFAL/TEM-3. This report was submitted by the authors in December, 1973.

A substantial amount of the research described in Part II of this report constituted the doctoral research of Mr. Mohamed A. Hidayet. The report has been designated Radiation Laboratory Report Number 004970-2-T for internal control purposes.

ACKNOWLEDGMENT

Mr. Mark Halverson and Mr. Philip Saldanha participated in technical supporting activities including experimental and computational efforts.

This report has been reviewed and is approved.

ABSTRACT

The analysis of finite planar arrays of slots is developed. This analysis includes as special cases the linear array of slots with weak coupling and the linear array with strong coupling. This strong coupling case has not been available heretofore in the literature. Likewise the analysis of the finite planar array is presented for the first time in this report. The degenerate or special case of the linear array with the weak coupling of slots is presented with experimental confirmation of results. The experiments of others were used to verify the finite planar array analysis. A complete and error free program has been written in Fortran IV language during this study. This program will enable the sponsor to fully utilize the advanced methods of calculation of array performance without the necessity of making expensive experimental models of planar arrays. This type of early design calculation also makes it possible to avoid "blind spots" in the projected array performance. The analysis may be adapted to arrays using other than slot elements through the use of the same basic approximation methods as well as with full use of reciprocity and symmetry.

The report also includes a detailed analysis of mutual coupling effects in linear and planar finite phased arrays of rectangular slots in a perfectly conducting ground plane. Internal TE and TM waveguide modes with unknown coefficients are assumed inside the waveguide. The electromagnetic field outside is evaluated in terms of the waveguide illuminations at the array aperture. The resulting infinite set of linear equations relating the illumination to the incident amplitudes in the guides is then truncated. The finite set of equations is further simplified by neglecting the contribution among modes not directly excited by waveguide feeds. This new approximation greatly reduces the size of the resulting matrix and one is left with an augmented matrix equation which directly relates the main mode illuminations to the main mode excitations. The entries in this augmented matrix include the effects of unexcited

modes implicitly. The importance of such a matrix in practical applications cannot be overemphasized. Deep insight was given to the mechanism giving rise to the so-called "blind spot" phenomenon. Computer programs were developed which accommodated linear as well as planar arrays of both rectangular grid arrangement and isosceles triangular grid arrangement.

The study presented here, besides having the advantage of being adaptable to finite arrays at reasonable costs, would give information related to the center element as well as any other elements including edge elements. Another advantage is that the matrix thus calculated is scan-independent. These features should be contrasted to what is available for a study based upon the infinite array assumption around a center element. Thus the matrix here represents information about the physical dimensions of the array and the geometry of the array grid; such information would be particularly useful in designing array feed networks and computer controlled phased arrays. Although the basic analysis can accommodate non-uniformly spaced arrays, great savings in the computations cost is realized with uniformly spaced arrays. This includes nonuniformly filled arrays of uniform grids.

A means for "blind spot" control is suggested, based on the suppression of modes of different parity along the direction of scan from that of the excited mode. Preliminary calculation did show the plausibility of this suggestion.

Studies of multi-terminal, multi-mode slot elements were made. It is shown that a limited amount of scan in the H-plane can be obtained through the proper proportioning of the amount of TE_{10} and TE_{20} excitation. A means is required for keeping the time phase between the two modes constant at 90^{o}. To propagate the higher mode a larger slot is required. Also the amount of scan possible is extremely limited. Scanning in this manner is also characterized by the build-up of a large unwanted side lobe which for large scan angles from broadside may approach the same magnitude as the main lobe but is located on the opposite side. It is possible to scan a slot even less effectively by varying the relative time phase

of the two modes. It was concluded that scanning in the H-plane through the use of additional modes is not justified within the objectives of the present study. No great saving of space would be accomplished and much complication would be added. Mode scanning in the E-plane appears even less feasible. However, it should be mentioned that the planar array analysis described can be adapted to the slot excitation of more than one mode.

TABLE OF CONTENTS

TABLE OF CONTENTS

continued

LIST OF ILLUSTRATIONS

LIST OF TABLES

PREFATORY MATERIAL

0.1 Introduction

This contract as amended 13 October 1972 involved three tasks (1) Fifteen-Element Linear Array, (2) Fifteen by Fifteen-Element Planar Array, and (3) the Use of Multi-Terminal/Multi-Mode Elements for Scanning. Each of the topics listed is given some coverage in this report. However, most of the effort was concentrated on the first two mentioned topics. The effort devoted to the study of Multi-Terminal Elements was relatively small, perhaps 15 percent of the total time.

0.2 Linear Arrays of Slots

In Task 1 on the Fifteen-Element Linear Array emphasis was placed upon an adequate formulation for the boundary value problem applicable to a linear array of slots arranged in a weak coupling manner. That is the slots were in line and were oriented so that the magnetic lines of one slot were colinear with the magnetic lines of the next slot. The relatively low level of coupling enabled some simplification to be made in the computational methods used for such an array. Basically the problem in the Fifteen-Element Linear Array was to solve a matrix equation where a matrix operator including elements which represented Green's functions operated on a column vector which represented the illuminations at each slot and this in turn yielded the required feed parameters for each slot. It was necessary to have several modes represented for each slot in order to achieve the needed accuracy. This was done and is fully described in Chapter II. Chapter III includes numerous examples of computer studies which justify the assumptions and approximations made in the analysis. Experimental results on linear arrays are also given in Chapter III.

0.3 Planar Arrays of Slots

In Task 2 a more difficult boundary problem was considered in the study of planar arrays. Although this task calls for a 15 x 15 element planar array economics dictated that smaller planar arrays would first be studied. For this purpose, then a 7 x 7 triangular grid array and a 13 x 13 rectangular grid array were studied. Actually the number of elements in an array is not truly representative of the difficulties and length of the computer program necessary. It is extremely important to consider the number of modes which must be represented for each slot in the array. A major part of this task was the study and evaluation of the modes which were required for an adequate representation of this problem. Significant improvements and scientific contributions were made by a detailed study of the contribution of various modes to the electromagnetic mutual coupling problem. It is believed that some of the achievements in the simplification of the analysis represent a very distinct and original contribution in the solution of such electromagnetic problems. Chapters II and III of this report cover in detail the technical work done on Task 2.

0.4 Single Slot Scanning

The last section or Task 3 of the amended work statement dealt with the Use of Multi-Terminal/Multi-Mode Elements for Scanning. Both theoretical and experimental studies were made in order to develop elements which would facilitiate scanning in an array. An objective was to obtain some scanning by an individual element and thereby reduce or simplify the overall scanning requirements of the entire array. In this sense it means that one element would in effect take the place of two or three elements. The multi-terminal elements which were used offered a means of scanning in the H-plane. Such elements have been studied in considerable detail by other workers in the field. Some of the work in this report follows

closely that given in the reference (29) by Kitsuregawa and Tachikawa. In other instances information was utilized from a report (30) by Thiele, Wagner and Walter. Actually the earlier reports on multi-mode or multi-terminal antennas were sufficient to show the possibilities of scanning an individual slot. In the work done on this project primary emphasis has been made on scanning a slot using the TE_{10} and the TE_{20} modes. The use of multi-terminal or multi-mode slots is somewhat attractive until full consideration of electromagnetic coupling is invoked. Then it appears that the larger size slots needed to support higher order modes, adds additional complication in the electromagnetic boundary value problem. A detailed discussion of the multi-mode slots work is given in Chapter V.

CHAPTER I

INTRODUCTION

1.0

The work described here has provided a successful analysis for the input impedance of different slots in a finite phased array. The mechanism which gives rise to coupling accumulation, causing "blind spots", at scan angles within the scan range has been disclosed. New means for avoiding such effects are introduced. Also, some of the already existing suggestions for "blind spot" reduction are discussed.

This analysis is based upon the integral equation formulation of the boundary value problem. The solution of the integral equation is approximated by a solution of a truncated set of linear equations. To this end, the set of internal TE and TM waveguide modes was used as a basis for field representation inside the radiating slots. This formulation in its raw form requires a prohibitive computational effort. A new simplifying assumption is used which, together with symmetry and reciprocity properties, reduces computational costs to very reasonable limits. This assumption does not neglect the effect of higher order modes, but rather it neglects the interactions among unexcited modes.

Using the above approximation it has been possible for the first time to generate a matrix that relates the main mode illuminations on the array face to the incident components of that mode, where the effects of unexcited modes are included in the matrix coefficients. A relationship beyond the usual symmetry and reciprocity which relates normalized coupling coefficients between the M_1N_1 and M_2N_2 modes to the normalized coupling coefficient between the M_1N_2 and M_2N_1 or the M_2N_1 and M_1N_2 coupling coefficients for similar elements was observed. M and N refer to modal indices.

Since a vast amount of work has been done on phased arrays in general (1), only a brief survey of the work related to the problem of finite phased arrays will be given.

1.1 Phased Arrays and Methods of Analysis

Arrays capable of high speed scanning and multi-target tracking and/or simultaneous operation of multiple physical functions are in increasing demand. Electronically controlled phased arrays can have such capabilities. While large phased arrays of the narrow beam type have wide applications in modern radar systems and radio astronomy, arrays of limited size are used in a variety of applications. An example is collision avoidance radar for automobiles.

Several approaches exist for the phased array analysis. Classical array theory (which neglects mutual coupling) and approximate analytical methods (which neglect the effects of higher order modes) are, in most cases, incapable of explaining the behavior around anomalous nulls in the radiation pattern as the beam is scanned off broadside. The design of phased arrays, especially ones of large size, by experimental methods is expensive and time consuming. Analysis based on an infinite array environment is adequate for elements in the midst of a large array but not for elements close to or at the edge of such arrays. Semi-infinite array analysis, which depends on the solutions of the infinite array, can provide information on elements near one edge of such large arrays. Hence, the need exists for an analysis of finite arrays which have no limitation on array size, and can supply information about all elements in such arrays.

This work concentrates on finite array analysis on a rigorous basis and provides an understanding of the anomalous null or "blind spot" behavior and means for "blind spot" reduction. Emphasis has been placed on arrays of open-ended rectangular waveguides; however, the same methods can be utilized for other types of elements. While the pattern of an array of given dimensions can be easily calculated from classical array theory, the input impedances of the various elements require the consideration of the near field situation at the array aperture. The analysis given here deals with the input impedance as a function of the main beam direction for finite arrays.

At the present state of knowledge one would expect to formulate the boundary value problem into an integral equation. An exact analytical solution for such problems is not guaranteed, especially for finite arrays. Instead, the integral equation is reduced to an infinite set of linear algebraic equations which can then be truncated. Hence, the solution of the boundary value problem requires the evaluation of the coefficients involved in these equations by solving the matrix equation. Reduction of the integral equation into an infinite set of algebraic equations is usually achieved by expressing the unknown field quantities (and sometimes the kernel under the integration) as an infinite series of a convenient set of basis functions with unknown coefficients. This set of functions, of course, has to be complete over the intervals where the field quantities are represented. The solution of the matrix equation yields the unknown coefficients. The rate of convergence of the solution depends on the choice of the basis of representation. In this work the orthogonal set of waveguide TE and TM modes were chosen as a basis set. From the geometry of the problem, this appears to be a natural choice. First, because severe discontinuities in the span of the aperture do not exist; therefore, relatively few components are required for adequate field representation. Secondly, the results are readily interpretable from the engineering point of view. Indeed, the results do show that a limited number of modes can predict input impedance variation as a function of beam direction. It turns out that coupling due to modes of different parity (odd or even) along the direction of scan, especially those close to cut off, tends to add up near beam pointing directions where blind spots are observed.

1.2 History of Developments

A large amount of work has been done on phased arrays in general. Recently a book by Amitay, Galindo and Wu (1) was published on theory and analysis of phased array antennas where a reasonably complete account of work on infinite arrays is included.

The classical array theory which neglects the effects of higher order

modes, provides satisfactory information about array patterns, even for large arrays at broadside. However, deep nulls in the power transmission pattern were observed for scan angles well within the normal scan range of the array (1-7). This phenomenon, termed "blind spot", has since been the subject of intensive research aimed at understanding and finding means to avoid the problem. Knittel et al. (2), in 1968, differentiated between two basic types of the so-called "blind spot" phenomenon, those supported by modes inside the waveguides and those supported by modes outside the waveguides due to external structures like fences. The internal waveguide higher order modes at the slots are essential for realization of the first type. Such might not be the case for the second type where contributions from external structures are most likely.

Lechtreck (3), in 1965, obtained experimentally the first evidence of "blind spot" behavior using an array of circularly polarized coaxial horns with hemispherical radomes on each element. This was designated as external resonance by Oliner (4) in 1970. Farrell and Kuhn (5), in 1966, analyzed the infinite triangular grid and expected a null in both the H-plane scan and the E-plane scan for that grid. The null in the H-plane was confirmed experimentally on a 7×7 triangular grid array. Diamond (6), in 1967, analyzed the same grid and an infinite rectangular grid of square waveguide slots. He was able to detect the H-plane null for the triangular grid and E-plane null for the rectangular grid. Diamond also showed the importance of the TE_{20}, TE_{11}, TM_{11}, TE_{12} and TM_{12} modes on studying the "blind spot" phenomenon.

In 1968, Farrell and Kuhn (7) again studied mutual coupling in infinite planar arrays of rectangular waveguide horns both for rectangular and triangular grids. The convergence of the solution was studied and the numbers of external free space and internal waveguide modes necessary for an adequate representation were given. Comparison with experiments was made for the rectangular grid 169-element array (see Fig. 1-1)) and the triangular grid (95-element array (see Fig. 1-2)). The measured H-plane

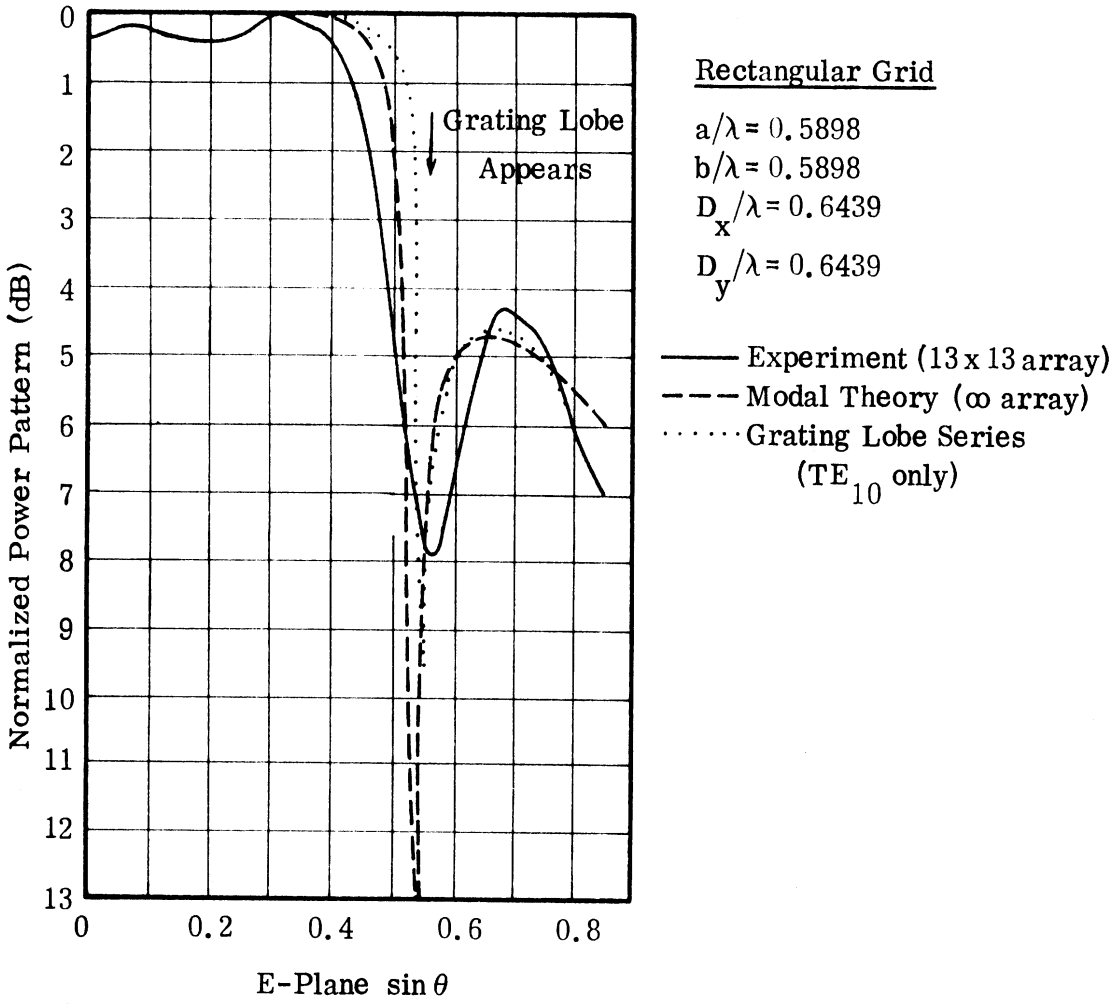

(a)

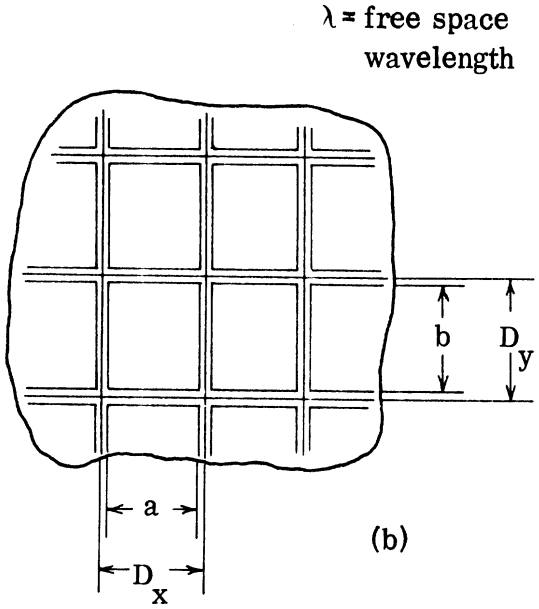

(b)

Fig. 1-1: Infinite array theory of rectangular grid and measurements for an array of 13 x 13 elements of square waveguides: (a) comparison between theory and experiment, (b) array configuration.

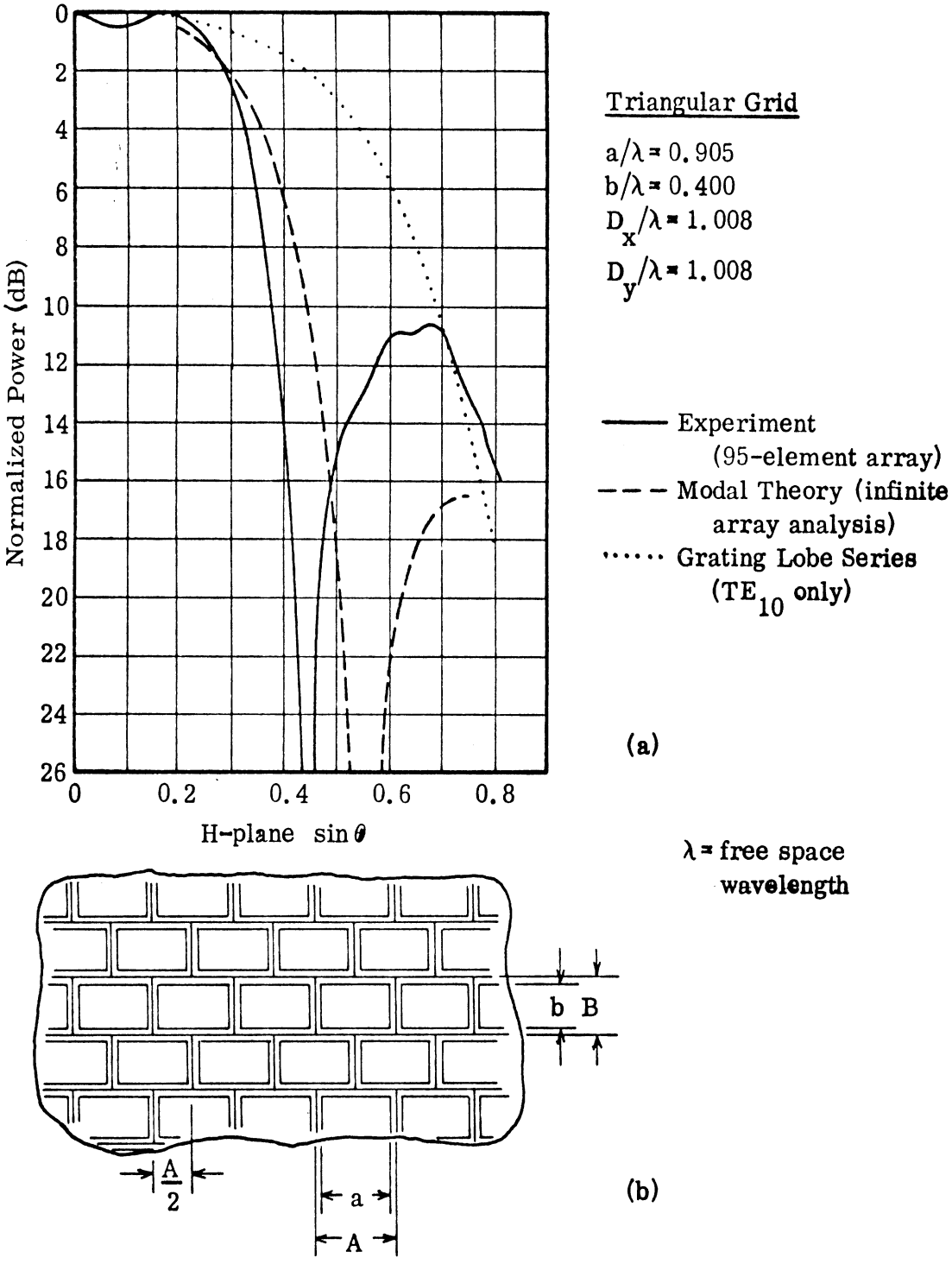

Fig. 1-2: Infinite array theory of triangular grid and measurements for an array of 95 elements of rectangular waveguides: (a) comparison between theory and experiment, (b) array configuration.

pattern for the triangular grid exhibited a 32 dB null well inside the grating lobe onset position. This was in agreement with the computed results except that the measured null was closer to broadside than the computed null. The measurements did not detect an E-plane null as was expected from calculation. For the rectangular grid, both theory and experiment show a null in E-plane scan approximately at the grating lobe onset position. The variation from the experiment was attributed to the limited size of the experimental array.

In the same year Borgiotti (8) obtained a new expression for the mutual admittance between two identical radiating apertures in the form of a Fourier transform of a function related to the power radiation pattern of the element. Later the same author (9) obtained the driving-point admittance of a radiating aperture in an infinite periodic planar phased array. Also, in 1968 Knittel et al. (10) related the element pattern nulls in an infinite phased array to waves guided by the array face (external modes effect). Galindo and Wu (11) investigated the asymptotic decay of coupling for infinite phased arrays.

In 1969 Mailloux (12) studied the near field coupling between two collinear open-ended waveguide slots. He formulated the problem into an integral equation which was then solved approximately by expanding the aperture field into a Fourier series of LSE modes. The special case of one isolated slot in a ground plane was solved first; then the case of two collinear coupling waveguide slots was solved by the same numerical method using the symmetry properties of the geometry. The same author (13) in 1969 treated a first order solution for the mutual coupling between waveguide slots, which propagate two orthogonal modes. The waveguides ended in a common ground plane and had parallel walls but the relative positions were arbitrary. The first order analysis was based on the method of moments and used a single-mode approximation to the aperture field for each polarization. An improved first order analysis was also presented which used a higher order mode solution for the self-admittance. In the first of these studies Mailloux was motivated by the need for a finite array study based upon individually coupled elements in order to directly compare theory with

experiment. Furthermore, the analysis may be extended quite naturally to consider the edge behavior of small or large arrays. In addition to these factors the second study was motivated by the existence of cross polarized modes at the array surface when slots have walls of finite thickness.

Earlier, Lyon et al. (14) studied coupling between various radiating structures including two open-ended waveguides in a common ground plane with arbitrary orientation and spacing. The theoretical part of the study was based on a single-mode approximation to the aperture field of the excited slot and on the assumption that the waveguide-backed parasitic slot has a total magnetic field equal to that which would exist if the slot were absent. In this manner the solution of an integral equation was avoided.

In 1970 Wu (15) analyzed the coupling between parallel plate waveguides in an infinite array environment with and without dielectric plugs. An analysis of a finite parallel plate waveguide array was also presented by the same author later in the year. The finite parallel plate waveguide array is a good approximation to the semi-infinite rectangular waveguide array in the H-plane scan. In a probabilistic study, Argwal and Lo (16), in 1972, showed that coupling accumulation as a cause for "blind spots" was highly improbable for a randomly spaced array.

Very recently, Wasylkiwskyj, 1973 (17) introduced an analysis of mutual coupling effects in linear and planar uniformly spaced semi-infinite arrays. The solutions for the active reflection coefficient as well as the mutual coupling coefficient were expressed in terms of the active impedance in a phased infinite array. Cha (18), in 1973, presented the advantages of the basic formulation for finite arrays in a recent publication.

1.3 Finite Array Analysis

The need for an analysis that can predict the behavior of finite arrays has been demonstrated by some authors (12, 18). Pattern information is available from classical array theory assuming the illumination of each array element. The driving point admittance cannot be predicted without considera-

tion of mutual effects. The reflected component of the field in any slot is the sum of the reflection due to the abrupt change in the feeding guide geometry and the coupling from other slots in the vicinity. Thus, the reflection coefficient for individual elements is generally a function of scan angle. Furthermore, these coupling coefficients are themselves dependent on the antenna array geometry. As the main beam is scanned by adjusting the phases of different elements, the vector sum of these coupling components is going to change. This makes the element input impedance a function of the steering phases or, in other words, a function of the beam direction. The accumulation of these couplings at some scan angle to a large reflected component, in any one element, will cause a serious impedance mismatch at this particular angle. If the array has a uniform grid, then by symmetry, the same phenomenon will occur for most elements and will result in a null in the array transmission power pattern or "blind spot". The understanding of element input impedance behavior can lead to different methods to avoid such an undesirable effect.

The finite array analysis here evaluates the coupling coefficients between the illumination of different TE and TM modes in different apertures and the incident or the reflected components of those modes in the same or other apertures. This is a direct interpretation of the integral equation formulation. The result is a matrix equation that relates the column vector whose entries represent illumination to the column vector whose entries represent either the incident or reflected components as desired. These two versions are suitable for the problem of a transmitting or a receiving array, respectively. In both cases, however, the matrix entries representing coupling, contain information about the dimensions and geometry of the array and the frequency of operation. Since both the array geometry and the modes inside the aperture are scan independent the whole matrix is scan invariant. Changes in the steering phases are accounted for by a complex exponential factor in each of the entries of the illumination column. These same viewpoints were shared by Cha (18).

However, at this stage the amount of computational cost involved is

extremely high. A simplifying assumption is introduced which, together with the symmetry and reciprocity properties inherent in the problems, greatly reduces the computational effort. The assumption does not neglect entirely the effect of unexcited modes. The classes of coupling considered are these: (1) coupling of an excited mode to an excited mode in the same or another slot, (2) coupling of an excited mode to an unexcited mode and then the coupling of this unexcited mode back to an excited mode. The neglected effect on the excited modes would be that due to two or more consecutive steps of unexcited mode coupling, e.g., coupling from an excited mode to an unexcited mode and thence to the same or another unexcited mode before again coupling to an excited mode. The use of this approximation allows generation of the entries of an augmented matrix and greatly reduces the number of matrix entries to be calculated. These entries represent the relations between the illuminations of the excited mode or modes and either the incident or reflected components of these modes. The coefficients of this augmented matrix include the effects of unexcited modes as intermediate couplers between different main mode illuminations. In this fashion the array environment is fully described.

The matrix thus obtained is very useful in array analysis and application. In analysis the reflection coefficient and hence the input impedance can be calculated for a given scan angle without the need to invert the matrix. For an application requiring a certain scan angle the required incident component can be calculated for all elements by a straightforward matrix multiplication. Such a feature can be very useful in computer controlled phased arrays.

Finally, the role played by different modes internal to the slots is revealed. A new method for avoiding such an effect based on suppression of these modes at the apertures is studied, together with other means for the same objective.

Chapter II contains the finite array formulation, symmetry and reciprocity characteristics and the new approximation discussed above. Comparisons of the results obtained using finite array analysis with experimental data for one linear array and two planar arrays are included in Chapter III. The

relation between modes of different parity along the direction of scan and the occurrence of "blind spots" is explained in Chapter IV. Discussions and conclusions are also included in Chapter IV.

CHAPTER II

FINITE ARRAY FORMULATION

2.1 Preliminaries

The effects of coupling between waveguide slots as elements of an array have been considered by many authors using the simplifying assumption of an infinite (1, 5, 6, 11, 18) or a semi-infinite (17) array environment. The infinite array environment assumption makes use of the periodicity of the electromagnetic field on the array surface to focus the attention on a unit cell. For the same reason the electromagnetic field beyond the array surface is expanded in a series of Floquet modes. The results thus obtained predict the behavior of the central elements of a large finite array. Because of complications the infinite array analysis is usually scalar and one-dimensional only. It is therefore useful for special types of scanning such as H-plane or quasi E-plane scans (1). The semi-infinite array study expresses the behavior of edge elements explicitly in terms of the infinite array solution. The above-mentioned studies are only valid for cases where the infinite array environment assumption is justified. Since Floquet modes are scan dependent, these formulations are likewise.

The analysis presented here deals with the problem of the actual environment in any finite planar array of rectangular elements. The array consists of a number of rectangular slots in an infinitely conducting ground plane of infinite extent. Each slot is fed by a rectangular waveguide of the same cross section as that of the slot. The assumption of infinite conductivity is well justified. The finite array analysis presented in this chapter is capable of predicting the input impedance of any element of a uniformly spaced finite array of the type just described at any scan angle. A new simplifying assumption which neglects the interactions among unexcited modes is introduced. This assumption, together with symmetry and reciprocity properties of the problem, made the solution amenable for computer handling.

2.2 Formulation of the Boundary Value Problem

In the following paragraphs the formal presentation of the problem is explained. The arrays considered consist of open-ended rectangular waveguides of arbitrary dimensions and arranged arbitrarily in an otherwise perfectly conducting infinite ground plane. However, considerable computational efforts can be saved in the case of identical waveguide slot openings arranged in either a rectangular pattern as shown in Fig. 2-1(a) or an isosceles triangular pattern as shown in Fig. 2-1(b). Such lattice arrangements provide a high degree of symmetry and this, together with the principle of reciprocity, provides a major means of achieving a substantial savings in analytical and computational effort.

2.2.1 General Procedures

The electromagnetic field above the plane of the array of elements can conveniently be represented in terms of the tangential electric field at the aperture plane using an integral expression. The fields inside each slot aperture are expressed in a series of waveguide TE and TM modes of unknown coefficients. The boundary condition is then applied for the continuity of the tangential magnetic field. The normal electric flux across the apertures automatically fulfills the same condition of continuity. The orthogonality properties of waveguide modes are then used. There results an infinite set of linear equations in an infinite number of unknown coefficients. The factors multiplying these coefficients contain quadruple integrations. Using a simple change of variables the kernel of the integration involved in computing these factors can be rendered independent of two of the new integration variables with respect to which the integration can be carried out explicitly and thereby the quadruple integration is reduced to a double integration. The procedure used as described above in reducing the quadruple integrals is very similar to the procedure used by A. T. Adams (19). After an appropriate but necessary truncation of the infinite equation set and the numerical evaluation of the coefficients involving the double integration, the system is then reduced to a

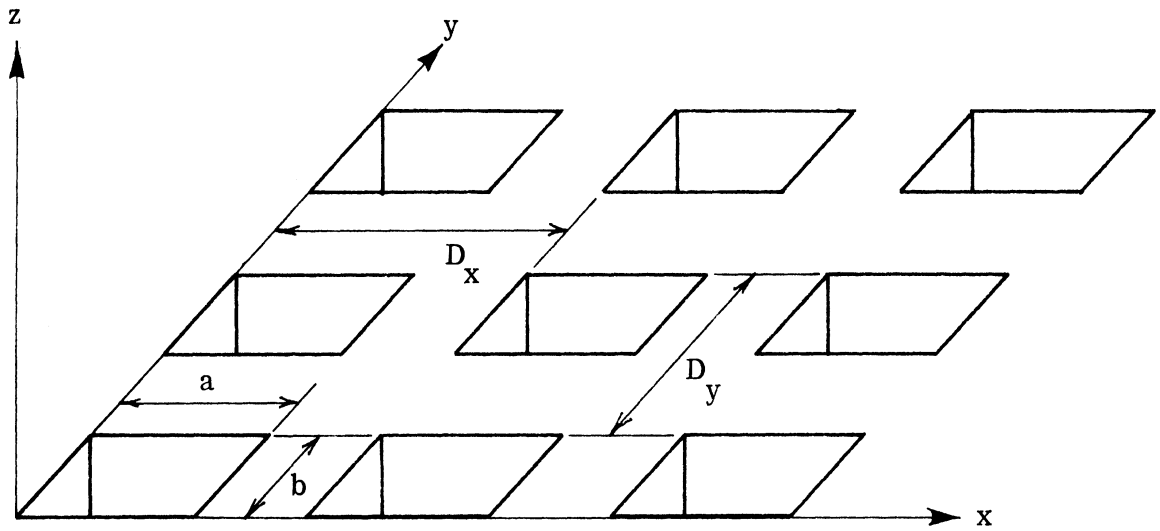

(a)

G = Grid parameter

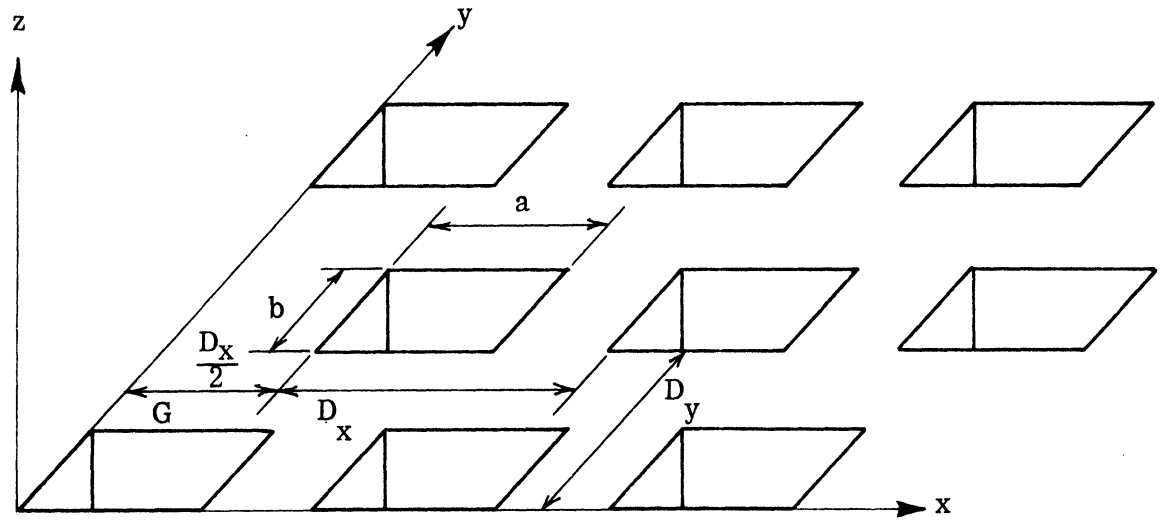

(b)

Fig. 2-1: Planar array of rectangular waveguide slots: (a) Rectangular grid (b) Triangular grid.

finite set of linear equations in a finite number of unknown modal coefficients.

2.2.2 Mathematical Formulation

It is well known that the electromagnetic field in a source-free region can be expressed in terms of the tangential components of the field over the closed surface surrounding the region. The analysis presented here uses Huygen's principle formulated in a vector form utilizing a vector Green's function (20).

Let a vector $\overline{F}$ satisfy the homogeneous vector wave equation:

$$\nabla x \nabla x \overline{F} - k^2 \overline{F} = 0 \qquad (2.1)$$

where k is the propagation constant.* Let $\overline{G}$ be the vector Green's function described by

$$\overline{G} = \nabla x (g\hat{a}) \quad ,$$

and

$$g = \frac{e^{-jk\left|\overline{R}-\overline{r}'\right|}}{4\pi\left|\overline{R}-\overline{r}'\right|} \quad ,$$

where

$\hat{a}$ is an arbitrary unit vector,

$\overline{R}$ is the position vector of the field point, and

$\overline{r}'$ is the position vector of the source point.

$\overline{G}$ clearly satisfies the homogeneous vector wave equation (2.1) except at the point where $\overline{R} = \overline{r}'$.

Then, in reference to Fig. 2-2, applying Green's second identity to $\overline{F}$ and $\overline{G}$, and taking the limit as the surface σ shrinks to zero (20):

$$(\nabla x \overline{F}) \cdot a = \iint_S (\overline{G} x \nabla x \overline{F}(\overline{r}') - \overline{F}(\overline{r}') x \nabla x \overline{G}) \cdot \hat{n} \, ds' \qquad (2.2)$$

where S and σ bound the region of volume V and $\hat{n}$ is the outward normal to

---

*$e^{j\omega t}$ time convention is used throughout.

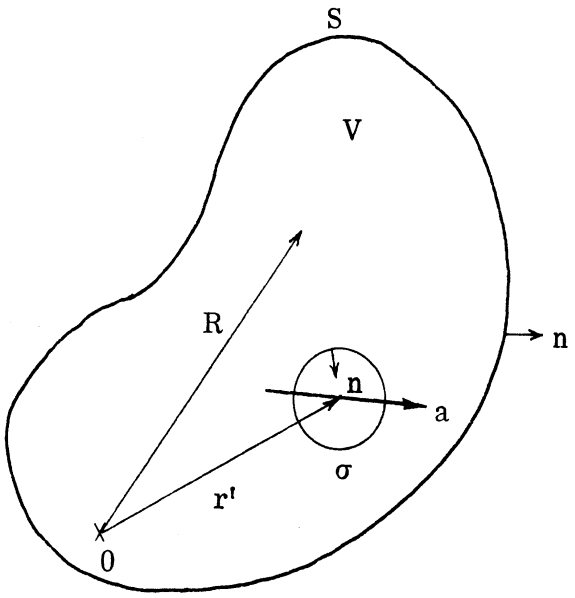

Fig. 2-2: Region of Integration.

the surface bounding V.

Inasmuch as modifying the Green's function, by adding to it any vector function satisfying the homogeneous vector wave equation throughout the volume bounded by S, will not alter the result of equation (2.2), such a part can be chosen to make:

$$\hat{n} \times \hat{G}_1 = 0$$

or

$$\hat{n} \times \nabla \times \hat{G}_2 = 0$$

where both $\bar{G}_1$ and $\bar{G}_2$ include the free space Green's function plus a homogeneous part. Since both the electric and the magnetic fields ($\bar{E}$ and $\bar{H}$ respectively) satisfy the vector wave equation,

$$\bar{E}(\bar{R}) \cdot \hat{a} = \frac{1}{j\omega\epsilon} \iint \left[\nabla \times \bar{G}_1(\bar{R}, \bar{r}') \times \bar{H}(\bar{r}') \right] \cdot \hat{n} \, ds' \qquad (2.3a)$$

$$= \iint \left[\bar{\bar{G}}_2(\bar{R}, \bar{r}') \times \bar{E}(\bar{r}') \right] \cdot \hat{n} \, ds' \tag{2.3b}$$

$$\bar{H}(\bar{R}) \cdot \bar{a} = \frac{-1}{j\omega\mu} \iint \left[\nabla \times \bar{\bar{G}}_1(\bar{R}, \bar{r}') \times \bar{E}(\bar{r}') \right] \cdot \hat{n} \, ds' \tag{2.3c}$$

$$= \iint \left[\bar{\bar{G}}_2(\bar{R}, \bar{r}') \times \bar{H}(\bar{r}') \right] \cdot \hat{n} \, ds' \quad . \tag{2.3d}$$

Thus the electric or magnetic field intensity within a source free volume is determined by the tangential component of either the electric or magnetic field intensity alone on the bounding surface. An exception would be for the cases of normal modes; e.g., resonant oscillations in closed cavities (20).

When applying the above to the problem of open-ended waveguides in an otherwise infinite perfectly conducting ground plane equations (2.3b) and (2.3c) are particularly suitable since $n \times E = 0$ on the ground plane and one is left only with integrations over the apertures. Equations (2.3b) and (2.3c) can now be rewritten as shown below:

$$E_x(\bar{R}) = -2 \iint E_x(\bar{r}') \frac{\partial G}{\partial z} \, ds' \tag{2.4a}$$

$$E_y(\bar{R}) = -2 \iint E_y(\bar{r}') \frac{\partial G}{\partial z} \, ds' \tag{2.4b}$$

$$E_z(\bar{R}) = 2 \iint \left[E_x(\bar{r}') \frac{\partial G}{\partial x} + E_y(\bar{r}') \frac{\partial G}{\partial y} \right] ds' \tag{2.4c}$$

$$H_x(\bar{R}) = \frac{2j}{\omega\mu} \iint \left[E_x(\bar{r}') \frac{\partial^2 G}{\partial x \, \partial y} - E_y(\bar{r}') \left(\frac{\partial^2 G}{\partial x^2} + k^2 G \right) \right] ds' \tag{2.4d}$$

$$H_y(\bar{R}) = \frac{2j}{\omega\mu} \iint \left[E_x(\bar{r}') \left(\frac{\partial^2 G}{\partial y^2} + k^2 G \right) - E_y(\bar{r}') \frac{\partial^2 G}{\partial x \, \partial y} \right] ds' \tag{2.4e}$$

$$H_z(\bar{R}) = \frac{2j}{\omega\mu}\iint\left[E_x(\bar{r}')\frac{\partial^2 G}{\partial y\,\partial z} - E_y(\bar{r}')\frac{\partial^2 G}{\partial x\partial z}\right] ds' \quad . \qquad (2.4f)$$

The above equations are the same as those in the paper by Tai (21) on the MMF method. The equivalence between the Fourier transform method and the MMF method is pointed out in the same reference.

2.3 Analysis of Uniformly Spaced Planar Array

Although the same type of formulation can accommodate non-uniform dimensions, uniform array dimensions are utilized from here on to reduce the complexity of the notation. The following notation will be adopted throughout (see Fig. 2-3).

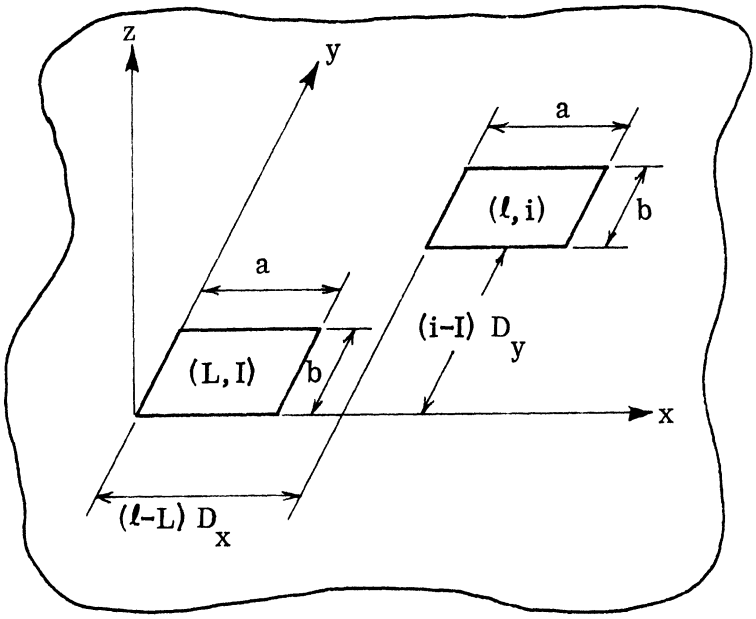

Fig. 2-3: Spacing between elements of the array.

L, ℓ refer to the column positions of the field and source slots, respectively,

I, i refer to the row positions of the field and source slots, respectively,

capitalized superscripts and subscripts refer to field quantities,

lower case superscripts and subscripts refer to source quantities,

M, m, N, n are modal indices for TE modes,

P, p, Q, q are modal indices for TM modes,

a, b are slot width and height, respectively,

D_x is the distance between two consecutive elements in the same row,

D_y is the distance between two consecutive rows.

Since the electromagnetic field inside the waveguides satisfy the vector wave equation, they can be written as an infinite series of TE and TM modes.

$$\bar{E}^{\ell i} = \sum_m \sum_n (A_{TE}^{\ell imn} e^{-jhz^{mn}} + B_{TE}^{\ell imn} e^{jhz^{mn}}) \left[-\frac{n\pi}{b} \cos(\frac{m\pi}{a}x) \sin(\frac{n\pi}{b}y)\hat{x} + \right.$$

$$\left. + \frac{m\pi}{a} \sin(\frac{m\pi}{a}x) \cos(\frac{n\pi}{b}y)\hat{y} + 0\,\hat{z} \right] +$$

$$+ \frac{j}{\omega\epsilon} \sum_p \sum_q (A_{TM}^{\ell ipq} e^{-jhz^{pq}} + B_{TM}^{\ell ipq} e^{jhz^{pq}})(jh^{pq}) \left[(\frac{p\pi}{a}) \cos(\frac{p\pi}{a}x) \sin(\frac{q\pi}{b}y)\hat{x} + \right.$$

$$\left. + (\frac{q\pi}{b}) \sin(\frac{p\pi}{a}x) \cos(\frac{q\pi}{b}y)\hat{y} \right] -$$

$$- (A_{TM}^{\ell ipq} e^{-jhz^{pq}} - B_{TM}^{\ell ipq} e^{jhz^{pq}})(k_c^{pq})^2 \sin(\frac{p\pi}{a}x) \sin(\frac{q\pi}{b}y)\hat{z} \qquad (2.5)$$

$$\bar{H}^{\ell i} = \frac{j}{\omega\mu} \nabla \times \bar{E}^{\ell i} \qquad (2.6)$$

$$\bar{H}^{\ell i} = \frac{j}{\omega\mu} \sum_m \sum_n (A_{TE}^{\ell imn} e^{-jhz^{mn}} - B_{TE}^{\ell imn} e^{jhz^{mn}})(jh^{mn}) \cdot$$

$$\left[\left(\frac{m\pi}{a}\right)\sin\left(\frac{m\pi}{a}x\right)\cos\left(\frac{n\pi}{b}y\right)\hat{x}+\left(\frac{n\pi}{b}\right)\cos\left(\frac{m\pi}{a}x\right)\sin\left(\frac{n\pi}{b}y\right)\hat{y}\right]+$$

$$+\left(A_{TE}^{\ell imn}e^{-jhz}+B_{TE}^{\ell imn}e^{jhz}\right)\left(k_c^{mn}\right)^2\cos\left(\frac{m\pi}{a}x\right)\cos\left(\frac{n\pi}{b}y\right)\hat{z}+$$

$$+\sum_p\sum_q\left(A_{TM}^{\ell ipq}e^{-jhz}-B_{TM}^{\ell ipq}e^{jhz}\right)\left[\left(\frac{q\pi}{b}\right)\sin\left(\frac{p\pi}{a}x\right)\cos\left(\frac{q\pi}{b}y\right)\hat{x}-\right.$$

$$\left.-\left(\frac{p\pi}{a}\right)\cos\left(\frac{p\pi}{a}x\right)\sin\left(\frac{q\pi}{b}y\right)\hat{y}+0\,\hat{z}\right] \qquad (2.7)$$

where

A is the incident mode amplitude (+z direction),

B is the reflected mode amplitude (-z direction),

$\overline{E}$ is the electric field vector,

$\overline{H}$ is the magnetic field vector,

$k = 2\pi/\lambda$, (2.8a)

λ = free space wavelength,

$$k_c^{mn} = \sqrt{\left(\frac{m\pi}{a}\right)^2+\left(\frac{n\pi}{b}\right)^2}\ , \qquad (2.8b)$$

$$k_c^{pq} = \sqrt{\left(\frac{p\pi}{a}\right)^2+\left(\frac{q\pi}{b}\right)^2}\ , \qquad (2.8c)$$

$$jh^{mn} = j\sqrt{k^2-k_c^{mn\,2}}\ , \qquad (2.8d)$$

and $$jh^{pq} = j\sqrt{k^2-k_c^{pq\,2}}\ . \qquad (2.8e)$$

positive square root

Substitute equations (2.5) and (2.7) into equations (2.4c, d and e) and let z approach the array surface where $z = 0$. Then using the continuity of the normal component of the electric flux (ϵE_z) and the tangential components of the magnetic field (H_x, H_y) across the boundary (array surface), the following can be written:

$$E_z = \sum_P \sum_Q -\frac{j}{\omega\epsilon}(A_{TM}^{LIPQ} - B_{TM}^{LIPQ})(k_c^{LIPQ})^2 \sin\left[\frac{P\pi}{a}(x-(L-1)D_x)\right] \cdot$$

$$\sin\left[\frac{Q\pi}{b}(y-(I-1)D_y)\right] =$$

$$= 2\sum_{\ell}\sum_{i}\iint_{s'_{\ell i}}\left\{\sum_m\sum_n (A_{TE}^{\ell imn} + B_{TE}^{\ell imn})\left[-\left(\frac{n\pi}{b}\right)\cos\left[\frac{m\pi}{a}(x'-(\ell-1)D_x)\right]\cdot\right.\right.$$

$$\sin\left[\frac{n\pi}{b}(y'-(i-1)D_y)\right]\frac{\partial G}{\partial x} + \left(\frac{m\pi}{a}\right)\sin\left[\frac{m\pi}{a}(x'-(\ell-1)D_x)\right]\cdot$$

$$\left.\cos\left[\frac{n\pi}{b}(y'-(i-1)D_y)\right]\frac{\partial G}{\partial y}\right] + \frac{j}{\omega\epsilon}\sum_p\sum_q (A_{TM}^{\ell ipq} + B_{TM}^{\ell ipq})(jh^{\ell ipq})\cdot$$

$$\left[\left(\frac{p\pi}{a}\right)\cos\left[\frac{p\pi}{a}(x'-(\ell-1)D_x)\right]\sin\left[\frac{q\pi}{b}(y'-(i-1)D_y)\right]\frac{\partial G}{\partial x} + \right.$$

$$\left.\left.\left(\frac{q\pi}{b}\right)\sin\left[\frac{p\pi}{a}(x'-(\ell-1)D_x)\right]\cos\left[\frac{q\pi}{b}(y'-(i-1)D_y)\right]\frac{\partial G}{\partial y}\right]\right\} dx'\,dy' \qquad (2.9)$$

$$H_x = \sum_M\sum_N (A_{TE}^{LIMN} - B_{TE}^{LIMN})(jh^{LIMN}\frac{M\pi}{a})\sin\left[\frac{M\pi}{a}(x-(L-1)D_x)\right]\cdot$$

$$\cos\left[\frac{N\pi}{b}(y-(I-1)D_y)\right] - j\omega\mu\sum_P\sum_Q (A_{TM}^{LIPQ} - B_{TM}^{LIPQ})(\frac{Q\pi}{b})\cdot$$

$$\sin\left[\frac{P\pi}{a}(x-(L-1)D_x)\right]\cos\left[\frac{Q\pi}{b}(y-(I-1)D_y)\right] =$$

$$= 2\sum_{\ell}\sum_{i}\iint_{s'_{\ell i}}\left\{\sum_m\sum_n (A_{TE}^{\ell imn} + B_{TE}^{\ell imn})\left[-(\frac{n\pi}{b})\cos\left[\frac{m\pi}{a}(x'-(\ell-1)D_x)\right]\cdot\right.\right.$$

$$\left.\left.\sin\left[\frac{n\pi}{b}(y'-(i-1)D_y)\right]\frac{\partial^2 G}{\partial x\partial y} - (\frac{m\pi}{a})\sin\left[\frac{m\pi}{a}(x'-(\ell-1)D_x)\right]\cdot\right.\right.$$

$$\cos\left[\frac{n\pi}{b}(y'-(i-1)D_y)\right]\left(\frac{\partial^2 G}{\partial x^2}+k^2 G\right)\Bigg]+\frac{j}{\omega\epsilon}\sum_p\sum_q (A_{TM}^{\ell ipq}+B_{TM}^{\ell ipq})(jh^{\ell ipq})\cdot$$

$$\left[\left(\frac{p\pi}{a}\right)\cos\left[\frac{p\pi}{a}(x'-(\ell-1)D_x)\right]\sin\left[\frac{q\pi}{b}(y'-(i-1)D_y)\right]\frac{\partial^2 G}{\partial x\partial y}-\left(\frac{q\pi}{b}\right)\cdot\right.$$

$$\left.\sin\left[\frac{p\pi}{a}(x'-(\ell-1)D_x)\right]\cos\left[\frac{q\pi}{b}(y'-(i-1)D_y)\right]\left(\frac{\partial^2 G}{\partial x^2}+k^2 G\right)\right]\Bigg\}dS'_{\ell i} \qquad (2.10)$$

$$H_y=\sum_M\sum_N (A_{TE}^{LIMN}-B_{TE}^{LIMN})(jh^{LIMN}\frac{N\pi}{b})\cos\left[\frac{M\pi}{a}(x-(L-1)D_x)\right]\cdot$$

$$\sin\left[\frac{N\pi}{b}(y-(I-1)D_y)\right]+j\omega\mu\sum_P\sum_Q (A_{TM}^{LIPQ}-B_{TM}^{LIPQ})\left(\frac{P\pi}{a}\right)\cdot$$

$$\cos\left[\frac{P\pi}{a}(x-(L-1)D_x)\right]\sin\left[\frac{Q\pi}{b}(y-(I-1)D_y)\right]=2\sum_\ell\sum_i\iint_{S'_{\ell i}}\Bigg\{\sum_m\sum_n$$

$$(A_{TE}^{\ell imn}+B_{TE}^{\ell imn})\left[-\frac{n\pi}{b}\cos\left[\frac{m\pi}{a}(x'-(\ell-1)D_x)\right]\sin\left[\frac{n\pi}{b}(y'-(i-1)D_y)\right]\cdot\right.$$

$$\left.\left(\frac{\partial^2 G}{\partial y^2}+k^2 G\right)-\frac{m\pi}{a}\sin\left[\frac{m\pi}{a}(x'-(\ell-1)D_x)\right]\cos\left[\frac{n\pi}{b}(y'-(i-1)D_y)\right]\frac{\partial^2 G}{\partial x\partial y}\right]\cdot$$

$$dS'_{\ell i}+\frac{j}{\omega\epsilon}\sum_p\sum_q (A_{TM}^{\ell ipq}+B_{TM}^{\ell ipq})(jh^{\ell ipq})\left[\frac{p\pi}{a}\cos\left[\frac{p\pi}{a}(x'-(\ell-1)D_x)\right]\cdot\right.$$

$$\sin\left[\frac{q\pi}{b}(y'-(i-1)D_y)\right]\left(\frac{\partial^2 G}{\partial y^2}+k^2 G\right)-\frac{q\pi}{b}\sin\left[\frac{p\pi}{a}(x'-(\ell-1)D_x)\right]\cdot$$

$$\left.\cos\left[\frac{q\pi}{b}(y'-(i-1)D_y)\right]\frac{\partial^2 G}{\partial x\partial y}\right]\Bigg\}dS'_{\ell i}\ . \qquad (2.11)$$

Only two of the above three equations are linearly independent. Making use of the orthogonality properties of trigonometric functions one can multiply Eq.(2.9) by:

$$\sin\left[\frac{p\pi}{a}(x-(L-1)D_x)\right]\sin\left[\frac{Q\pi}{b}(y-(I-1)D_y\right]$$, and equation (2.10) by

$$\sin\left[\frac{M\pi}{a}(x-(L-1)D_x)\right]\cos\left[\frac{N\pi}{b}(y-(I-1)D_y\right]$$, and integrate over the LI^{th} aperture. The integrals on the right hand side do exist (see Reference (22), p. 624). Integrating by parts and using the identity $\frac{\partial G}{\partial x_i} = -\frac{\partial G}{\partial x_i'}$, where $x_i = x$, y or z and $x_i' = x'$, y' or z', one can eliminate the derivative of G under the integral sign, e.g., for arbitrary A, B, A' and B';

$$\int_B^{B+b}\int_A^{A+a}\int_{B'}^{B'+b}\int_{A'}^{A'+a}\sin\left[\frac{P\pi}{a}(x-A)\right]\sin\left[\frac{Q\pi}{b}(y-B)\right]\cdot\cos\left[\frac{m\pi}{a}(x'-A')\right]\cdot$$

$$\sin\left[\frac{n\pi}{b}(y'-B')\right]\frac{\partial G}{\partial x}\,dx'\,dy'\,dx\,dy = -\int_B^{B+b}\int_A^{A+a}\int_{B'}^{B'+b}\int_{A'}^{A'+a}\left(\frac{p\pi}{a}\right)\cos\left[\frac{P\pi}{a}(x-A)\right]\cdot$$

$$\sin\left[\frac{Q\pi}{b}(y-B)\right]\cos\left[\frac{m\pi}{a}(x'-A')\right]\sin\left[\frac{n\pi}{b}(y'-B')\right]G\,dx'\,dy'\,dx\,dy \qquad (2.12)$$

$$\int_B^{B+b}\int_A^{A+a}\int_{B'}^{B'+b}\int_{A'}^{A'+a}\sin\left[\frac{P\pi}{a}(x-A)\right]\sin\left[\frac{Q\pi}{b}(y-B)\right]\cdot\sin\left[\frac{m\pi}{a}(x'-A')\right]\cdot$$

$$\cos\left[\frac{n\pi}{b}(y'-B')\right]\frac{\partial G}{\partial y}\,dx'\,dy'\,dx\,dy = -\int_B^{B+b}\int_A^{A+a}\int_{B'}^{B'+b}\int_{A'}^{A'+a}\left(\frac{Q\pi}{b}\right)\sin\left[\frac{P\pi}{a}(x-A)\right]\cdot$$

$$\cos\left[\frac{Q\pi}{b}(y-B)\right]\sin\left[\frac{m\pi}{a}(x'-A')\right]\cos\left[\frac{n\pi}{b}(y'-B')\right]G\,dx'\,dy'\,dx\,dy \qquad (2.13)$$

and

and

$$\int_{B}^{B+b}\int_{A}^{A+a}\int_{B'}^{B'+b}\int_{A'}^{A'+a} \sin\left[\frac{M\pi}{a}(x-A)\right]\cos\left[\frac{N\pi}{b}(y-B)\right]\cos\left[\frac{p\pi}{a}(x'-A')\right]\cdot$$

$$\sin\left[\frac{q\pi}{b}(y'-B')\right]\frac{\partial^2 G}{\partial x\partial y}\,dx'\,dy'\,dx\,dy = -\int_{B}^{B+b}\int_{A}^{A+a}\int_{B'}^{B'+b}\int_{A'}^{A'+a}\left(\frac{M\pi}{a}\right)\left(\frac{q\pi}{b}\right)\cdot$$

$$\cos\left[\frac{M\pi}{a}(x-A)\right]\cos\left[\frac{N\pi}{b}(y-B)\right]\cos\left[\frac{p\pi}{a}(x'-A')\right]\cos\left[\frac{q\pi}{b}(y'-B')\right]G\,dx'\,dy'\,dx\,dy\ . \tag{2.14a}$$

In a like manner:

$$\int_{B}^{B+b}\int_{A}^{A+a}\int_{B'}^{B'+b}\int_{A'}^{A'+a} \sin\left[\frac{M\pi}{a}(x-A)\right]\cos\left[\frac{N\pi}{b}(y-B)\right]\sin\left[\frac{m\pi}{a}(x'-A')\right]\cdot$$

$$\cos\left[\frac{n\pi}{b}(y'-B')\right]\frac{\partial^2 G}{\partial x^2}\,dx'\,dy'\,dx\,dy = -\int_{B}^{B+b}\int_{A}^{A+a}\int_{B'}^{B'+b}\int_{A'}^{A'+a}\left(\frac{M\pi}{a}\right)\left(\frac{m\pi}{a}\right)\cdot$$

$$\cos\left[\frac{M\pi}{a}(x-A)\right]\cos\left[\frac{N\pi}{b}(y-B)\right]\cos\left[\frac{m\pi}{a}(x'-A')\right]\cos\left[\frac{n\pi}{b}(y'-B')\right]G\,dx'\,dy'\,dx\,dy\ ; \tag{2.14b}$$

also:

$$\int_{B}^{B+b}\int_{A}^{A+a}\int_{B'}^{B'+b}\int_{A'}^{A'+a} \cos\left[\frac{M\pi}{a}(x-A)\right]\sin\left[\frac{N\pi}{b}(y-B)\right]\cos\left[\frac{m\pi}{a}(x'-A')\right]\cdot$$

$$\sin\left[\frac{n\pi}{b}(y'-B')\right]\frac{\partial^2 G}{\partial y^2}\,dx'\,dy'\,dx\,dy = -\int_{B}^{B+b}\int_{A}^{A+a}\int_{B'}^{B'+b}\int_{A'}^{A'+a}\left(\frac{N\pi}{b}\right)\left(\frac{n\pi}{b}\right)\cdot$$

$$\cos\left[\frac{M\pi}{a}(x-A)\right]\cos\left[\frac{N\pi}{b}(y-B)\right]\cos\left[\frac{m\pi}{a}(x'-A')\right]\cos\left[\frac{n\pi}{b}(y'-B')\right]G\,dx'\,dy'\,dx\,dy\,. \tag{2.14c}$$

Finally

$$\int_{B}^{B+b}\int_{A}^{A+a}\int_{B'}^{B'+b}\int_{A'}^{A'+a}\cos\left[\frac{M\pi}{a}(x-A)\right]\sin\left[\frac{N\pi}{b}(y-B)\right]\sin\left[\frac{m\pi}{a}(x'-A')\right]\cdot$$

$$\cos\left[\frac{n\pi}{b}(y'-B')\right]\frac{\partial^2 G}{\partial x\partial y}\,dx'\,dy'\,dx\,dy = -\int_{B}^{B+b}\int_{A}^{A+a}\int_{B'}^{B'+b}\int_{A'}^{A'+a}\left(\frac{N\pi}{b}\right)\left(\frac{m\pi}{a}\right)\cdot$$

$$\cos\left[\frac{M\pi}{a}(x-A)\right]\cos\left[\frac{N\pi}{b}(y-B)\right]\cos\left[\frac{m\pi}{a}(x'-A')\right]\cos\left[\frac{n\pi}{b}(y'-B')\right]G\,dx\,dy\,dx'\,dy'\,. \tag{2.14d}$$

Using identities (2.12) and (2.13) in connection with equation (2.9) one gets

$$-\frac{j}{\omega\epsilon}\left(A_{TM}^{LIPQ}-B_{TM}^{LIPQ}\right)\left(k_c^{PQ}\right)^2\frac{ab}{4} = 2\sum_{\ell}\sum_{i}\iint_{s_{LI}}\iint_{s'_{\ell i}}\left\{\sum_{m}\sum_{n}\cdot\right.$$

$$\left(A_{TE}^{\ell imn}+B_{TE}^{\ell imn}\right)\left[\left(\frac{n\pi}{b}\right)\left(\frac{P\pi}{a}\right)\cos\left[\frac{P\pi}{a}(x-(L-1)D_x)\right]\sin\left[\frac{Q\pi}{b}(y-(I-1)D_y\right]\cdot\right.$$

$$\cos\left[\frac{m\pi}{a}(x'-(\ell-1)D_x\right]\sin\left[\frac{n\pi}{b}(y'-(i-1)D_y\right]-\left(\frac{m\pi}{a}\right)\left(\frac{Q\pi}{b}\right)\sin\left[\frac{P\pi}{a}(x-(L-1)D_x)\right]\cdot$$

$$\left.\left.\cos\left[\left(\frac{Q\pi}{b}(y-(I-1)D_y\right)\right]\sin\left[\frac{m\pi}{a}(x'-(\ell-1)D_x\right]\cos\left[\frac{n\pi}{b}(y'-(i-1)D_y\right)\right]\right]$$

$$-\frac{j}{\omega\epsilon}\sum_{P}\sum_{Q}\left(A_{TM}^{\ell ipq}+B_{TM}^{\ell ipq}\right)\left(jh^{\ell ipq}\right)\left[\left(\frac{P\pi}{a}\right)\left(\frac{p\pi}{a}\right)\cos\left[\frac{P\pi}{a}(x-(L-1)D_x\right]\cdot\right.$$

$$\left.\sin\left[\frac{Q\pi}{b}(y-(I-1)D_y\right]\cos\left[\frac{p\pi}{a}(x'-(\ell-1)D_x\right]\sin\left[\frac{q\pi}{b}(y'-(i-1)D_y\right]+\left(\frac{Q\pi}{b}\right)\left(\frac{q\pi}{b}\right)\cdot\right.$$

$$\sin\left[\frac{P\pi}{a}(x-(L-1)D_x)\right]\cos\left[\frac{Q\pi}{b}(y-(I-1)D_y)\right]\sin\left[\frac{p\pi}{a}(x'-(\ell-1)D_x)\right]\cdot$$

$$\cos\left[\frac{q\pi}{b}(y'-(i-1)D_y)\right]\Bigg\} G\,dx'\,dy\,dx\,dy \quad . \qquad (2.15)$$

Identities (2.14a), (2.14b) and equation (2.10) yield:

$$\left[(A_{TE}^{LIMN}-B_{TE}^{LIMN})(jh^{MN}\frac{M\pi}{a})-j\omega\mu\,(A_{TM}^{LIMN}-B_{TM}^{LIMN})(\frac{N\pi}{b})\right]\frac{ab}{4}(1+\delta_{ON})=$$

$$2\sum_{\ell}\sum_{i}\iint_{s_{LI}}\iint_{s'_{\ell i}}\Bigg\{\sum_{m}\sum_{n}(A_{TE}^{\ell imn}+B_{TE}^{\ell imn})\left[(k_c^{mn})^2(\frac{M\pi}{a})\cdot\right.$$

$$\cos\left[\frac{M\pi}{a}(x-(L-1)D_x)\right]\cos\left[\frac{N\pi}{b}(y-(I-1)D_y)\right]\cos\left[\frac{m\pi}{a}(x'-(\ell-1)D_x)\right]\cdot$$

$$\cos\left[\frac{n\pi}{b}(y'-(i-1)D_y)\right]-k^2(\frac{m\pi}{a})\sin\left[\frac{M\pi}{a}(x-(L-1)D_x)\right]\cos\left[\frac{N\pi}{b}(y-(I-1)D_y)\right]\cdot$$

$$\sin\left[\frac{m\pi}{a}(x'-(\ell-1)D_x)\right]\cos\left[\frac{n\pi}{b}(y'-(i-1)D_y)\right]-\frac{j}{\omega\epsilon}\sum_{p}\sum_{q}$$

$$(A_{TM}^{\ell ipq}+B_{TM}^{\ell ipq})(jh^{pq})\,k^2(\frac{q\pi}{b})\sin\left[\frac{M\pi}{a}(x-(L-1)D_x)\right]\cos\left[\frac{N\pi}{b}(y-(I-1)D_y)\right]\cdot$$

$$\left.\sin\left[\frac{p\pi}{a}(x'-(\ell-1)D_x)\right]\cos\left[\frac{q\pi}{b}(y'-(i-1)D_y)\right]\right\}G\;dx'\,dy'\,dx\,dy \qquad (2.16)$$

In a like manner identities (2.14c), (2.14d) and equation (2.11) yield:

$$\left[(A_{TE}^{LIMN}-B_{TE}^{LIMN})(jh^{MN}\frac{N\pi}{b})+j\omega\mu\,(A_{TM}^{LIMN}-B_{TM}^{LIMN})(\frac{M\pi}{a})\right]\frac{ab}{4}(1+\delta_{OM})=$$

$$2\sum_{\ell}\sum_{i}\iint_{s_{LI}}\iint_{s'_{\ell i}}\Bigg\{\sum_{m}\sum_{n}(A_{TE}^{\ell imn}+B_{TE}^{\ell imn})\left[(k_c^{mn})^2(\frac{N\pi}{b})\cdot\right.$$

$$\cos\left[\frac{M\pi}{a}(x-(L-1)D_x)\right]\cos\left[\frac{N\pi}{b}(y-(I-1)D_y)\right]\cos\left[\frac{m\pi}{a}(x'-(\ell-1)D_x)\right]\cdot$$

$$\cos\left[\frac{n\pi}{b}(y'-(i-1)D_y)\right] - k^2\left(\frac{n\pi}{b}\right)\cos\left[\frac{M\pi}{a}(x-(L-1)D_x)\right]\sin\left[\frac{N\pi}{b}(y-(I-1)D_y)\right]\cdot$$

$$\cos\left[\frac{m\pi}{a}(x'-(\ell-1)D_x)\right]\sin\left[\frac{n\pi}{b}(y'-(i-1)D_y)\right] + \frac{j}{\omega\epsilon}\sum_p\sum_q$$

$$(A_{TM}^{\ell ipq} + B_{TM}^{\ell ipq})(jh^{pq})\,k^2\left(\frac{p\pi}{a}\right)\cos\left[\frac{M\pi}{a}(x-(L-1)D_x)\right]\sin\left[\frac{n\pi}{b}(y-(I-1)D_y)\right]\cdot$$

$$\cos\left[\frac{p\pi}{a}(x'-(\ell-1)D_x)\right]\sin\left[\frac{q\pi}{b}(y'-(i-1)D_y)\right]\Bigg\}\, G\, dx'\, dy'\, dx\, dy \qquad (2.17)$$

where,
$$\delta_{ON} = \begin{cases} 1 & \text{for } N = 0, \\ 0 & \text{otherwise.} \end{cases}$$

Multiplying equation (2.16) by $(1+\delta_{OM})(\frac{M\pi}{a})$, (2.17) by $(1+\delta_{ON})(\frac{N\pi}{b})$ and adding:

$$(A_{TE}^{LIMN} - B_{TE}^{LIMN})(jh^{MN})(k_c^{MN})^2\,\frac{ab}{4}(1+\delta_{ON})(1+\delta_{OM}) =$$

$$= 2\sum_\ell\sum_i \iint_{s_{LI}}\iint_{s'_{\ell i}}\Bigg\{\sum_m\sum_n (A_{TE}^{\ell imn} + B_{TE}^{\ell imn})\Bigg[(k_c^{mn})^2(k_c^{MN})^2\cdot$$

$$\cos\left[\frac{M\pi}{a}(x-(L-1)D_x)\right]\cos\left[\frac{N\pi}{b}(y-(I-1)D_y\right]\cos\left[\frac{m\pi}{a}(x'-(\ell-1)D_x)\right]\cdot$$

$$\cos\left[\frac{n\pi}{b}(y'-(i-1)D_y)\right] - k^2\left(\frac{M\pi}{a}\right)\left(\frac{m\pi}{a}\right)\sin\left[\frac{M\pi}{a}(x-(L-1)D_x)\right]\cdot$$

$$\cos\left[\frac{N\pi}{b}(y-(I-1)D_y)\right]\sin\left[\frac{m\pi}{a}(x'-(\ell-1)D_x)\right]\cos\left[\frac{n\pi}{b}(y'-(i-1)D_y)\right] -$$

$$k^2\left(\frac{N\pi}{b}\right)\left(\frac{n\pi}{b}\right)\cos\left[\frac{M\pi}{a}(x-(L-1)D_x)\right]\sin\left[\frac{N\pi}{b}(y-(I-1)D_y)\right]\cdot$$

$$\cos\left[\frac{m\pi}{a}(x'-(\ell-1)D_x)\right]\sin\left[\frac{n\pi}{b}(y'-(i-1)D_y)\right]\Bigg] + \frac{j}{\omega\epsilon}\sum_p\sum_q$$

$$(A_{TM}^{\ell ipq}+B_{TM}^{\ell ipq})(jh^{pq})\,k^2\left[(\frac{N\pi}{b})(\frac{p\pi}{a})\cos\left[\frac{M\pi}{a}(x-(L-1)D_x)\right]\cdot\right.$$

$$\sin\left[\frac{N\pi}{b}(y-(I-1)D_y)\right]\cos\left[\frac{p\pi}{a}(x'-(\ell-1)D_x)\right]\sin\left[\frac{q\pi}{b}(y'-(i-1)D_y)\right]-$$

$$(\frac{M\pi}{a})(\frac{q\pi}{b})\sin\left[\frac{M\pi}{a}(x-(L-1)D_x)\right]\cos\left[\frac{N\pi}{b}(y-(I-1)D_y)\right]\cdot$$

$$\left.\sin\left[\frac{p\pi}{a}(x'-(\ell-1)D_x)\right]\cos\left[\frac{q\pi}{b}(y'-(i-1)D_y)\right]\right]\Bigg\}\,G\,dx'\,dy'\,dx\,dy\quad.\qquad(2.18)$$

Equations (2.15) and (2.18) are linearly independent. Multiplying both sides of equation (2.15) by $\frac{jh^{PQ}k^2}{\omega^2\epsilon^2}$ to realize symmetry with equation (2.18) and rewritting equation (2.18) in a more compact form we get:

$$(A_{TE}^{LIMN}-B_{TE}^{LIMN})(jh^{MN})(k_c^{MN})^2\,\frac{ab}{2}(1+\delta_{OM})(1+\delta_{ON})=$$

$$\frac{1}{2}\sum_{\ell}\sum_{i}\Bigg\{\sum_{m}\sum_{n}(A_{TE}^{\ell imn}+B_{TE}^{\ell imn})\left[I_1^{LIMN}\left[(k_c^{MN}k_c^{mn})^2+k^2\left(\frac{Mm\pi^2}{a^2}+\frac{Nn\pi^2}{b^2}\right)\right]+\right.$$

$$+I_2^{LIMN}\left[(k_c^{MN}k_c^{mn})^2-k^2\left(\frac{Mm\pi^2}{a^2}-\frac{Nn\pi^2}{b^2}\right)\right]$$

$$+I_3^{LIMN}\left[(k_c^{MN}k_c^{mn})^2+k^2\left(\frac{Mm\pi^2}{a^2}-\frac{Nn\pi^2}{b^2}\right)\right]$$

$$\left.+I_4^{LIMN}\left[(k_c^{MN}k_c^{mn})^2-k^2\left(\frac{Mm\pi^2}{a^2}+\frac{Nn\pi^2}{b^2}\right)\right]\right]$$

$$+\frac{j}{\omega\epsilon}\sum_{p}\sum_{q}(A_{TM}^{\ell ipq}+B_{TM}^{\ell ipq})\,jh^{pq}\,k^2\left[(I_1^{LIMN}-I_4^{LIMN})\left[\frac{Mq\pi^2}{ab}-\frac{Np\pi^2}{ab}\right]+\right.$$

$$\left(I_3^{\ell ipq\,LIMN} - I_2^{\ell ipq\,LIMN}\right)\left[\frac{Mq\pi^2}{ab} + \frac{Np\pi^2}{ab}\right]\Bigg]\Bigg\} . \tag{2.19}$$

Likewise, equation (2.15) becomes:

$$(A_{TM}^{LIPQ} - B_{TM}^{LIPQ})(jh^{PQ})(k_c^{PQ})^2 \frac{ab}{4} Z_o^2 =$$

$$\frac{1}{2}\sum_{\ell}\sum_{i}\Bigg\{\sum_{p}\sum_{q}(A_{TM}^{\ell ipq} + B_{TM}^{\ell ipq}) Z_o^2 (h^{pq} h^{PQ})\Bigg[\left(I_1^{\ell ipq\,LIPQ} - I_4^{\ell ipq\,LIPQ}\right)\left[\frac{Pp\pi^2}{a^2} + \frac{Qq\pi^2}{b^2}\right]$$

$$- \left(I_3^{\ell ipq\,LIPQ} - I_2^{\ell ipq\,LIPQ}\right)\left[\frac{Pp\pi^2}{a^2} - \frac{Qq\pi^2}{b^2}\right]\Bigg] +$$

$$+ \frac{j}{\omega\epsilon}\sum_{m}\sum_{n}(A_{TE}^{\ell imn} + B_{TE}^{\ell imn})\, jh^{PQ} k^2 \Bigg[\left(I_1^{\ell imn\,LIPQ} - I_4^{\ell ipq\,LIPQ}\right)\left[\frac{Qm\pi^2}{ab} - \frac{Pn\pi^2}{ab}\right] +$$

$$\left(I_3^{\ell imn\,LIPQ} - I_2^{\ell imn\,LIPQ}\right)\left[\frac{Qm\pi^2}{ab} + \frac{Pn\pi^2}{ab}\right]\Bigg]\Bigg\} , \tag{2.20}$$

where $Z_o^2 = \dfrac{k^2}{\omega^2 \epsilon^2}$.

$$I_1^{\ell imn\,LIMN} = \int_{(I-1)D_y}^{(I-1)D_y+b} dy \int_{(L-1)D_x}^{(L-1)D_x+a} dx \int_{(i-1)D_y}^{(i-1)D_y+b} dy' \int_{(\ell-1)D_x}^{(\ell-1)D_x+a} dx'$$

$$\Bigg\{\cos\left[\frac{N\pi}{b}(y-(I-1)D_y) + \frac{n\pi}{b}(y'-(i-1)D_y)\right]\cos\left[\frac{M\pi}{a}(x-(L-1)D_x) +\right.$$

$$\left.\frac{m\pi}{a}(x'-(\ell-1)D_x)\right] G(x-x', y-y')\Bigg\} \tag{2.21a}$$

$$I_2^{\ell imn}{}^{LIMN} = \int_{(I-1)D_y}^{(I-1)D_y+b} dy \int_{(L-1)D_x}^{(L-1)D_x+a} dx \int_{(i-1)D_y}^{(i-1)D_y+b} dy' \int_{(\ell-1)D_x}^{(\ell-1)D_x+a} dx'$$

$$\left\{ \cos\left[\frac{N\pi}{b}(y-(I-1)D_y)+\frac{n\pi}{b}(y'-(i-1)D_y)\right] \cos\left[\frac{M\pi}{a}(x-(L-1)D_x)-\frac{m\pi}{a}(x'-(\ell-1)D_x)\right] G(x-x', y-y') \right\} \qquad (2.21b)$$

$$I_3^{\ell imn}{}^{LIMN} = \int_{(I-1)D_y}^{(i-1)D_y+b} dy \int_{(L-1)D_x}^{(L-1)D_x+a} dx \int_{(i-1)D_y}^{(i-1)D_y+b} dy' \int_{(\ell-1)D_x}^{(\ell-1)D_x+a} dx'$$

$$\left\{ \cos\left[\frac{N\pi}{b}(y-(I-1)D_y)-\frac{n\pi}{b}(y'-(i-1)D_y)\right] \cos\left[\frac{M\pi}{a}(x-(L-1)D_x)+\frac{m\pi}{a}(x'-(\ell-1)D_x)\right] G(x-x', y-y') \right\} \qquad (2.21c)$$

$$I_4^{\ell imn}{}^{LIMN} = \int_{(I-1)D_y}^{(i-1)D_y+b} dy \int_{(L-1)D_x}^{(L-1)D_x+a} dx \int_{(i-1)D_y}^{(i-1)D_y+b} dy' \int_{(\ell-1)D_x}^{(\ell-1)D_x+a} dx'$$

$$\left\{ \cos\left[\frac{N\pi}{b}(y-(I-1)D_y)-\frac{n\pi}{b}(y'-(i-1)D_y)\right] \cos\left[\frac{M\pi}{a}(x-(L-1)D_x)-\frac{m\pi}{a}(x'-(\ell-1)D_x)\right] G(x-x', y-y') \right\} . \qquad (2.21d)$$

Since G in the equation specifying I_1 through I_4 is only a function of $x-x'$ and $y-y'$, a simple change of variable can be made after which G would be a function of only two of the integration variables. Simple integration can be performed with respect to the other pair of variables. That reduces the quadruple integrals to double integrals. See Appendix A for details.

The set of equations (2.19) and (2.20) relate the sum of all modal

components (A+B) or the illuminations of all modes at the apertures of all slots to the difference component (A - B) of any mode at any aperture. Adding or subtracting a factor $(A_{TE}^{LIMN}+B_{TE}^{LIMN})(jh^{MN})(k_c^{MN})^2 \frac{ab}{2}(1+\delta_{OM})(1+\delta_{ON})$ to both sides of equation (2.19) will yield a relation between the illumination and the incident (A) or reflected (B) components, respectively. The first form is suitable for the transmitting array problem and is used from here on. The second can prove more useful for the receiving array problem after adding suitable terms representing the incident wave. The evaluation of the integrals involved is the same, only a minor addition or subtraction is required to obtain one form or the other. Naturally, a similar comment applies in relation to equation (2.20).

By careful inspection of equations (2.19) and (2.20), it is evident that the coupling coefficient* $C^{LIUV}_{\ell iuv}$ remains unchanged if the values of the source and field superscripts are interchanged. In that sense, $C^{LIUV}_{\ell iuv}$ can be termed a normalized coupling coefficient since the matrix thus generated is symmetric. Interesting properties of these coefficients and their relation to symmetry and reciprocity properties will be the subject of the next section.

2.4 Properties of the Coupling Coefficients and Their Relation to Symmetry and Reciprocity

The coupling coefficients $C^{LIUV}_{\ell iuv}$ (see equations (2.19) and (2.20)) consist of a numerical factor multiplying the integrals $I_1^{LIUV}_{\ell iuv}$ through $I_4^{LIUV}_{\ell iuv}$. These numerical factors are functions of the modal indices but not the position indices. It is also important to notice that these factors are insensitive to the interchange of U and V simultaneous with u and v. Studying the equations for I_1 through I_4 (equations (A.2), (A.4), (A.5), (A.7),

*U, V, u, v can be any modal indices M, N, m, n or P, Q, p, q, respectively and $C^{LIUV}_{\ell iuv}$ is the coefficient y $(A^{\ell iuv}+B^{\ell iuv})$ in the expression for $(A^{LIUV}-B^{LIUV})$.

(A. 8), (A. 10)-(A. 13) in Appendix A), the following rules can be established:

1. Interchanging the values of L and ℓ superscripts is equivalent to exchanging the relative horizontal positions (column numbers) of the two slots under consideration. The values of the integrals I_1 through I_4 before and after the exchange are related by

$$I_{\alpha}^{\ell IUV\ Liuv} = (-1)^{U+u} I_{\alpha}^{LIUV\ \ell iuv} \qquad (2.22)$$

where $\alpha = 1, 2, 3$ or 4.

Evidently, for the slot arrangement in Fig. 2-4, the normalized coupling

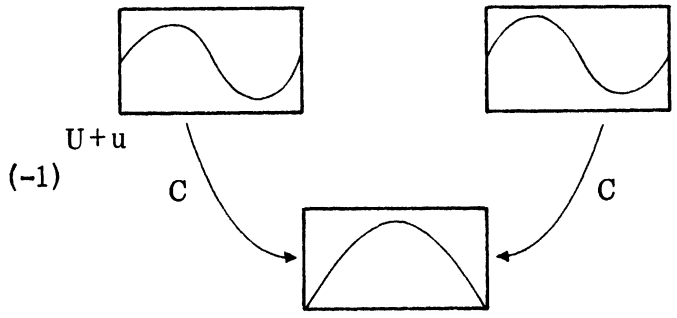

Fig. 2-4: Relation between the normalized coupling coefficients when the horizontal positions are interchanged between the source and field slots.

coefficient from one source mode in the right most slot to some field mode in the center slot is related to the normalized coupling coefficient from the same source mode in the left most slot to the same field mode in the center slot by a factor of $(-1)^{U+u}$.

2. Interchanging the values of I and i superscripts is equivalent to exchanging

the relative vertical positions (row numbers) of the two slots in question. The values of the integrals I_1 through I_4 before and after the exchange are related by

$$I_{\alpha}^{\ell Iuv\ LiUV} = (-)^{V+v} I_{\alpha}^{\ell iuv\ LIUV} \tag{2.23}$$

where $\alpha = 1, 2, 3, 4.$

This asserts that the normalized coupling coefficient from the same mode in the top or bottom slots in Fig. 2-5 to a mode in the center is related by

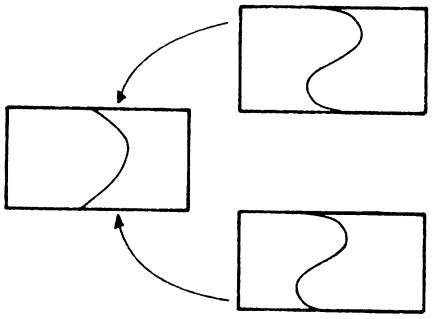

Fig. 2-5: Relation between the normalized coupling coefficients when the vertical positions are interchanged between the source and field slots.

the factor $(-1)^{V+v}$.

3. Interchanging the values of U and u superscripts will similarly yield the relation between the values of I_1 through I_4:

$$I_{\alpha}^{\ell iUv\ LIuV} = (-)^{U+u} I_{\alpha}^{\ell iuv\ LIUV} \tag{2.24}$$

where $\alpha = 1, 2, 3$ or 4.

In this case, however, the normalized coupling coefficients are not related by a simple sign relationship since the factors multiplying the integrals are going to change. The same statement is true when V and v superscripts are interchanged, where the integrals are related by:

$$I_{\alpha}^{\ell iuV}{}^{LIUv} = (-)^{V+v} I_{\alpha}^{\ell iuv}{}^{LIUV} \tag{2.25}$$

where $\alpha = 1, 2, 3$ or 4.

4. Evidently under simultaneous interchange of the values of U, V and u, v supercripts, respectively, the integrals are related by:

$$I_{\alpha}^{\ell iUV}{}^{LIuv} = (-)^{U+u+V+v} I_{\alpha}^{\ell iuv}{}^{LIUV} \tag{2.26}$$

where $\alpha = 1, 2, 3$ or 4.

Thus the normalized coupling coefficients, when the source and field slots remain unchanged but the source and field modes are interchanged, are related by $(-1)^{U+u+V+v}$.

5. The rules enunciated for the interchanging of slot positions either from one vertical position to another vertical position or from one horizontal position to another horizontal position as well as rules for changing the indices associated with modes are all consistent with the reciprocity requirement. This is illustrated in the following equation:

$$I_{\alpha}^{\ell iuv}{}^{LIUV} = I_{\alpha}^{\ell iuv}{}^{LIUV} \quad . \tag{2.27}$$

This can be interpreted as stating that the normalized coupling coefficient to the UV^{th} mode in the first slot from the uv^{th} mode in the second slot is equal to the normalized coupling coefficient to the uv^{th} mode in the

second slot from the UV^{th} mode in the first slot.

These basic relationships are essential to the understanding of the "blind spot" phenomenon. In addition, a sizable savings in the computational effort can be realized using these relations. For example, it is interesting to note that the third rule in the above goes beyond the usual symmetry and reciprocity relations to relate the integrals involved in evaluating the coupling between the u_1v_1 and u_2v_2 modes to those involved in evaluating the coupling between the u_1v_2 and u_2v_1 modes or the u_2v_1 and u_1v_2 modes. Also, the integrals used in evaluating the coupling coefficients depend only on the indices involved but not the type (TE or TM). This makes the same set of integrals usable for a number of coupling coefficients.

The application of these facts plus other measures to reduce the computational effort will be the subject of the next sections.

2.5 Matrix Description

Considering the transmitting array problem, the formulations described in the previous section ultimately lead to the major problem of solving a matrix equation of the form:

$$\left[C\right](\bar{A} + \bar{B}) = \left[C\right]\bar{Q} = \bar{A} \quad . \tag{2.28}$$

In this equation $[C]$ is the matrix whose entries represent coupling between different modes in different slots, $\bar{Q}$ is the column vector whose entries are complex numbers representing normalized modal illuminations at the apertures and $\bar{A}$ is the column vector of complex entries representing the normalized incident component of different modes in different slots. Usually arrays formed of open ended waveguides have only one propagating mode. Entries corresponding to modes below cut off in the excitation column vector A can then be zeroes if there is enough waveguide length directly behind the aperture to isolate it from any discontinuity in the guide.

Theoretically the array pattern requirements dictate the illumination $\bar{Q}$. The incident values can then be calculated from equation (2.28). The

reverse problem requires the inversion of [C]. Usually the array pattern is calculated based on the dominant mode illuminations alone and the higher order modal content is not specified. An approximation which will make it possible to reduce the problem to a matrix equation involving only the dominant mode or modes including the effect of higher order modes will be discussed in the next section.

First, a systematic method for filling the matrix and using the properties enunciated in the previous section will be described. Figure 2-6 shows a diagramatic representation of the antenna array and the matrix structure.

Legend for Fig. 2-6

Symbol	Meaning
LL	Number of columns in the antenna array
II	Number of rows in the antenna array
NOM	Number of modes considered
$C_{uv}^{\ell_i\, UV}$	Coupling coefficients from uv mode to UV mode where the source slot is i-1 rows above the field slot and ℓ-1 columns to the right of the field slot.
$s^{\ell i}$	Coupling matrix between two slots where the source slot is i-1 rows above the field slot and ℓ-1 columns to the right of the parasitic slot. Dimension of matrix = NOM.
R^{i}	Coupling matrix between two rows where the source row is i-1 rows above the field row. Dimension of modes = NOM x LL.
$s^{*\ell i}$	Coupling matrix between two slots where the same slot is i-1 rows above the field slot and ℓ-1 columns to the left of the field slot. Dimension of matrix = NOM.
R^{*i}	Coupling matrix between two rows where the source row is i-1 rows below the field row. Dimension of matrix = NOM x LL.

$[C] =$

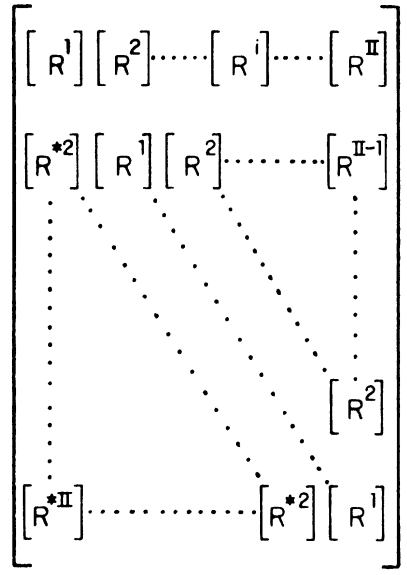

(a)

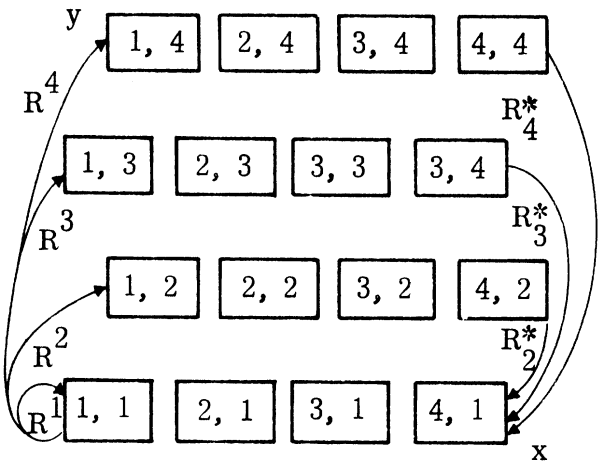

(b)

$[R^i] =$

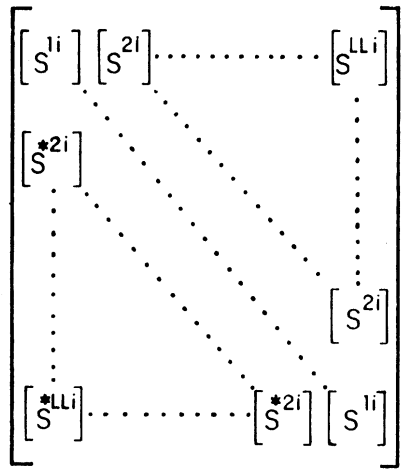

(c)

$[S^{\ell i}] =$

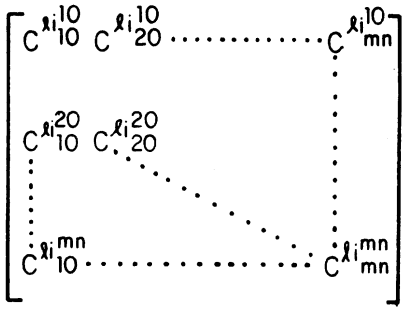

(d)

Fig. 2-6: Diagramatic sketch for the antenna array and the matrix representing the array: (a) Matrix structure, (b) Antenna array, (c) Sub-matrix representing the coupling between two rows, (i-1) rows apart, (d) Sub-matrix representing the coupling between two slots (i-1) rows apart and (ℓ-1) columns apart.

Based on relation number 5 in the previous section $[R^{*i}]$ can be derived from $[R^{*}]$ by transposing. For rectangular grid $[s^{*\ell i}]$ can be derived from $[s^{\ell i}]$. Also for isosceles triangular grid $[s^{*\ell i}]$ can be derived from $[s^{\ell-1,i}]$. Finally, only the elements in the upper triangle of the $[s^{\ell i}]$ matrix are necessary to fill the whole $[s^{\ell i}]$ matrix. In this fashion considerable simplification has been made. For an array of LL columns and II rows it is necessary to have only the elements of the upper triangles of the top rows of the $[s^{\ell i}]$ matrices in order to fill the entire matrix [C]. Hence, if NOM is the number of modes considered in each slot, then the number of coefficients to be calculated becomes:

$$LL \cdot II \cdot [NOM+(NOM-1)+(NOM-2)\ldots 1] = LL \cdot II \cdot (NOM+1) \cdot (NOM/2).$$

This is the actual number of coefficients relating all the modes in all of the slots to all of the modes in the L= 1, I = 1 slot.

2.6 Approximation Leading to Matrix Reduction

In designing a phased array, the array size and illuminations are implied by the pattern requirement. Usually, illuminations are calculated on a one mode basis. However, in actual operation several other modes can be excited at the array aperture. In the case of a transmitting array, for example, these modes are excited at any slot by coupling from the excited mode or modes in the same or surrounding slots. These modes couple back to the excited modes as well as to other unexcited modes. So even if the illumination by unexcited modes might not represent a large portion of the total illumination, these modes can still act as couplers between excited modes. Coupling accumulation at particular scan directions can lead to severe mismatch (27) when the beam is steered to these directions. This phenomenon was observed and is referred to as "blind spot". It is not associated with array pattern deterioration but rather with a severe mismatch for some scan directions. This indeed supports the belief that although the excited mode illuminations might still prevail, coupling accumu-

lation via unexcited modes as well as direct coupling between the excited modes in each slot gives rise to this unwanted effect. Studies made on the basis of the excited TE_{10} mode alone did not reveal the "blind spot" behavior (6, 7). One can then conclude that a major cause of this phenomenon is due to coupling via unexcited modes.

For transmitting array design one of the main interests is to determine the input impedance of different array elements as viewed by the unexcited mode. Based on the above discussion a simplifying approximation can be introduced. One can still take into account the existence of unexcited modes at the apertures, but only as contributions from the excited mode illuminations and neglecting further contributions from unexcited modes. This amounts to neglecting only some third and higher order coupling contributions on any excited mode. Third order means coupling from an excited mode to an unexcited mode and then to an unexcited mode before coupling back to an excited mode. The use of such an approximation leads to a tremendous savings of computational effort involved and the generation of an augmented matrix that relates the excited mode illuminations and excitations directly, where the effect of unexcited modes appear only implicitly in the augmented matrix entries.

Assuming one mode (TE_{10}) excitation of a rectangular or an isosceles triangular grid array of rectangular slots, then in reference to the matrix description in Fig. 2-6 d of the previous section, the use of the above-mentioned assumption is equivalent to calculating only the top row of the $[s^{li}]$ matrix. The first column can be obtained from the top row using the rules in section 2.4. The rest of the entries would be contributions among unexcited modes which can be set equal to zero based on the approximation just discussed. This means that only the top row of entries of the $[C]$ matrix (see the end of the previous section) need to be calculated and the whole matrix can then be considered filled. The number of coefficients one has to calculate, if only one mode is excited, corresponds to:

$$LL \times II \times NOM \quad .$$

This represents the number of coefficients relating the excited mode in the L = 1, I = 1 slot to all modes in all slots. Using this assumption equation (2.19) can be rewritten for M, N $\neq$ 1, 0 as:

$$-q_{TE}^{LIMN}(jh^{MN})(k_c^{MN})^2 \frac{ab}{2}(1+\delta_{ON})(1+\delta_{OM}) =$$

$$= \sum_{\ell}\sum_{i} q_{TE}^{\ell i10}\left[I_3^{\ell i10}\left(k_c^{MN}\left(\frac{\pi}{a}\right)^2 + k^2\left(\frac{M\pi^2}{a^2}\right)\right) + I_4^{LIMN}\left(k_c^{MN}\left(\frac{\pi}{a}\right)^2 - k^2\left(\frac{M\pi^2}{a^2}\right)\right)\right] \quad (2.29)$$

For M, N = 1, 0:

$$(A_{TE}^{LI10} - B_{TE}^{LI10})(jh^{10})\left(\frac{\pi}{a}\right)^2 \frac{ab}{2} =$$

$$= \sum_{\ell}\sum_{i}\left\{\sum_{m}\sum_{n} q_{TE}^{\ell imn}\left[I_3^{LIMN}\left(\left(\frac{\pi}{a}\right)^2 k_c^{2}{}_{mn} + k^2\left(\frac{m\pi^2}{a^2}\right)\right) + I_4^{LIMN}\left(\left(\frac{\pi}{a}\right)^2 k_c^{2}{}_{mn} - k^2\left(\frac{m\pi^2}{a^2}\right)\right)\right] + \right.$$

$$\left. + \frac{j}{\omega\epsilon}\sum_{p}\sum_{q} q_{TM}^{\ell ipq}\, jh^{pq}\, k^2\left(\frac{q\pi^2}{ab}\right)\left(I_3^{LI10}{}_{\ell ipq} - I_4^{LI10}{}_{\ell ipq}\right)\right\} \quad (2.30)$$

and (2.20) as follows:

$$-q_{TM}^{LIPQ}\left(k_c^{PQ}\right)^2 \frac{ab}{4} = \sum_{\ell}\sum_{i} j\omega\epsilon\left(\frac{Q\pi^2}{ab}\right) q_{TE}^{\ell i10}\left(I_3^{LIPQ}{}_{\ell i10} - I_4^{LIPQ}{}_{\ell i10}\right) \quad . \quad (2.31)$$

In the above equations, since the unexcited modes have no incident component, the illumination is equal to the reflected component ($q^{LIUV} = B^{LIUV}$). Also, the fact that N = 0 (for TE_{10} the excited mode) results in $I_3 = I_1$ and $I_2 = I_4$ (see Appendix A).

Substituting equations (2.29) and (2.31) into (2.30) and regrouping terms involving the same $q_{TE}^{\ell i10}$, one can write:

$$(A_{TE}^{LI10} - B_{TE}^{LI10}) = \sum_{\ell} \sum_{i} q_{TE}^{\ell i 10} \left[F^{LI10}_{\ell i 10} - \sum_{\ell' i'} \left(\sum_{mn}{}' F^{\ell' i' mn}_{\ell i 10} \, F^{LI10}_{\ell' i' mn} + \sum_{pq} F^{\ell' i' pq}_{\ell i 10} \, F^{LI10}_{\ell' i' pq} \right) \right] \tag{2.32}$$

where

$$F^{LI10}_{\ell i 10} = \frac{1}{jh^{10}\left(\frac{\pi}{a}\right)^2 \frac{ab}{2}} \left[I_3^{\ell i 10} \left(\frac{\pi^4}{a^4} + k^2 \frac{m\pi^2}{a^2} \right) + I_4^{\ell i 10} \left(\frac{\pi^4}{a^4} - k^2 \frac{m\pi^2}{a^2} \right) \right], \tag{2.33}$$

$$F^{\ell' i' mn}_{\ell i 10} = \frac{1}{jh^{mn}\left(k_c^{mn}\right)^2 \frac{ab}{4}} \left[I_3^{\ell' i' mn}{}_{\ell i 10} \left(\frac{\pi^2}{a^2} \left(k_c^{mn}\right)^2 + k^2 \frac{m\pi^2}{a^2} \right) + I_4^{\ell' i' mn}{}_{\ell i 10} \left(\frac{\pi^2}{a^2} \left(k_c^{mn}\right)^2 - k^2 \frac{m\pi^2}{a^2} \right) \right], \tag{2.34}$$

$$F^{LI10}_{\ell' i' mn} = \frac{1}{jh^{10}\left(\frac{\pi}{a}\right)^2 \frac{ab}{2}} \left[I_3^{LI10}{}_{\ell' i' mn} \left(\frac{\pi^2}{a^2} \left(k_c^{mn}\right)^2 + k^2 \frac{m\pi^2}{a^2} \right) + I_4^{LI10}{}_{\ell' i' 10} \left(\frac{\pi^2}{a^2} \left(k_c^{mn}\right)^2 - k^2 \frac{m\pi^2}{ab} \right) \right], \tag{2.35}$$

$$F^{\ell' i' pq}_{\ell i 10} = \frac{j\omega\epsilon}{\left(k_c^{pq}\right)^2 \frac{ab}{4}} \left(\frac{q\pi^2}{ab} \right) \left(I_3^{\ell' i' pq}{}_{\ell i 10} - I_4^{\ell' i' pq}{}_{\ell i 10} \right), \tag{2.36}$$

and

$$F^{LI10}_{\ell' i' pq} = \frac{-h^{pq}/\omega\epsilon}{jh^{10}\left(\frac{\pi}{a}\right)^2 \frac{ab}{2}} k^2 \left(\frac{q\pi^2}{ab} \right) \left(I_3^{LI10}{}_{\ell' i' pq} - I_4^{LI10}{}_{\ell' i' pq} \right). \tag{2.37}$$

The symbol $\sum_{mn}{}'$ implies summation excluding the case $m = 1$, $n = 0$.

Adding $A_{TE}^{LI10} + B_{TE}^{LI10}$ to both sides of equation (2.32) produces:

$$A_{TE}^{LI10} = \frac{1}{2} \sum_{\ell} \sum_{i} q_{TE}^{\ell i 10} \left[F^{LI10}_{\ell i 10} + \delta_{\substack{LI \\ \ell i}} - \sum_{\ell' i'} \left(\sum_{mn}{}' F^{\ell' i' mn}_{\ell i 10} \, F^{LI10}_{\ell' i' mn} + \sum_{pq} F^{\ell' i' pq}_{\ell i 10} \, F^{LI10}_{\ell' i' pq} \right) \right]. \tag{2.38}$$

Equation (2.38) expresses the relation between the incident modes in an array and the illuminations on the array face, including the effect of higher order modes but neglecting interaction among them. This form is particularly useful for application in computer controlled phased arrays since it represents the feed requirement for a given illumination. For the same reason it would be very convenient for designing an array feed network. The reflection coefficient and the normalized input admittance, for an arbitrary scan angle, can be expressed by:

$$R^{LI10} = \frac{q^{LI10}}{A^{LI10}} - 1 \quad , \tag{2.39}$$

$$Y^{LI10} = \frac{1 - R^{LI10}}{1 + R^{LI10}} \quad . \tag{2.40}$$

In the following chapter some study of the coupling between rectangular slots in a ground plane is carried out. Also, some phased array cases already studied theoretically and experimentally as reported in the literature (5, 6, 7) are now solved by the method described above. This method is shown to predict anomalous null or "blind spot" behavior. In the last chapter the occurrence of "blind spots" and the reasons for them will be discussed.

CHAPTER III

COMPUTATIONAL RESULTS AND COMPARISON WITH EXPERIMENT

3.0

Arrays chosen for detailed computational effort were a linear array of seven slot elements arranged for weak coupling, a planar array of 49 elements in a triangular grid and a rectangular grid array of 169 elements. In all cases the elements were open-ended waveguides. Familiar standard rectangular waveguides were used for the linear and the triangular grid array and square waveguides for the rectangular grid array. Limited experimental measurements were performed on the linear seven-element array. Aperture probing as well as reflection coefficient magnitude were provided for a few positions of the beam between broadside and 30^{o} scan. The results for the planar arrays were checked against previous work by Farrell and Kuhn (5, 7). In the next section a short description of the computer program used is given.

3.1 Computer Program Description

Due to the large number of coefficients that had to be calculated and the complex symmetry and reciprocity considerations involved, the program was best divided into several parts. The overall goal, of course, was to perform as small a number of calculations as possible, and secondly, to avoid using extremely large core storage which can be both as expensive as the calculation and may sometimes result in exceeding the storage capacity on the available computer. On the IBM 360/67 computer, available at The University of Michigan, the maximum size of one array of numbers that can be accommodated is roughly one million bytes; this number corresponds to 125,000 complex numbers. This is approximately the size of the basic matrix of a 25-element antenna array with 14 modes considered.

Several versions of the program were written and optimized. The final version is very compatible and has virtually no limitation on size due to storage requirements (by changing dimension statements the limit has now

become the number of modes per slot times the number of slots, NOM x NOS $< 125,000$). The cost as a function of the physical size of the antenna array and the number of modes represented is different for various parts of the program. Specific reference will be made as each section is described.

The first program, when given the specifications from the physical array (frequency, slot dimensions, grid type, grid dimensions and the number of rows and columns) and the modes to be considered, would calculate the top row of the basic matrix. The result together with the specifications are kept in a file. Evidently the cost is almost linear with the product of the number of TE modes times the number of slots. This corresponds physically to calculating the normalized coupling coefficients from all modes in all slots to the excited mode in the first slot. This program calls upon a subroutine which evaluates the integrals I_1 through I_4; this constitutes the major cost contribution in this part. These integrals are evaluated numerically (within one percent) for the near slots. Taylor's approximations for the distance between the field and source points and its inverse are utilized for the slots which are relatively far apart. In the following calculations the criterion used for slots being spaced far apart was empirically taken as $R \geq 4A$, where R is the distance between similar points on the slots and A is the slot width.

A separate subroutine was written which utilized the pertinent properties from section 2.4 to generate any desired row or column that is related to the top row. Given a row number and a column number this subroutine actually generates the corresponding row and column in the basic matrix representing the physical array. It can do this for rectangular as well as isosceles triangular lattice arrangements. The parameter G specifies the grid type by the designation $G = 0$ for a rectangular lattice arrangement and $G = 0.5$ for an isosceles triangular lattice arrangement.

The second part of the program calculates the reflection coefficient of any slot as a function of the beam pointing direction. This part calls on the above mentioned subroutine to generate the required rows and columns of the basic matrix, from which the entries of the augmented matrix are computed.

This task represents the major cost constituent for this part. For this reason only one row of the augmented matrix corresponding to the desired slot is generated. The entries in the augmented matrix are computed from the basic matrix using the approximation introduced in section 2.6. The program then proceeds to calculate the illuminations required for a desired beam direction. The incident component in the chosen slot is computed by a straightforward summation of the product of each illumination times the corresponding row entry. Using equation (2.37) the complex reflection coefficient and the relative power transmitted $(1 - |R|^2)$ are then computed. This is repeated throughout the range of main beam directions specified. The element position (row and column), the limits of the scan range (θ_{max}, θ_{min}, ϕ_{max}, ϕ_{min}) and the scan increments $\Delta\theta$ and $\Delta\phi$ are the inputs for this part. θ is the beam angle from broadside and ϕ is the azimuth direction (see Fig. 3-1); $\Delta\theta$ and $\Delta\phi$ are the respective increments.

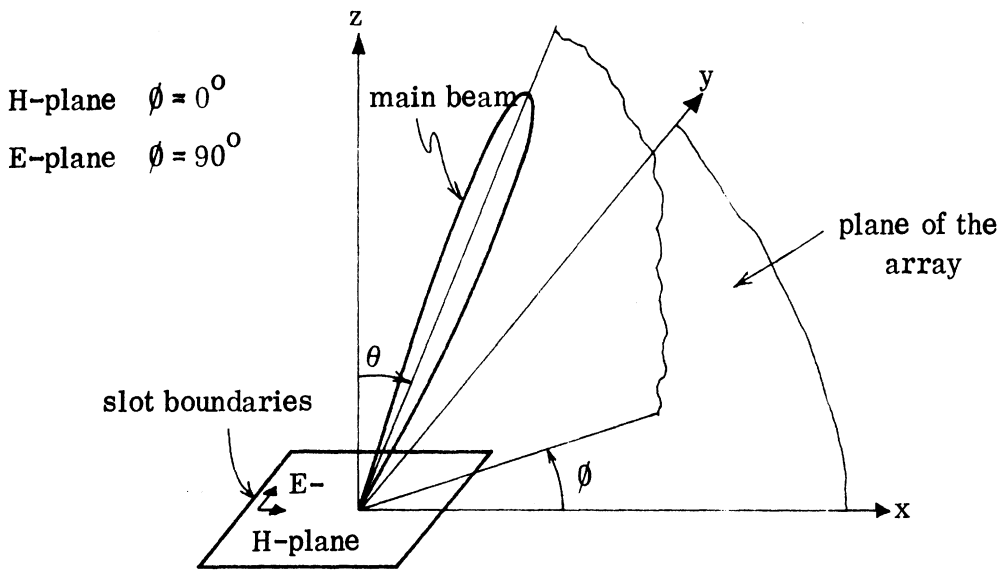

Fig. 3-1: Specification of the main beam direction.

In the arrangement described above the maximum mathematical array size to be stored is the top row of the basic mathematical matrix which contains number of slots times number of modes-elements. The limit on storage is then the maximum number of elements in the basic matrix row and this should be equal or less than the maximum allowable array size storable on the computer in use (125,000 on The University of Michigan IBM 360/67 computer). One can also notice that it is sufficient to calculate one row of the augmented matrix in order to study the scan characteristics of one of the array elements in the synthesis problem. In this context the synthesis problem is the one in which the aperture illumination is specified (from pattern requirements) and the reflection coefficient is calculated for each of the feeds to the antenna array. In this way there is a large cost advantage since the cost for calculating the augmented matrix elements goes up as the square of the number of elements times the number of modes. Another advantage present in this type of formulation is that the matrix need not be inverted.

3.2 Experimental Results

As a preliminary check on computer calculations a small slot array of seven elements was arranged with the slots oriented for weak coupling. This antenna array was built and tested. The money and time available limited the experimental studies on arrays to this one array. In comparison, construction of a large planar array of slots closely spaced would be extremely complicated and excessively costly. However, the method of computations was further checked against the experimental results obtained on a 7x7 element array having rectangular slots arranged in an isosceles triangular grid and a 13x13 element array having square slots arranged in a rectangular grid. Experimental data as well as analytical data based on the infinite array assumption on these arrays were reported in the literature by Farrell and Kuhn (5, 7). Close agreement was observed between the finite array calculations and the experimental results, both for the seven-element linear array tested in the laboratory as well as in the experimental data cited in the literature.

3.2.1 Linear Seven-Element Array

This array consists of seven open-ended X-band waveguides mounted on a 4' x 4' aluminum ground plane. Figures 3-2 to 3-6 show important details of the linear seven-element slot array which was designed and constructed in the laboratory. A feature of this array was that the slots were

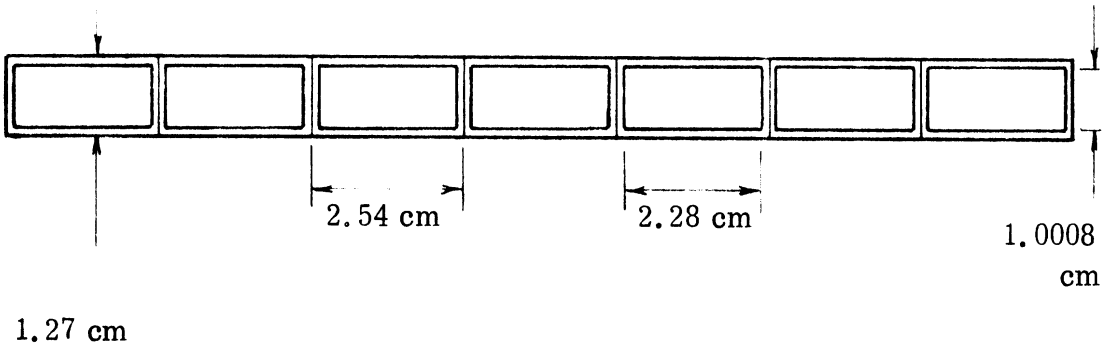

Fig. 3-2: Aperture of the seven-element linear array (X-Band).

formed from the open ends of X-band waveguides which were clamped with appropriate spacers. The slots could be oriented either for weak coupling or strong coupling. By loosening the clamps and inserting different spacers it was possible to have a different spacing between every two slots. However, for the experimental work done here only one spacing of slots was used. Likewise, only one orientation of slots was used and that was the one corresponding to the weak coupling from one slot to the other. The array was fed by means of a power divider which was also designed and constructed in the laboratory (see Fig. 3-7). The power divider was a nine-port network with one input port and eight output ports. One of the output ports went into a dummy load. The remaining seven output ports went into coaxial fittings and from this into line stretchers. From the line stretchers individual coaxial connections were made through appropriate coaxial fittings on each of the waveguides of the array. The construction was such that a directional

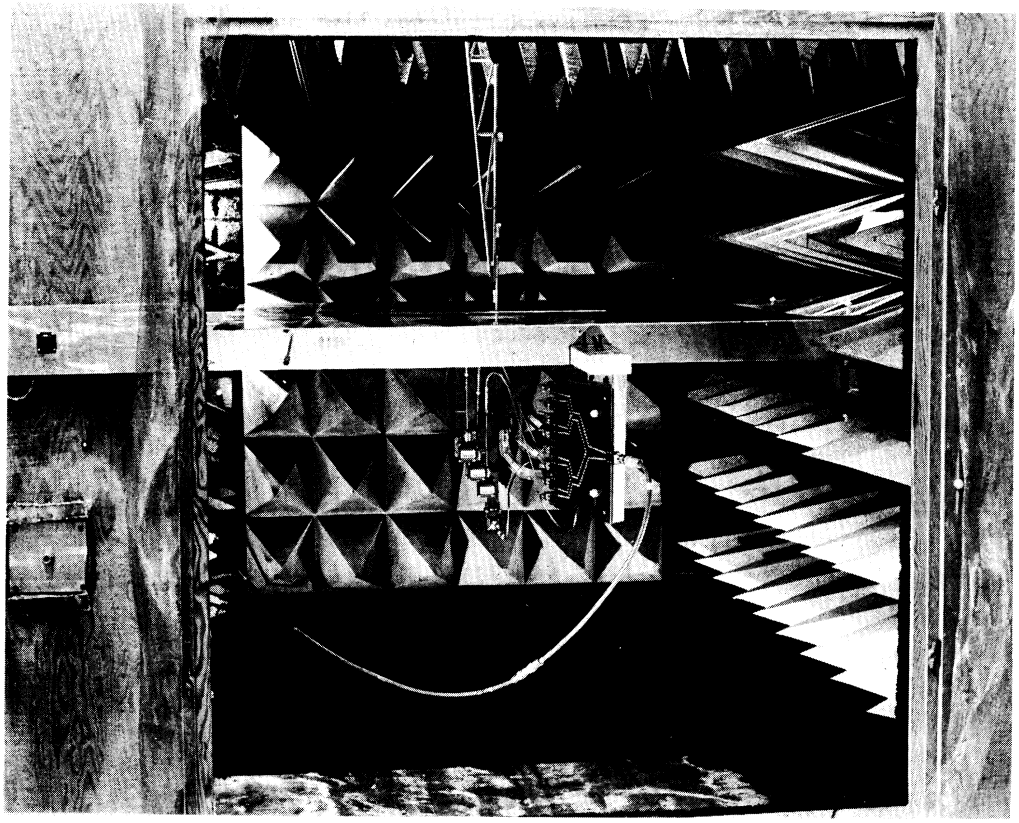

Fig. 3-3: Seven-element X-Band linear array inside anechoic chamber.

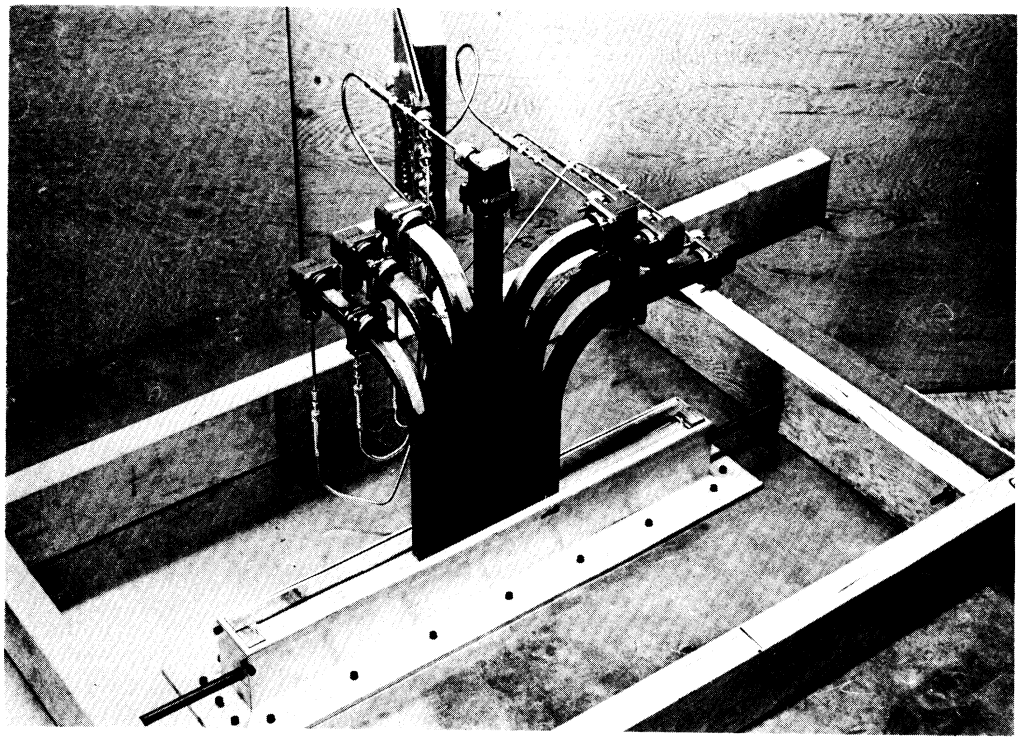

Fig. 3-4: Details of seven-element X-Band linear array behind the ground plane. Notice the coaxial line stretchers in the rigid coaxial lines between the power divider and the waveguide adapters.

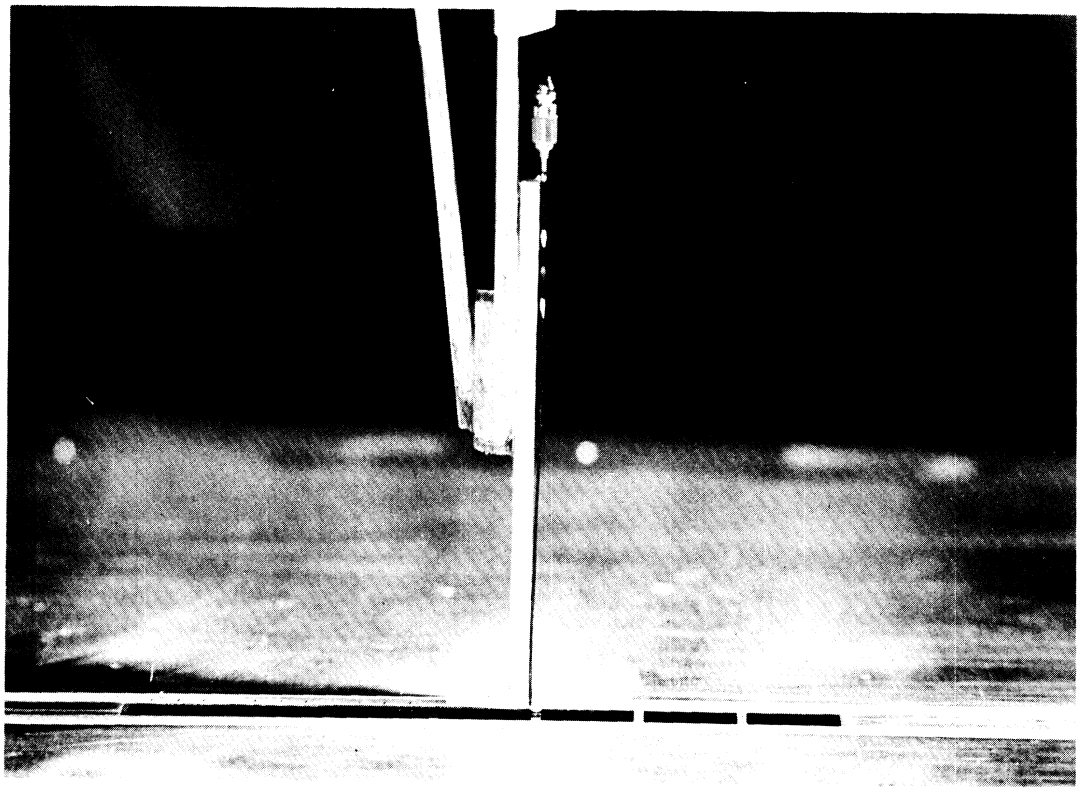

Fig. 3-5: Seven-element linear array as viewed from the top (above ground plane) and the field (H_z) probe.

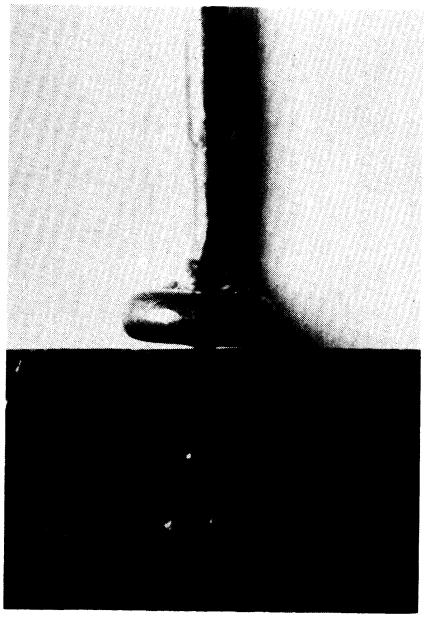

Fig. 3-6: A close-up of the normal magnetic field (H_z) probe. One division = 0.01 inch.

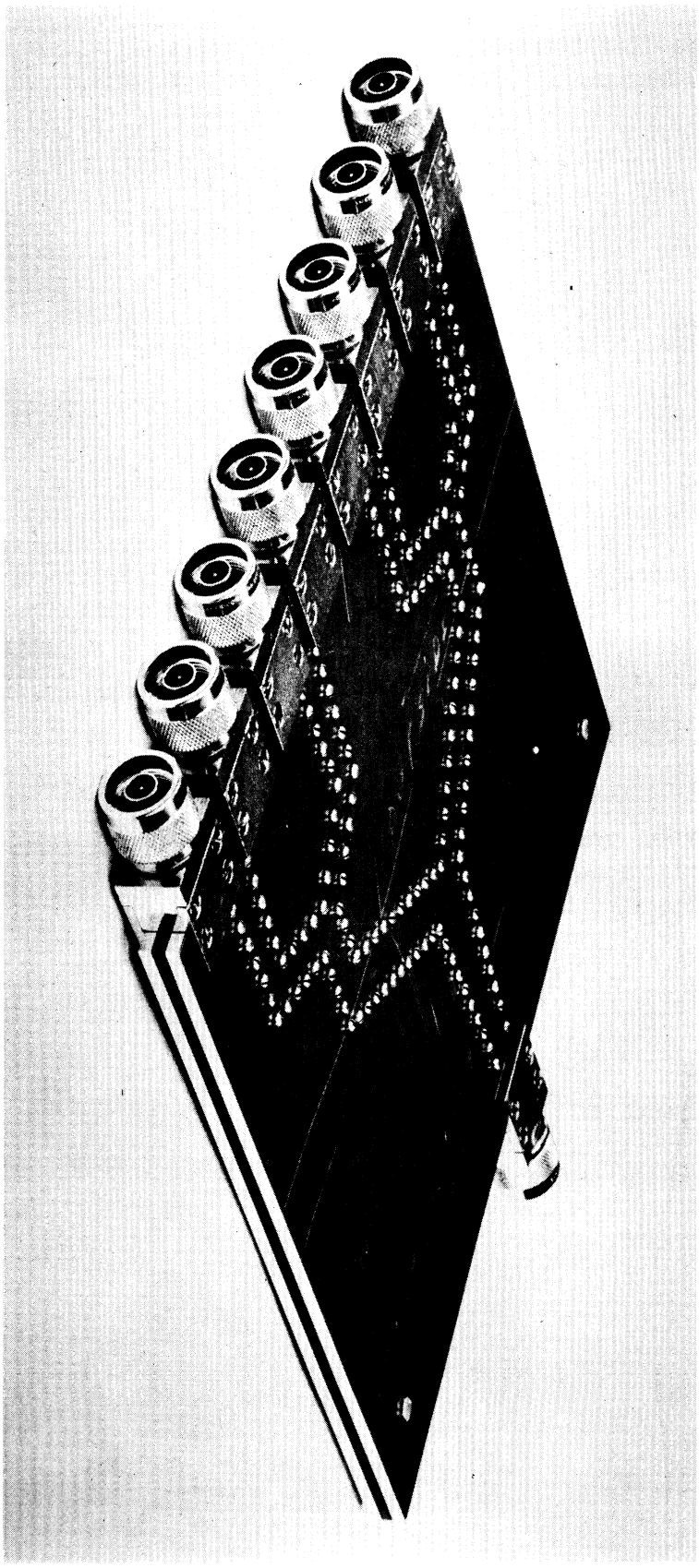

Fig. 3-7: The power divider.

coupler could be inserted in each of the feeds to the slots without changing the electrical length of the feed to the slot. The waveguide sections were constructed to have equal electrical lengths. The bends in the waveguides were used to allow physical clearance for the flanges, even for the minimum possible spacing between the waveguides. The rigid coaxial lines were also cut to have equal lengths. The line stretchers were used as a fine adjustment for the phase between slots for the broadside position. They were also used to provide the required phase gradient between slots for main lobe directions other than broadside. Since a single directional coupler was used the actual measurement required the coupler to be inserted first in one direction and then the other. In this manner a measurement can be obtained on the magnitude of the reflection factor at each of the ports of the seven-element array. No measurements were made of the phase of the reflection factor because of the difficulties of measuring this phase with sufficient precision.

Figure 3-8 shows a schematic diagram of the experimental setup used. The reflection coefficient for the central slot was measured at four different directions of the main beam. These scan angles were between 0^{o} or broadside position and 30^{o} from broadside. In order to obtain a given scan angle the illumination of each slot was adjusted to the appropriate phase as calculated for the desired scan angle. This measurement of phase was by means of a measurement of H_z through the use of a small probe. The small probe is shown in Fig. 3-6. The minute size of the probe resulted in only a slight perturbation of the field.

In Figs. 3-9 through 3-12 several probing patterns are shown, corresponding to the various scan angles studied. In each of these figures the topmost part shows the amplitude of the field. Keeping in mind that H_z is what is measured by the small probe, the sharp minimums in the upper diagrams in each figure represent the zero which is to be expected for the H_z component of the field of a slot with, of course, the dominant TE_{10} mode prevailing. The lower part of each figure shows the probing of the phase profile for each of the cases. The phase situation is somewhat complicated

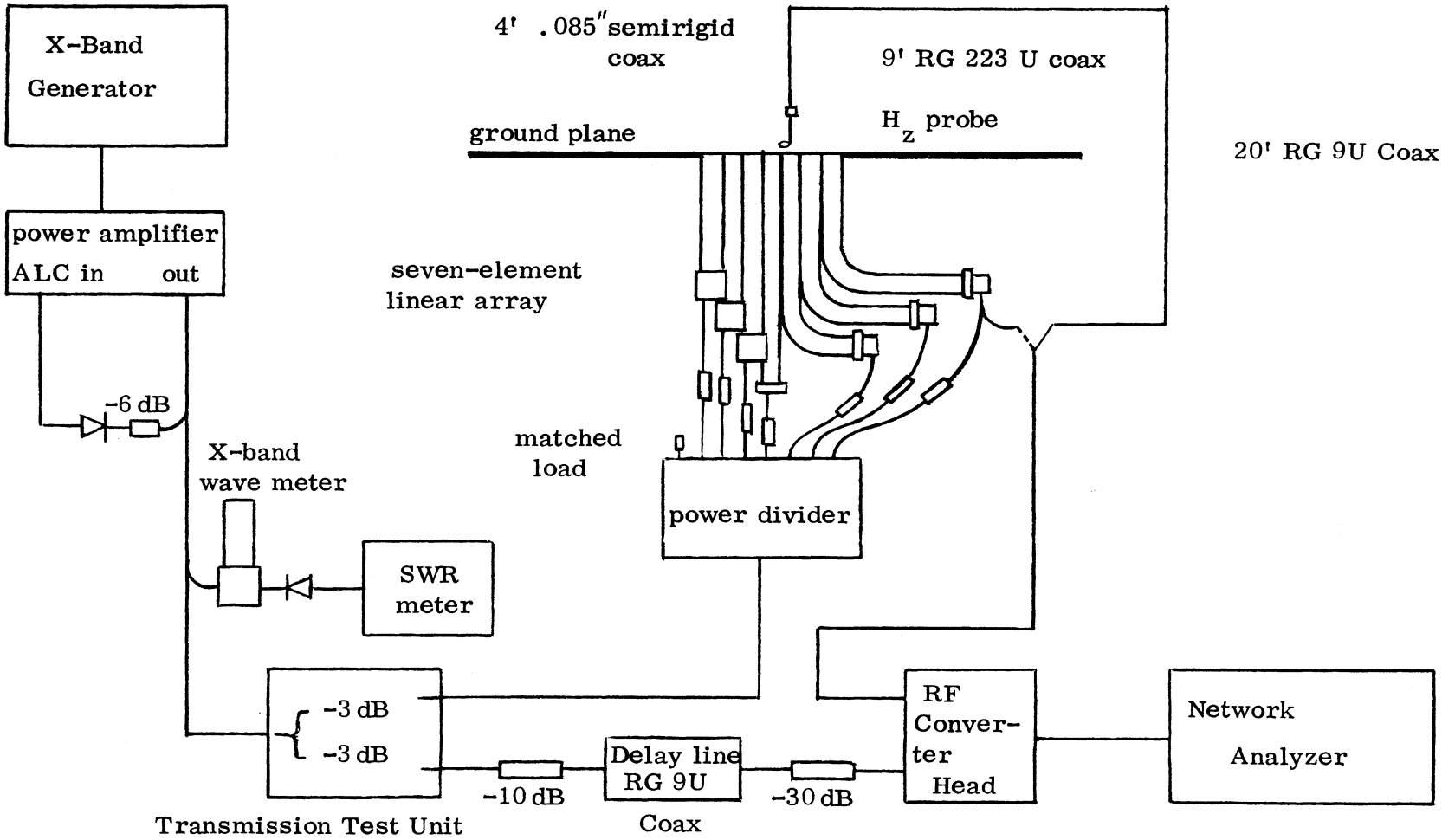

Fig. 3-8: Block diagram for the experimental set-up used for reflection coefficient and aperture measurement on the seven-element linear array.

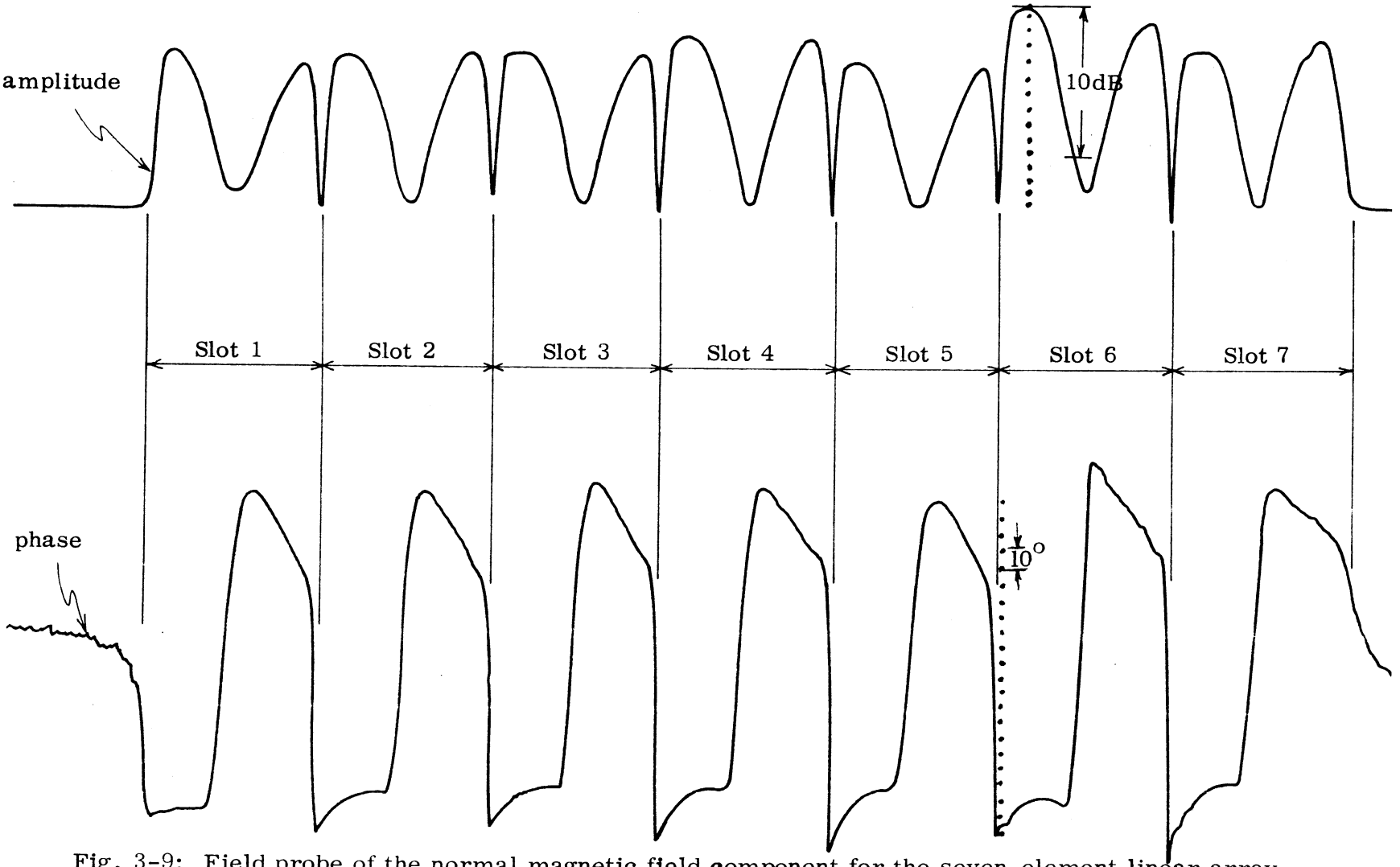

Fig. 3-9: Field probe of the normal magnetic field component for the seven-element linear array. Frequency 10 GHz. Phase shift per element = 0^{o}.

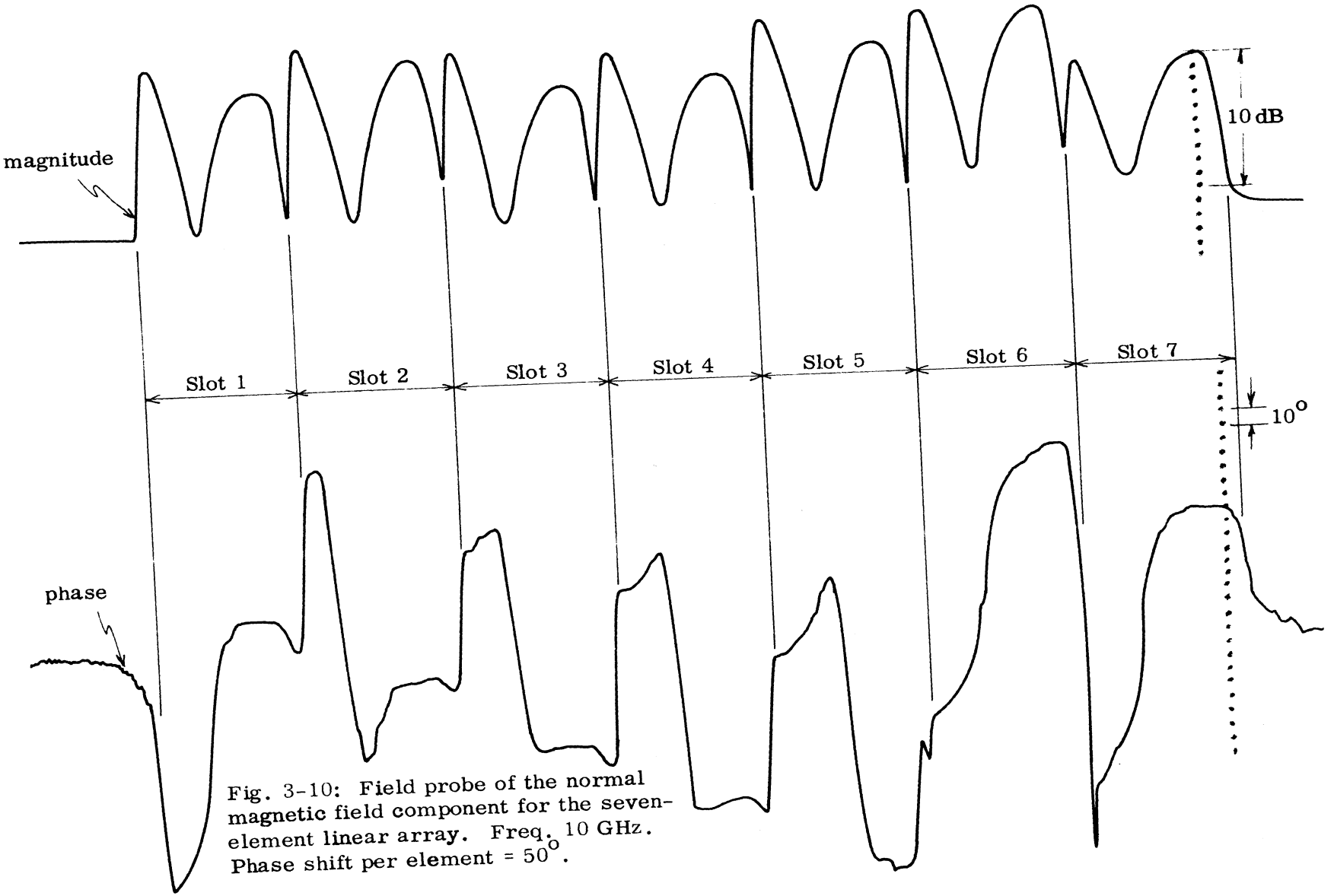

Fig. 3-10: Field probe of the normal magnetic field component for the seven-element linear array. Freq. 10 GHz. Phase shift per element = 50°.

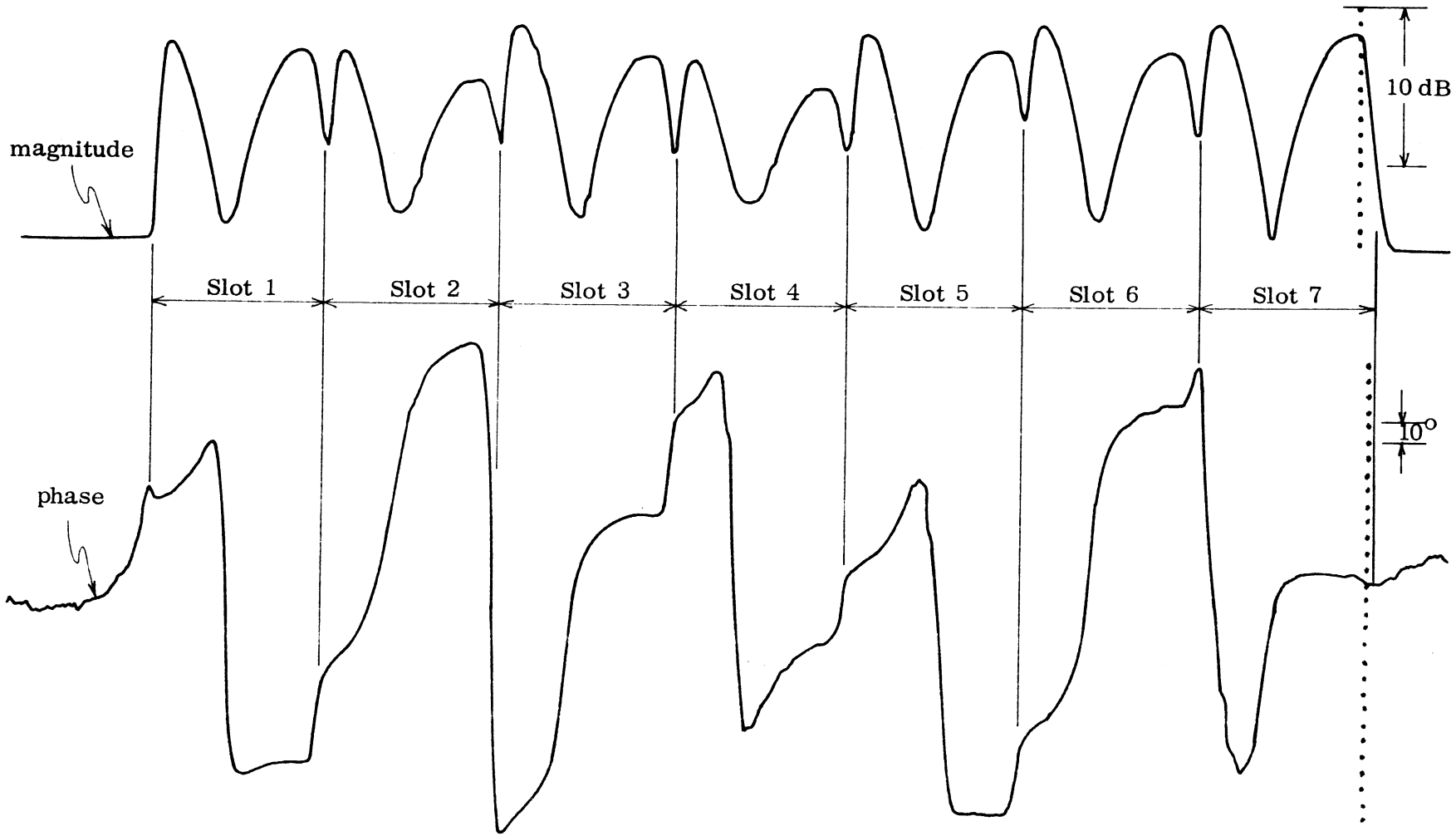

Fig. 3-11: Field probe of the normal magnetic field component for the seven-element linear array. Frequency 10 GHz. Phase shift per element = 100°.

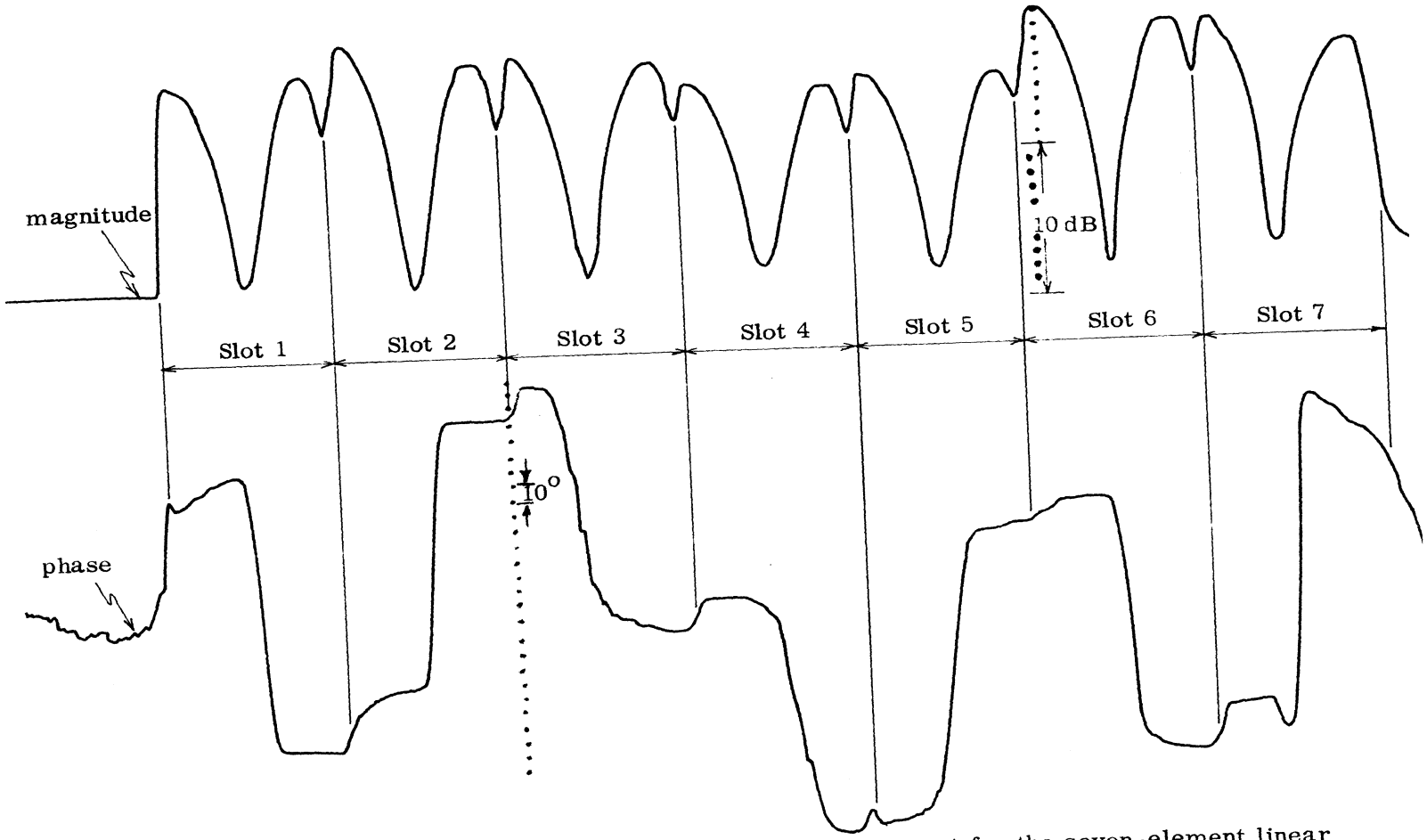

Fig. 3-12: Field probe of the normal magnetic field component for the seven-element linear array. Frequency 10 GHz. Phase shift per element = 150°.

in going from one figure to another since each scan position requires a different amount of stepping of the phase between slots. (Notice that the limits of the phase measuring device are $+180^{o}$ and -180^{o}.)

Table 3-1 shows the experimental results for the amplitudes of the

Table 3-1 Comparison between theory and experiment for the reflection coefficient of the center slot of the seven-element linear array. Frequency = 10 GHz.

Phase Shift Between Elements	Experimental Reflection Coeff. Mag.		Finite Array Calculation	
	dB	ratio	Magnitude	Phase
0^{o} (broadside)	-15.4	0.1698	0.1563	-61.7
50^{o} (7.9^{o} scan)	-14.2	0.1950	0.1910	-61.6
100^{o} (16^{o} scan)	-12.5	0.2371	0.2504	-67.23
150^{o} (24.4^{o} scan)	-11.5	0.2661	0.2820	-76.5

reflection coefficients for the various scan angles used and also the calculated amplitude and phase for the center slot of the seven slot linear array. Fig. 3-13 contains data showing the reflection coefficient versus scan angle as well as the relative power transmitted versus scan angle as predicted by the finite array analysis for this seven-element linear array.

3.2.2 49-Element Triangular Grid Planar Array

Isosceles triangular grid planar arrays are characterized by having the minimum element density for a given scan range before the grating lobe appears in the visible region. Accordingly, they represent the most economical array from this viewpoint. The elements in such an array are arranged in a brick-layer fashion. The array chosen as a study case was treated previously in the literature by Farrell and Kuhn (5) both experimentally and analytically, based on an infinite grid approximation. This array consists of seven rows of elements with seven elements per row. Alternate rows are displaced by $\frac{Dx}{2}$; here Dx is the distance between two consecutive slots in the same row. The elements are open-ended rectangular X-band

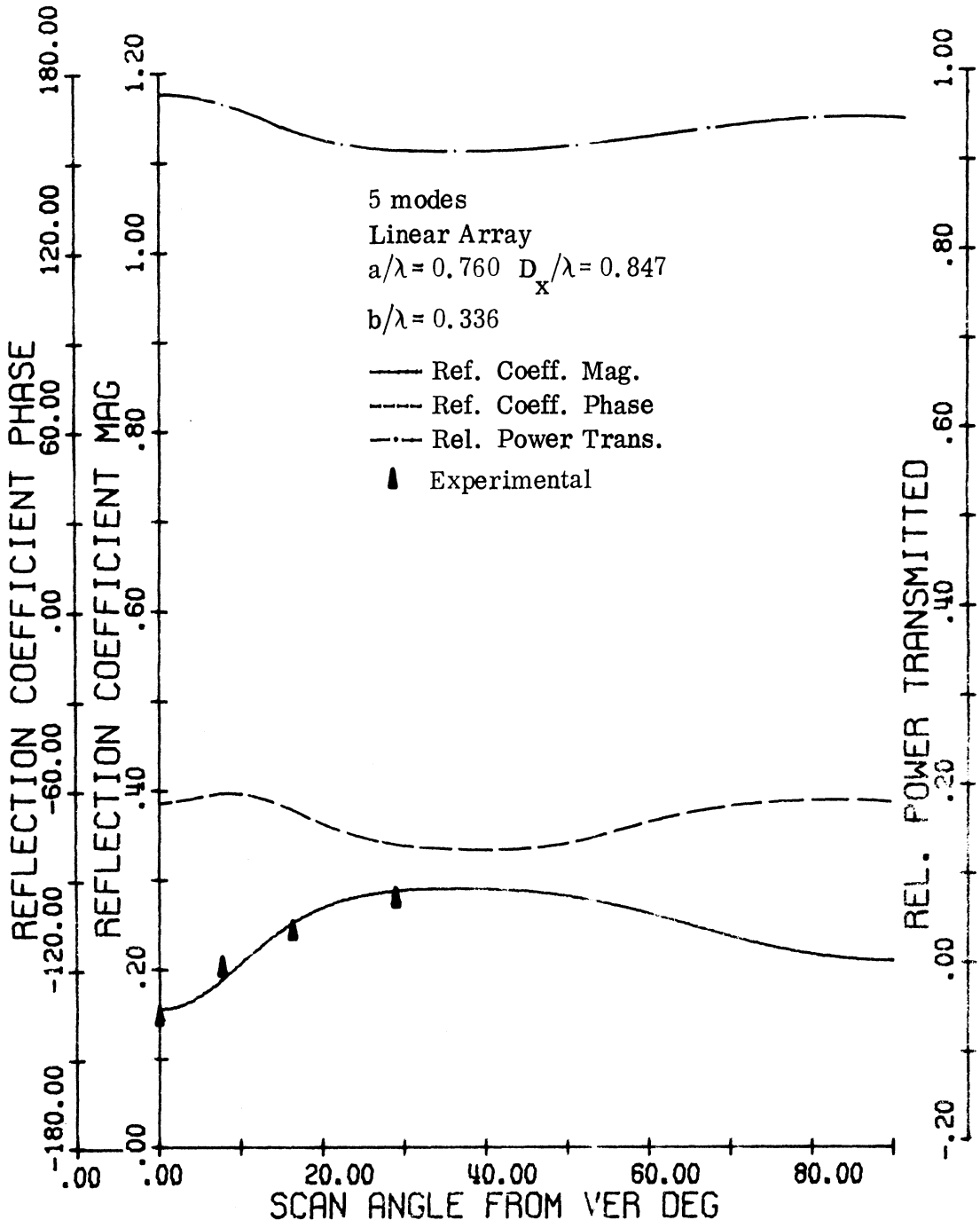

FIG. 3-13: 7-COLS. 1-ROWS ARRAY G=0.0 PHI= 0.0
F= 10000.000MHZ ELEMENT POS. (4, 1)

waveguides flush-mounted in an otherwise infinitely conducting ground plane. A schematic sketch of the physical array is shown in Fig. 3-14a.

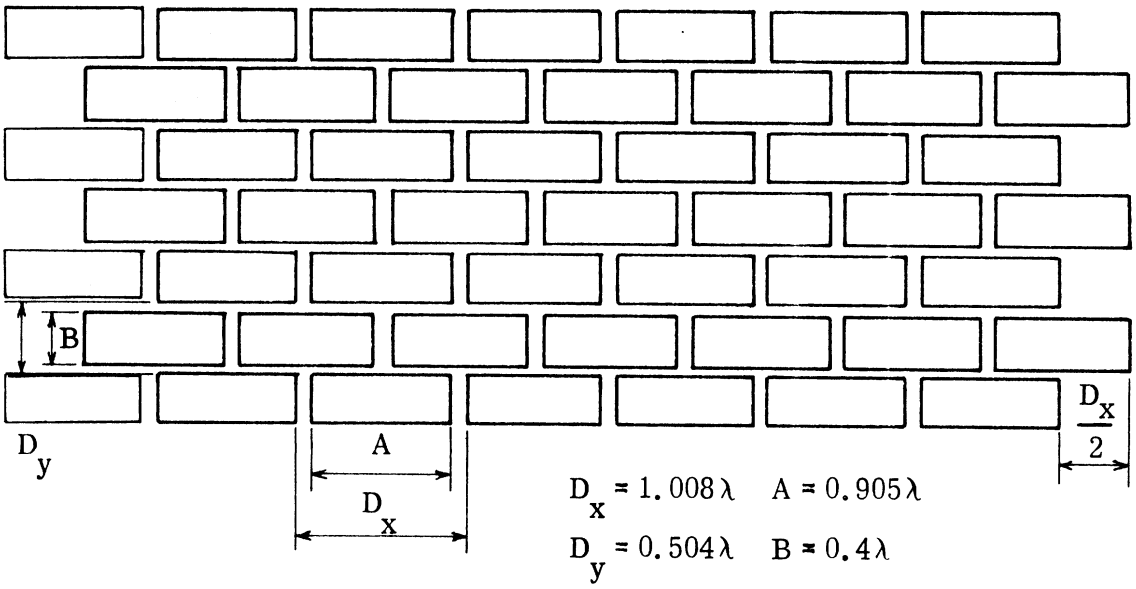

Fig. 3-14a: Schematic sketch for the aperture of the 49-element planar array with triangular grid.

Experimental results on the 49-element array were published in reference (5) and are shown in Fig. 3-14b. It is interesting to note that despite the small size of this array, the experimental pattern exhibits a null of 30 dB only 27^{o} from broadside in the H-plane scan. This null is far inside the grating lobe circle which passes through H-plane scan about 60^{o} from broadside. It is also worth mentioning that the same grid has been further considered by Diamond (6) and again by Farrell and Kuhn (7). Both analyses were again for infinite triangular grid arrangements. The results were compared to a larger array (95-element) of the same grid. The results by Diamond (Fig. 3-15) and those by Farrell and Kuhn (7) (Fig. 1-2) are similar. The infinite array approach in both cases detected a null; however, the measured null was somewhat closer to broadside than

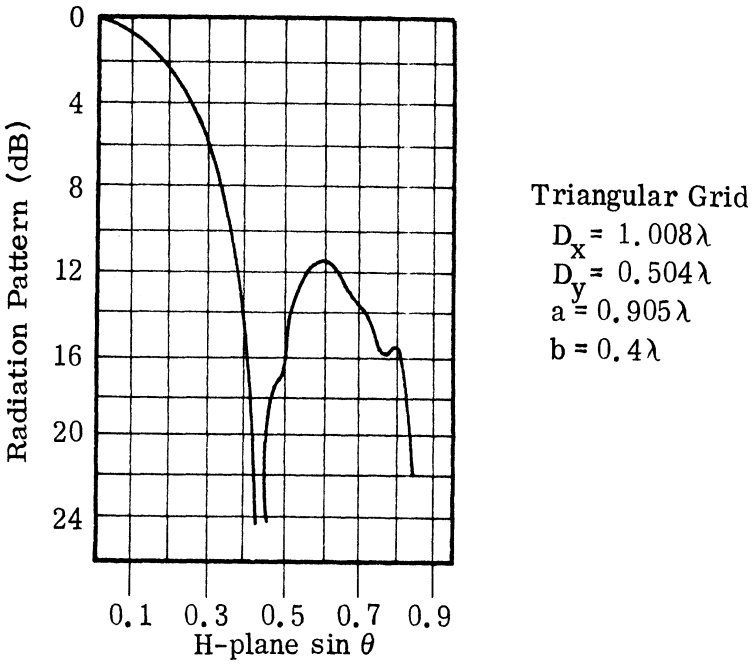

Fig. 3-14b: Experimental results for the 49-element triangular grid array. (Farrell and Kuhn)

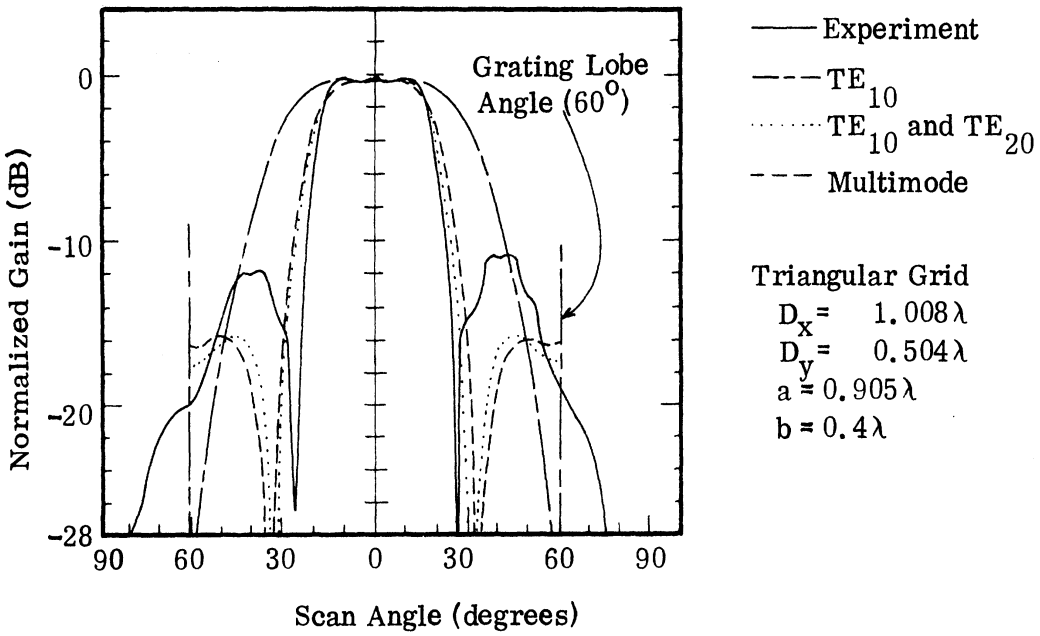

Fig. 3-15: Comparison of theoretical and experimental H-plane element patterns for 95-element triangular grid array. (Diamond)

that predicted by infinite array calculations. Farrell and Kuhn (7) also predicted a null in the E-plane pattern for the infinite triangular grid array. However, such a null was not detected experimentally on the 95-element experimental array. Departure of the theory from experiment was attributed to the limited size of the experimental array.

In comparing the computational method included in this report it is important to emphasize that the method is validated by closely predicting the position of the null. This is mainly because the finite array calculation deals exclusively with the input impedance aspect. The experimental data cited give the normalized gain or the radiation pattern (main beam) at any scan direction compared to that at broadside in decibels. These data include the effect of the input impedance variation as a function of scan angle as well as changes in the array pattern itself as a function of scan angle. This latter effect can simply be predicted from classical array theory.

In the figures showing the results of computations for the center slot of a finite 7x7 array (Figs. 3-16 through 3-24), it is to be noted that the reflection coefficient magnitude and phase are given versus the scan angle from the broadside position. Also the relative power transmitted is given versus the scan angle. Each of these curves is for a different cut. The meaning of cut corresponds to having for each selected value of ϕ a variation of the scan through the range of angle θ from 0 to 90^{o}. In this series of curves the array factor is not included. In other words, the data presented here correspond to that for the input impedance for one slot. Two sampling slots on the array are given. In these figures the location of the slot involved is given by the coordinates, row number and column number. In order to make the data obtained in this work conform to that presented in the references, it is necessary to add up the results for all the slots and include the effect of the radiation pattern change as a function of the main beam direction.

Two sets of data are provided for the center slot. One uses only two modes: TE_{10} and TE_{20}. The results are shown in Figs. 3-16 and 3-17 for

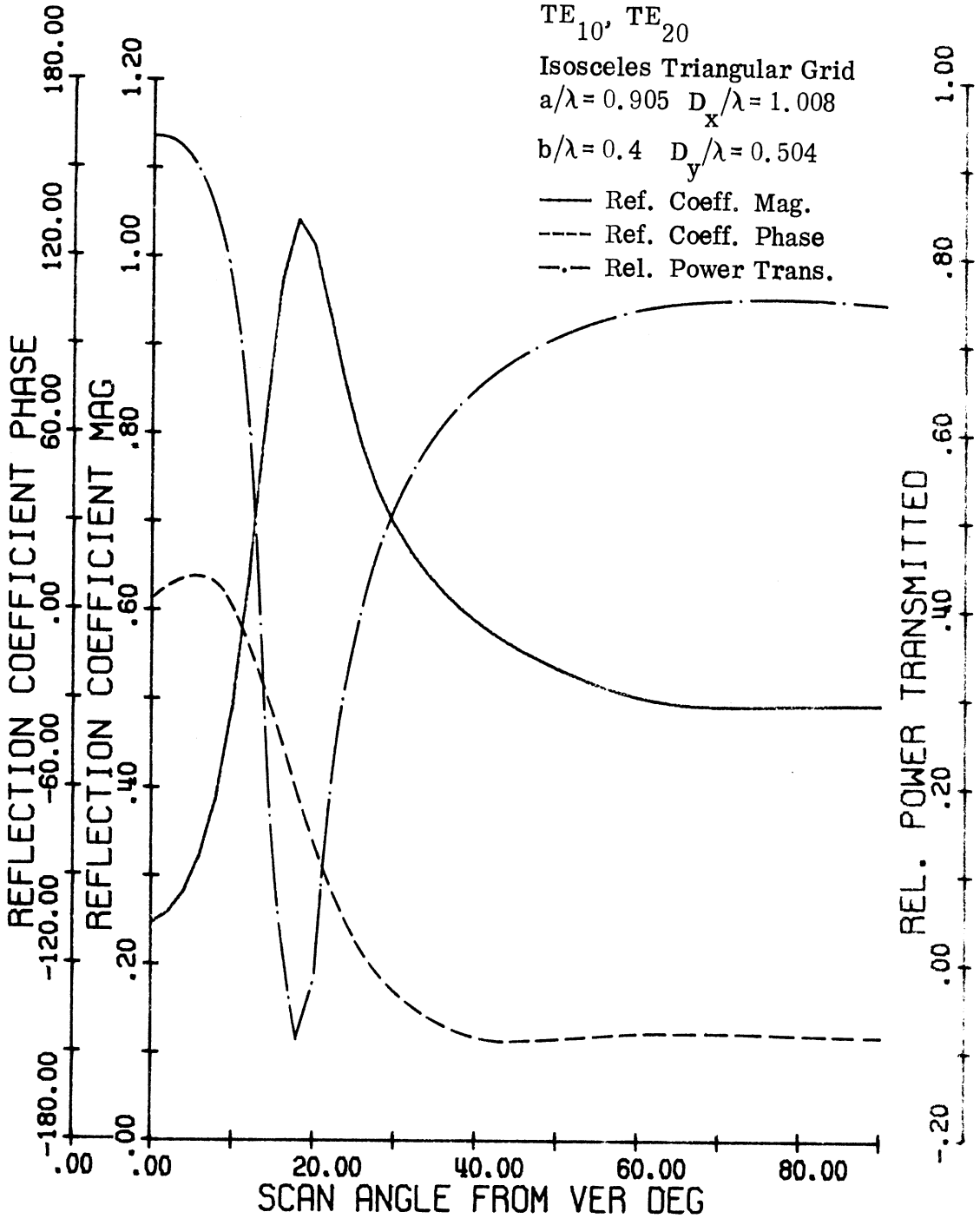

FIG. 3-16: 7COLS. 7ROWS ARRAY G=0.5 PHI= 0.0
F= 11900.000MHZ ELEMENT POS.(4, 4)

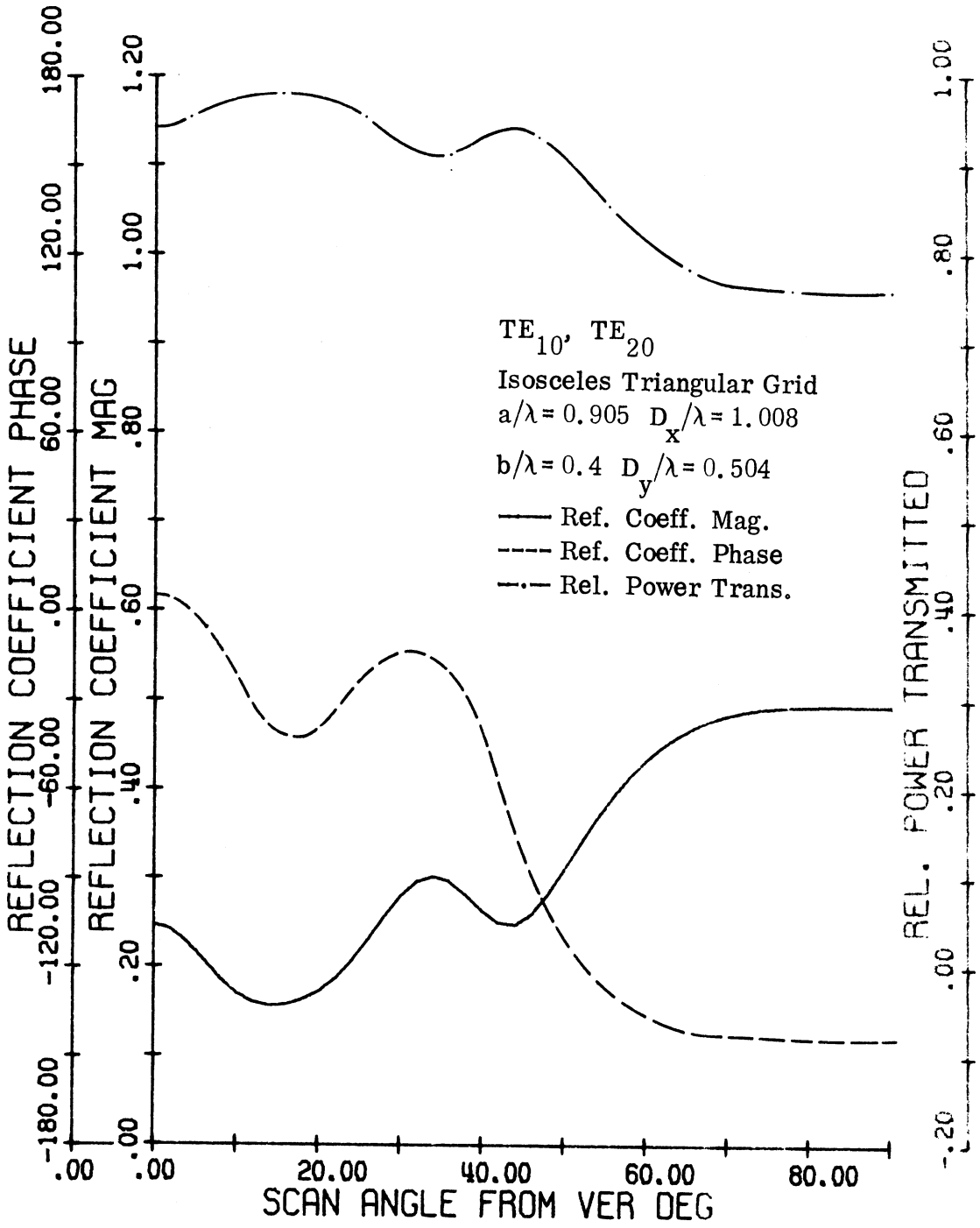

FIG. 3-17: 7COLS. 7ROWS ARRAY G=0.5 PHI= 90.00
F= 11900.000MHZ ELEMENT POS. (4, 4)

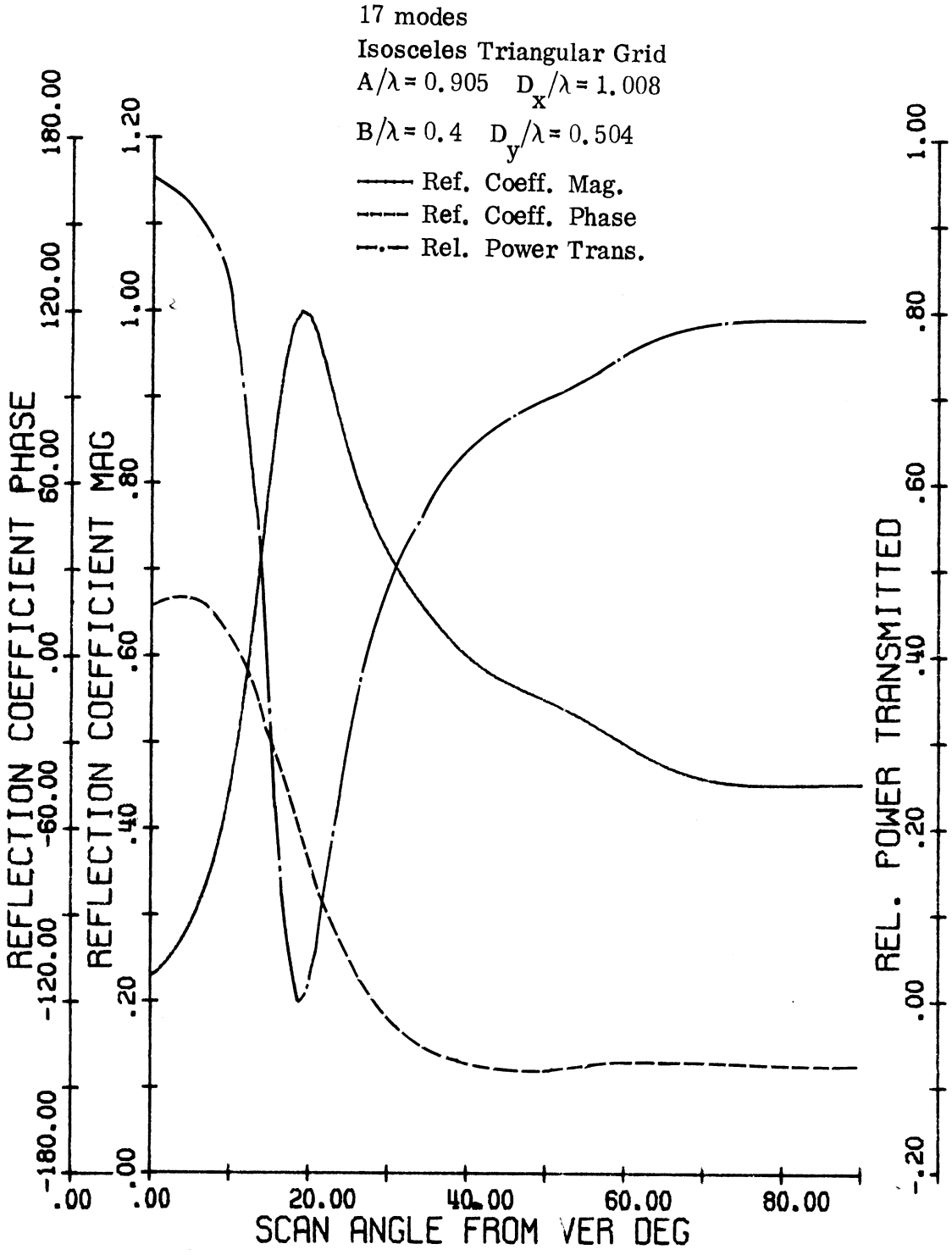

FIG. 3-18: 7COLS. 7ROWS ARRAY G=0.5 PHI= 0.0
F= 11900.000MHZ ELEMENT POS. (4, 4)

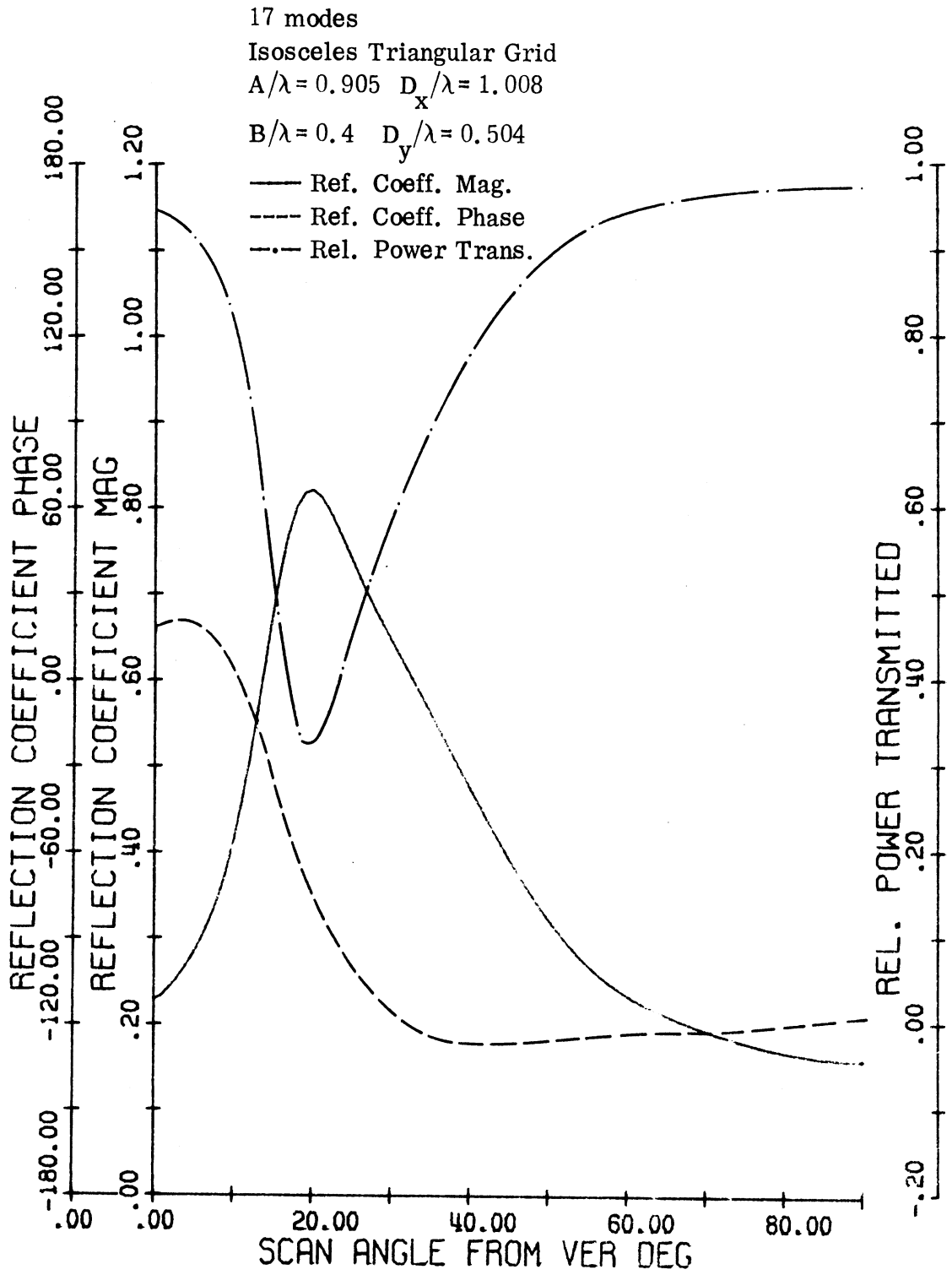

FIG. 3-19: 7COLS. 7ROWS ARRAY G=0.5 PHI= 15.00
F= 11900.000MHZ ELEMENT POS. (4, 4)

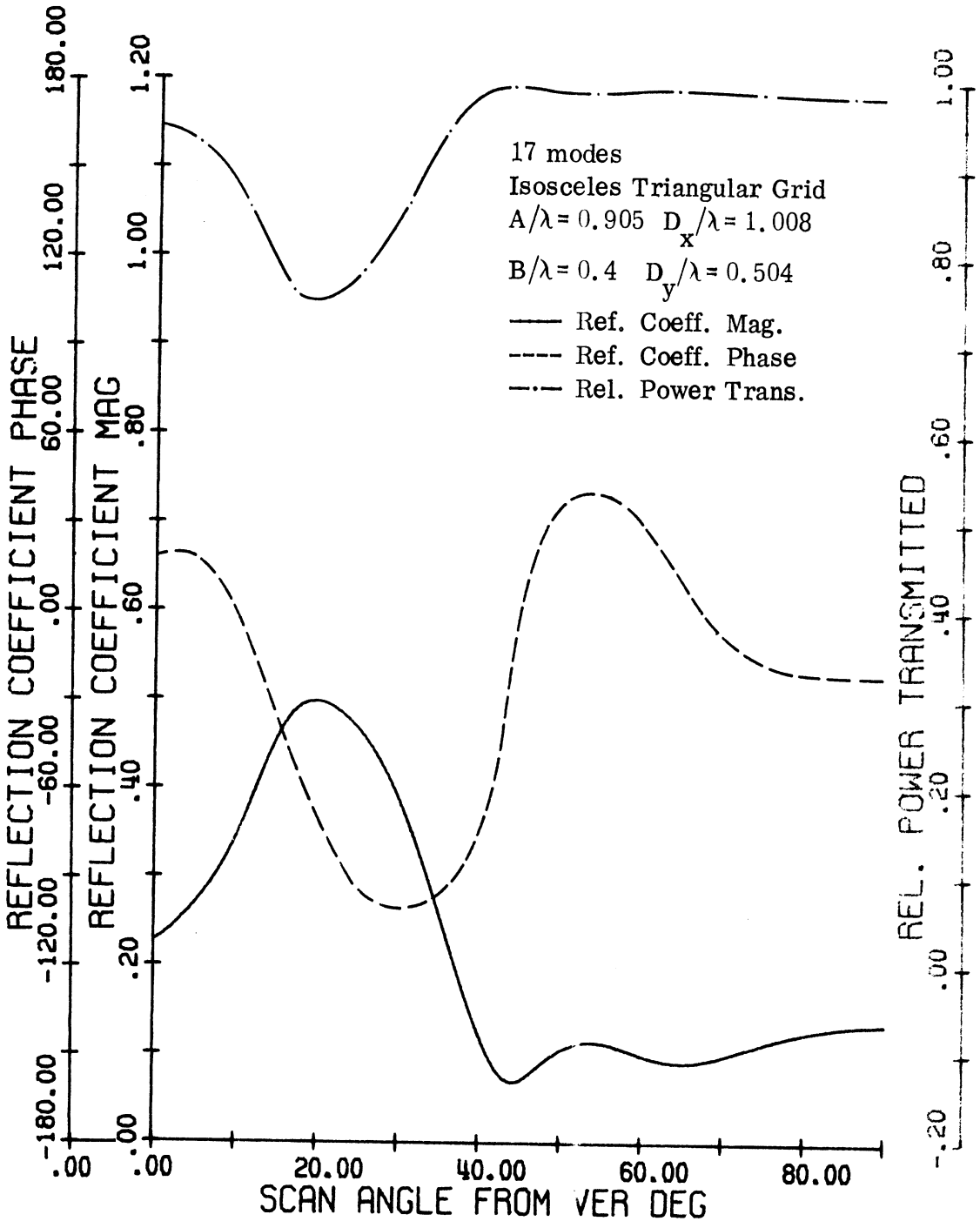

FIG. 3-20: 7COLS. 7ROWS ARRAY G=0.5 PHI= 30.00
F= 11900.000MHZ ELEMENT POS.(4, 4)

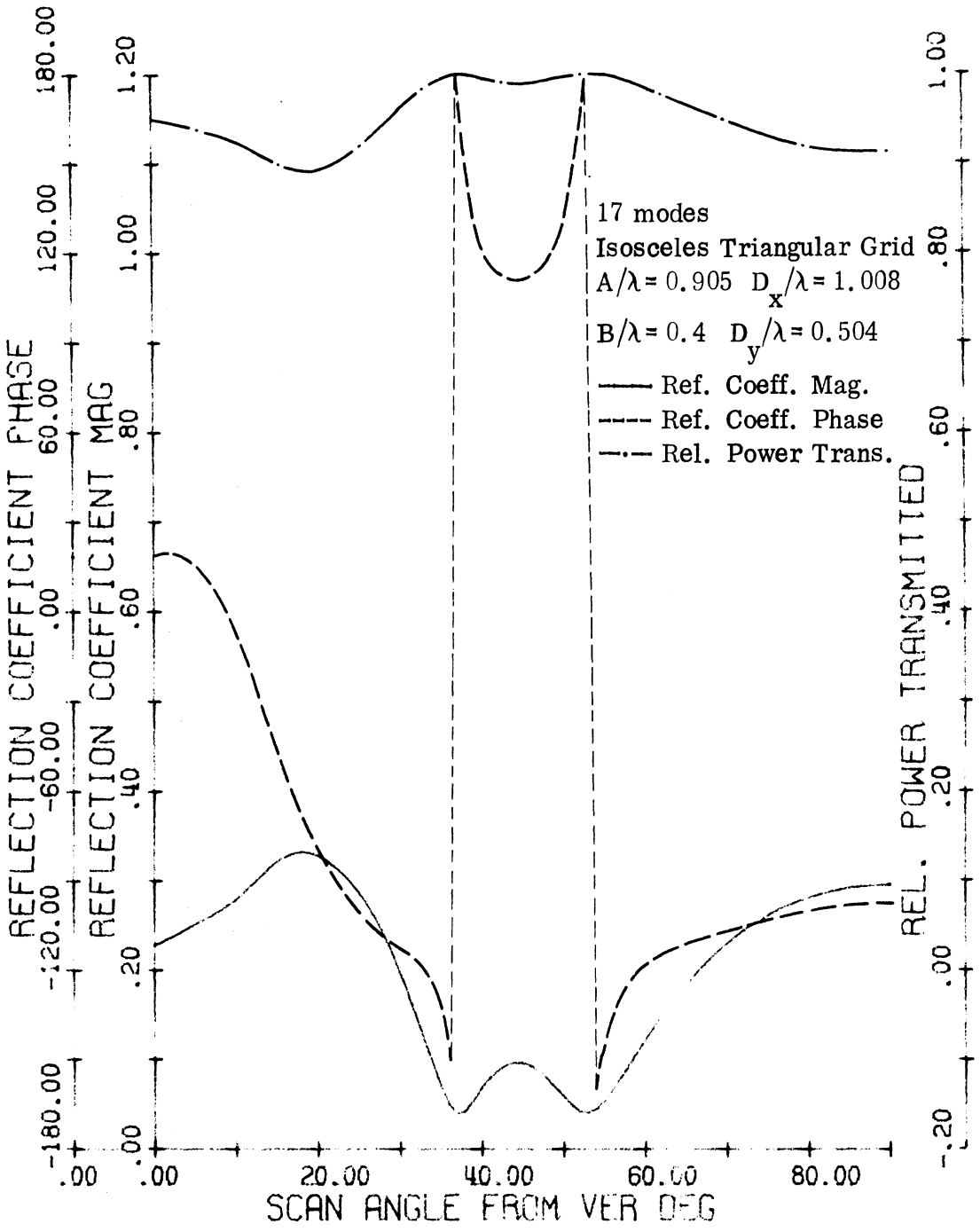

FIG. 3-21: 7COLS. 7ROWS ARRAY G=0.5 PHI= 45.00

F= 11900.000MHZ ELEMENT POS. (4, 4)

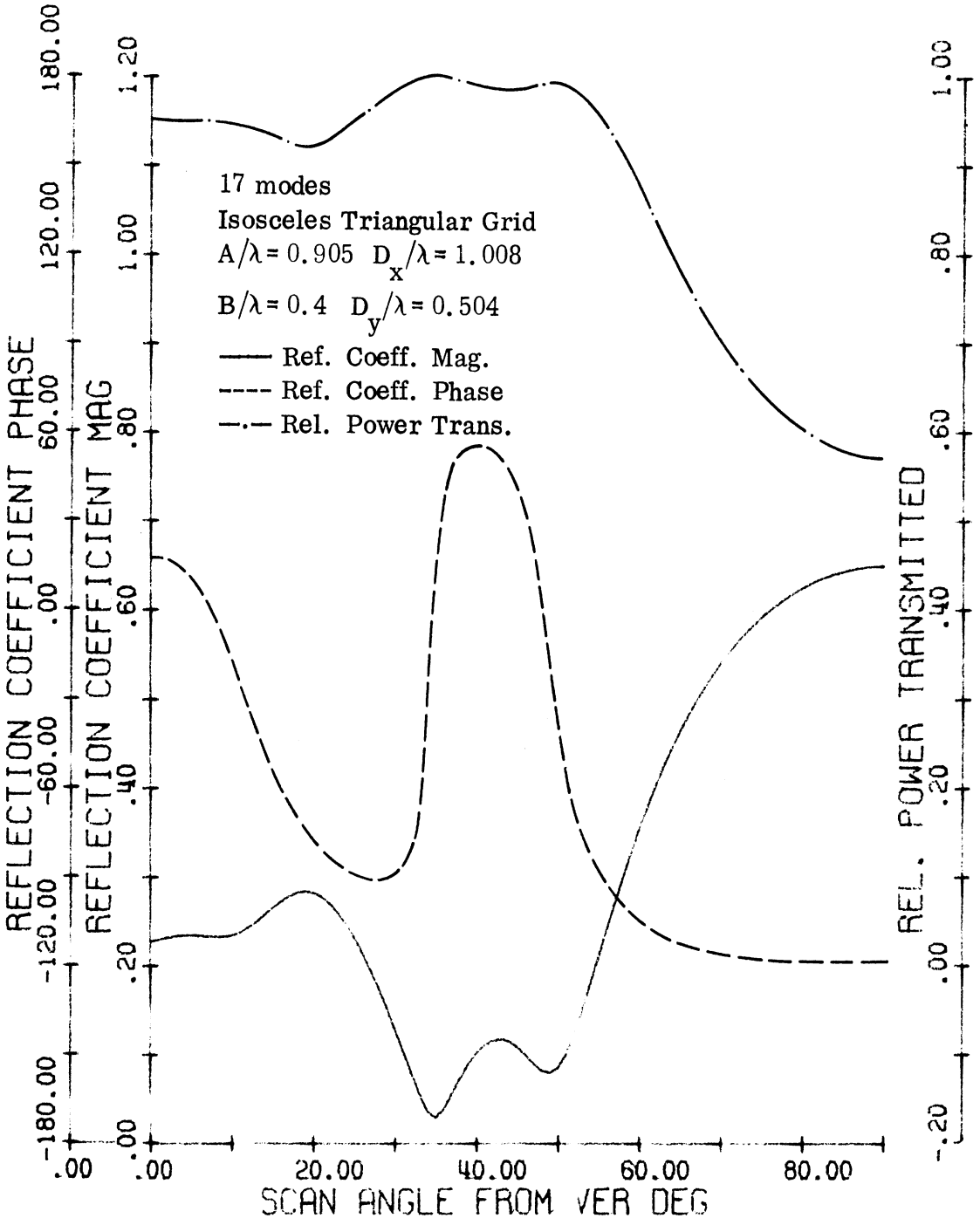

FIG. 3-22: 7COLS. 7ROWS ARRAY G=0.5 PHI= 60.00
F= 11900.000MHZ ELEMENT POS. (4, 4)

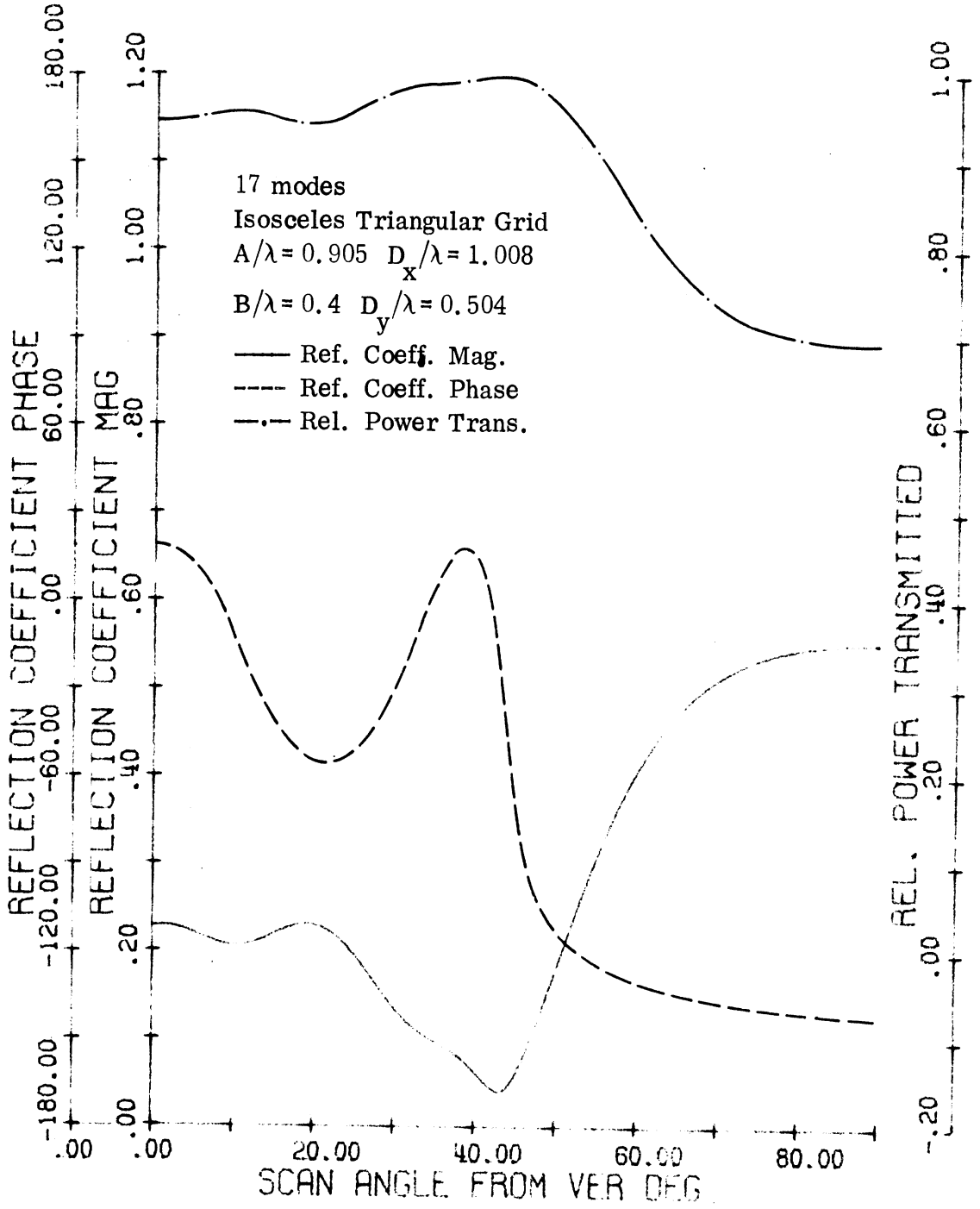

FIG. 3-23: 7COLS. 7ROWS ARRAY G=0.5 PHI= 75.00
F= 11900.000MHZ ELEMENT POS. (4, 4)

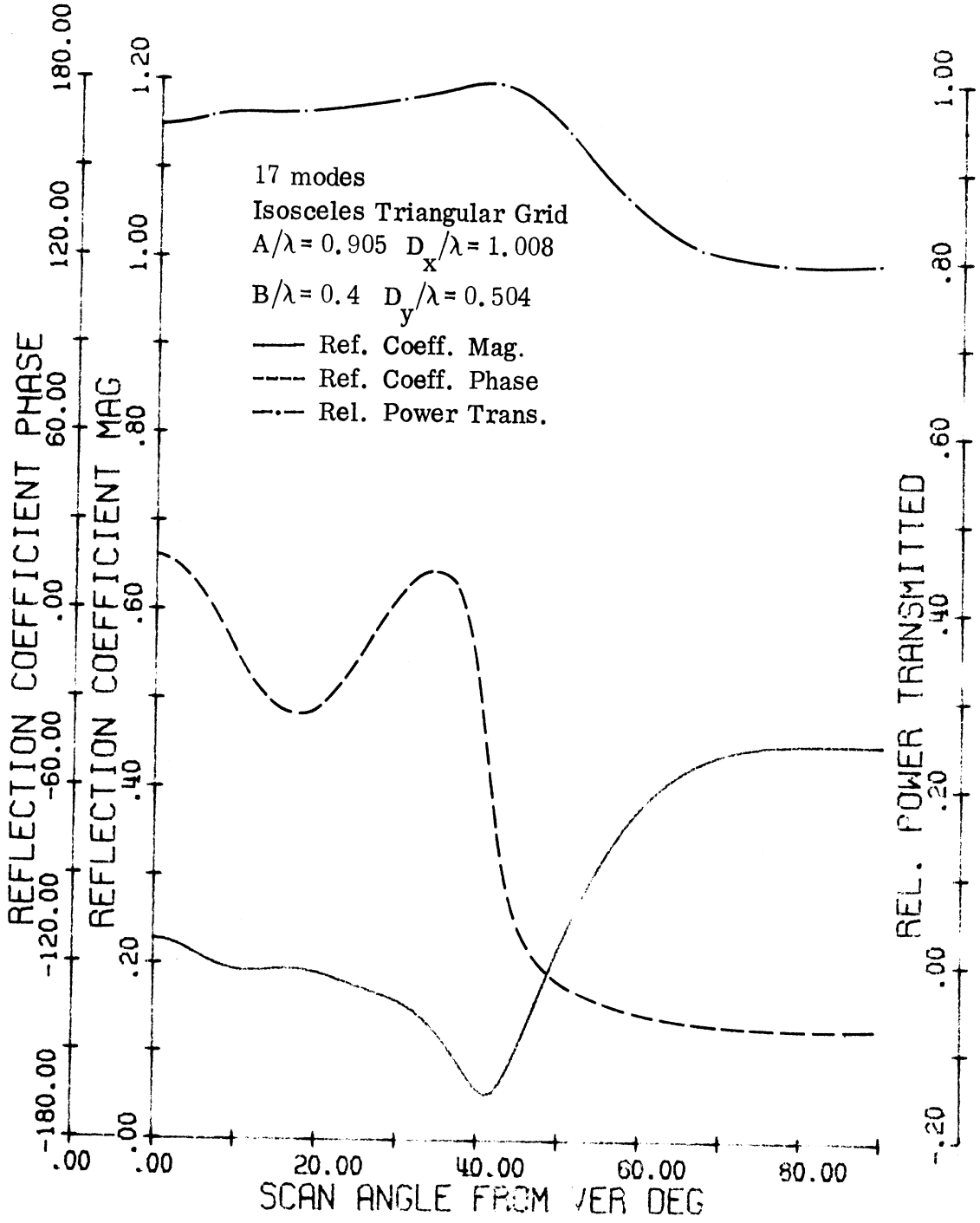

FIG. 3-24: 7COLS. 7ROWS ARRAY G=0.5 PHI= 90.00
F= 11900.000MHZ ELEMENT POS. (4, 4)

the H-plane and the E-plane, respectively. In the second set (Figs. 3-18 to 3-24) 17 modes were actually used in the analysis. These 17 modes included all the TE_{MN} and TM_{MN} modes which had an index value of M as high as 3 and N as high as 2. Curves based upon TE_{10} and TE_{20} alone show a null (a maximum for reflection coefficient) at about the same position in the H-plane scan ($\phi = 0^{o}$) as the 17-mode solution. This leads one to believe that the TE_{20} mode plays an important role in causing a "blind spot" in the H-plane scan for this array. The fact that the analysis using TE_{10} and TE_{20} can predict a null was also evident in the infinite array analysis (5-7) (see Figs. 1-2, 3-14b and 3-15).

It was observed in the curves for relative power transmitted that the null for the center slot (4, 4) is sharper and the angular position measured from broadside is smaller than what was indicated in the experimental data of the references. On the other hand, a corner slot such as (1, 1) (Figs. 3-25 through 3-31) has a shallower null for the relative power transmitted and this null occurs slightly farther out from the broadside position. The position of the null from the experimental data is between its counterparts for the center slot and the corner slot, but is closer to that of the corner slot. This seems satisfactory since for such a small array, elements close to the array periphery outnumber those that can be considered in the middle of this array. If all slots were considered then the reflection factor applying to the overall feed to all slots would have an angular position somewhere between these two nulls, which correspond to the two slots selected. In other words, it would be anticipated that a much better check on the experimental location of the null could be had through the use of all slots of the array. Obviously a reason for not pursuing this is the great increase in cost for making the computations for all slots. The scan for just one slot costs about $30.00. This cost factor has utilized many of the economies described earlier. Nevertheless, at $30 per slot the cost of taking into consideration the entire 49 slots of the antenna array approximates $1,500, which was not available for additional computation at the time of this research.

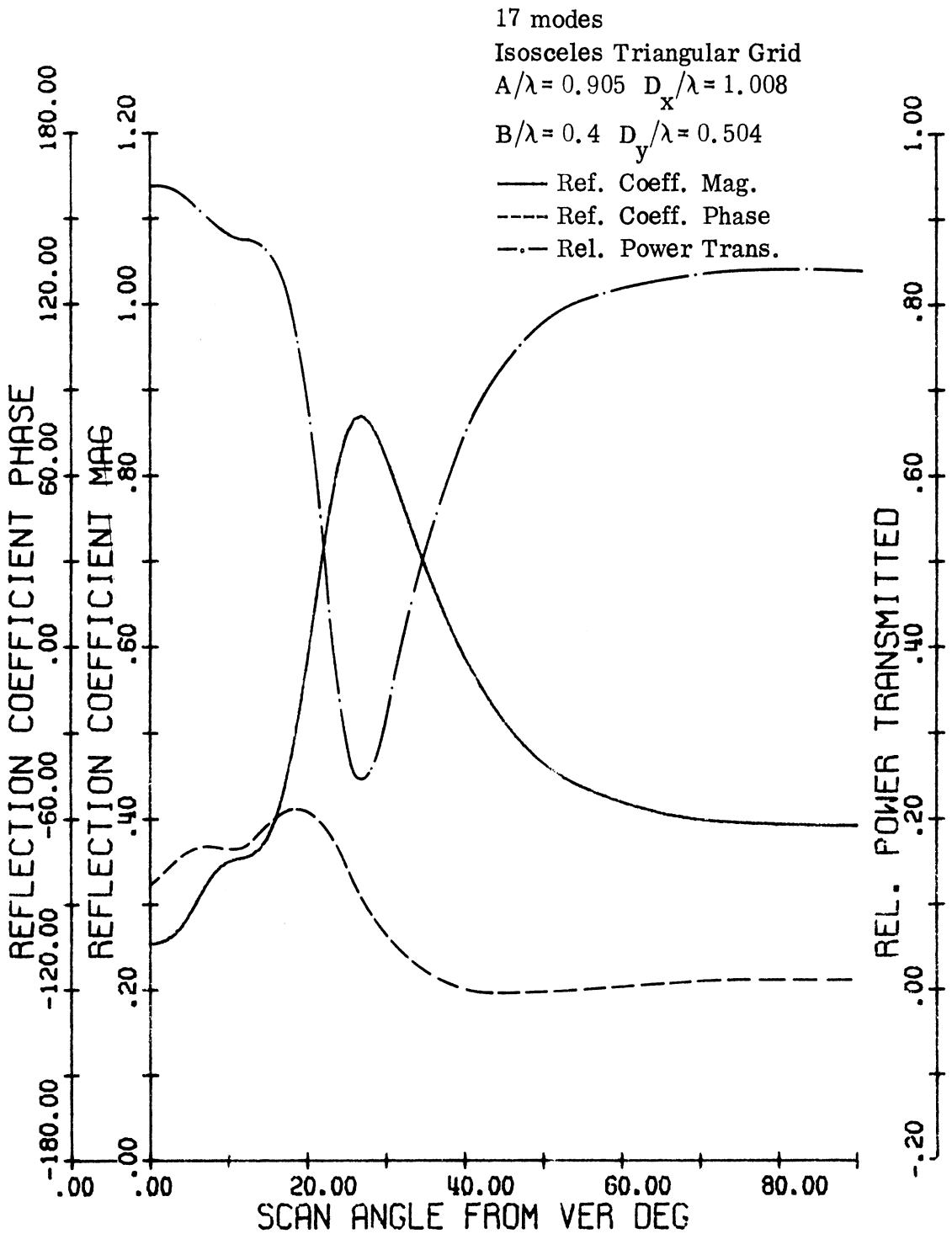

FIG. 3-25: 7-COLS. 7-ROWS ARRAY G=0.5 PHI= 0.0
F= 11900.000MHZ ELEMENT POS.(1, 1)

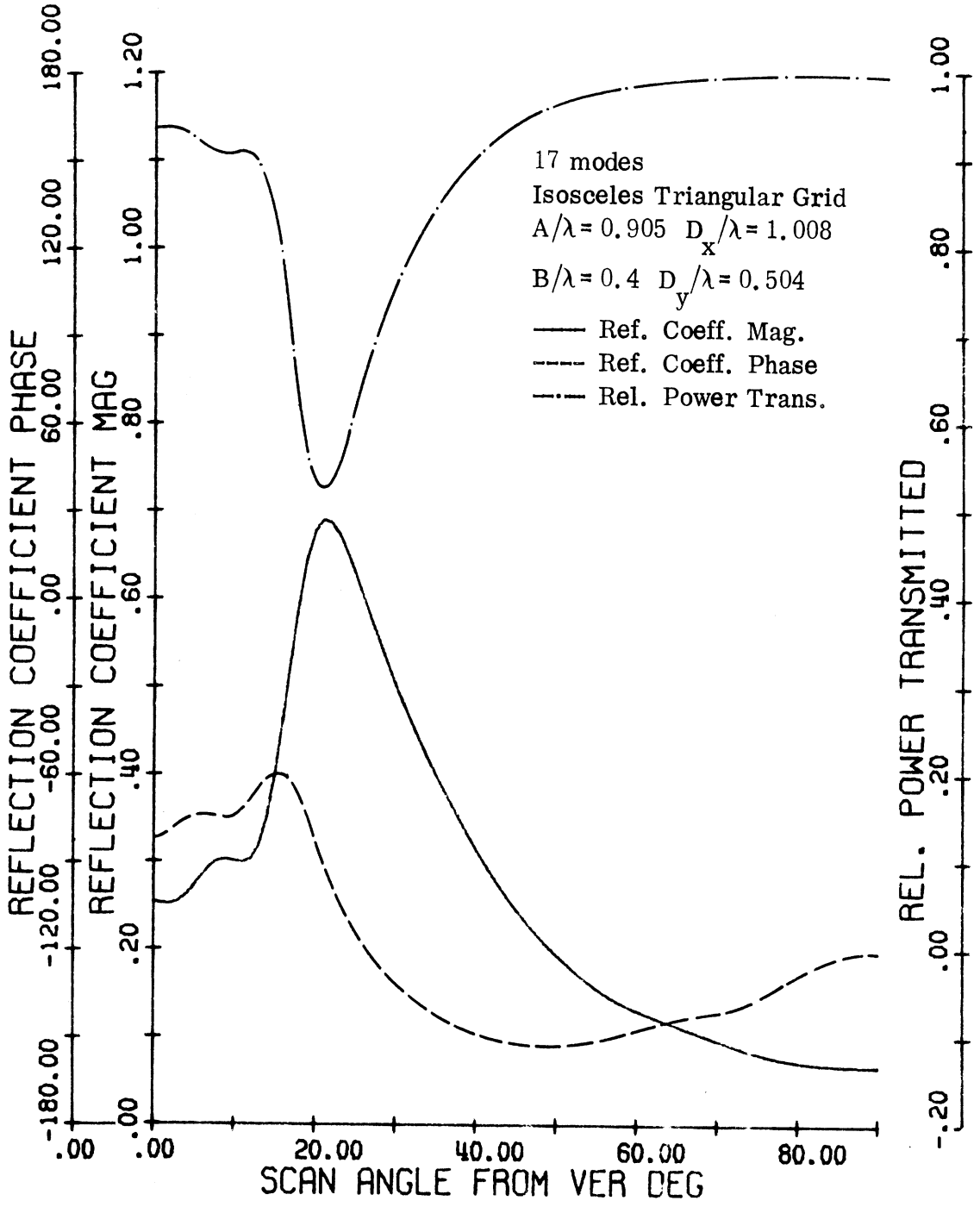

FIG. 3-26: 7-COLS. 7-ROWS ARRAY G=0.5 PHI= 15.00
F= 11900.000MHZ ELEMENT POS.(1, 1)

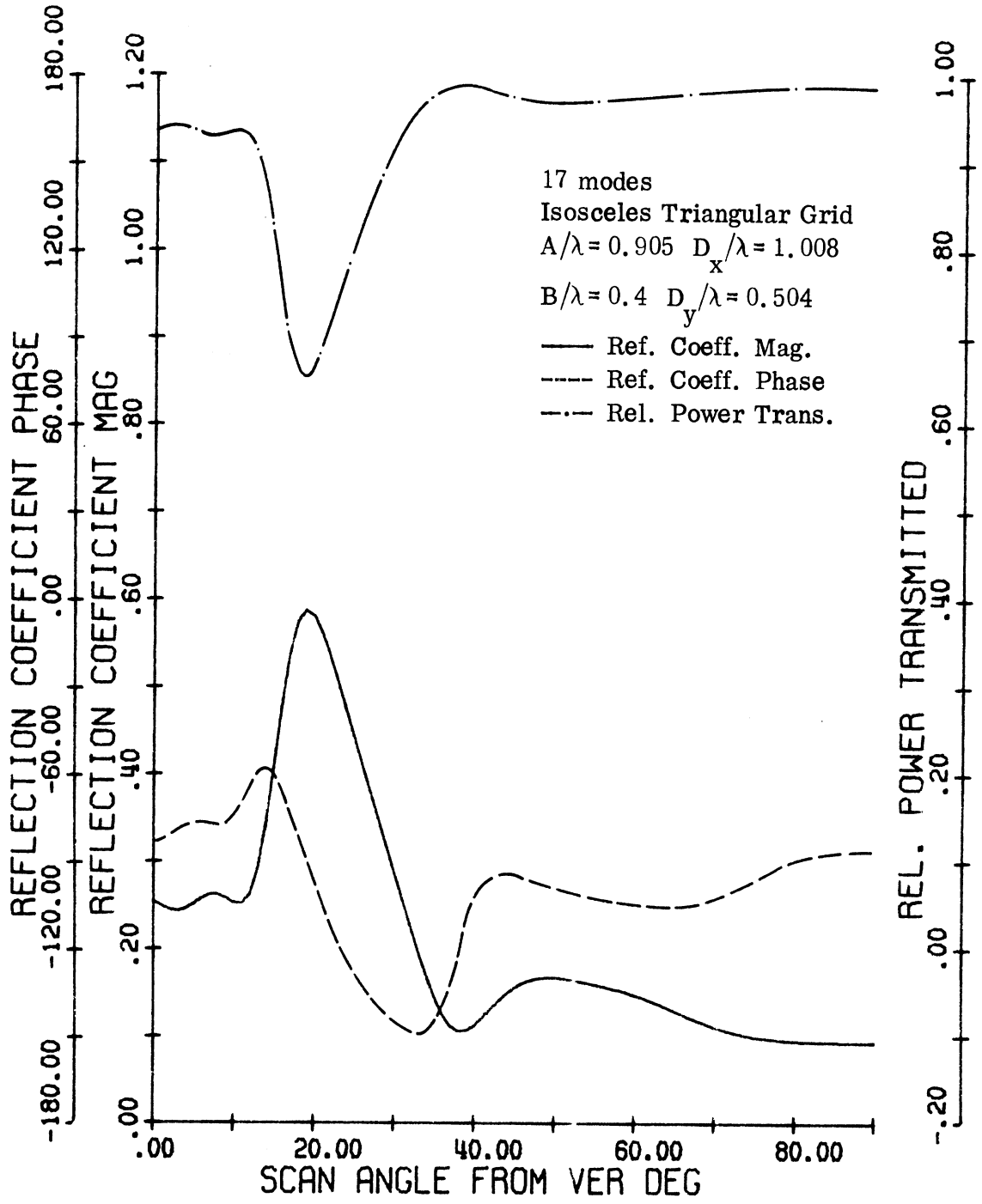

FIG. 3-27: 7-COLS. 7-ROWS ARRAY G=0.5 PHI= 30.00
F= 11900.000MHZ ELEMENT POS.(1, 1)

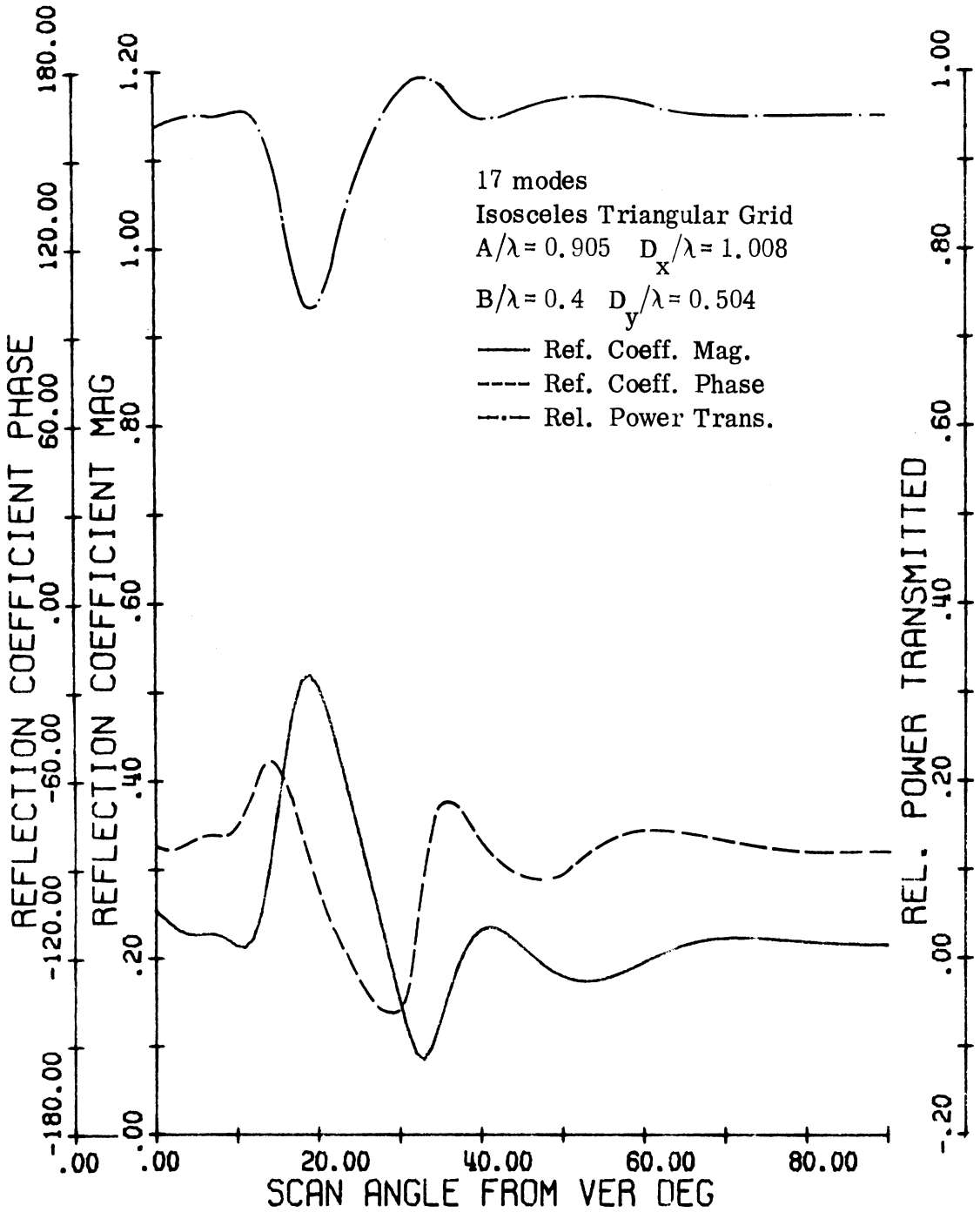

FIG. 3-28: 7-COLS. 7-ROWS ARRAY G=0.5 PHI= 45.00
F= 11900.000MHZ ELEMENT POS. (1, 1)

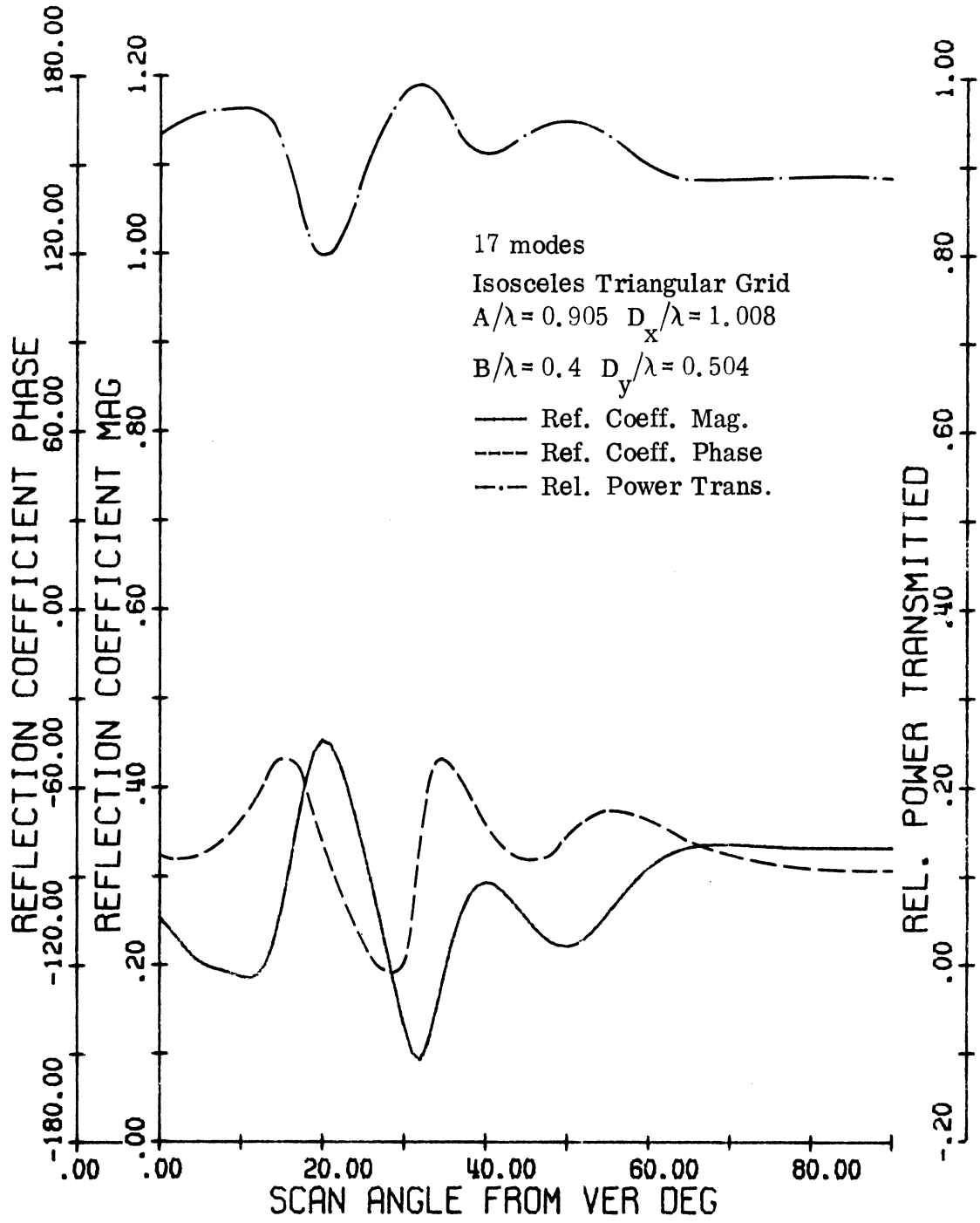

FIG. 3-29: 7-COLS. 7-ROWS ARRAY G=0.5 PHI= 60.00
F= 11900.000MHZ ELEMENT POS. (1, 1)

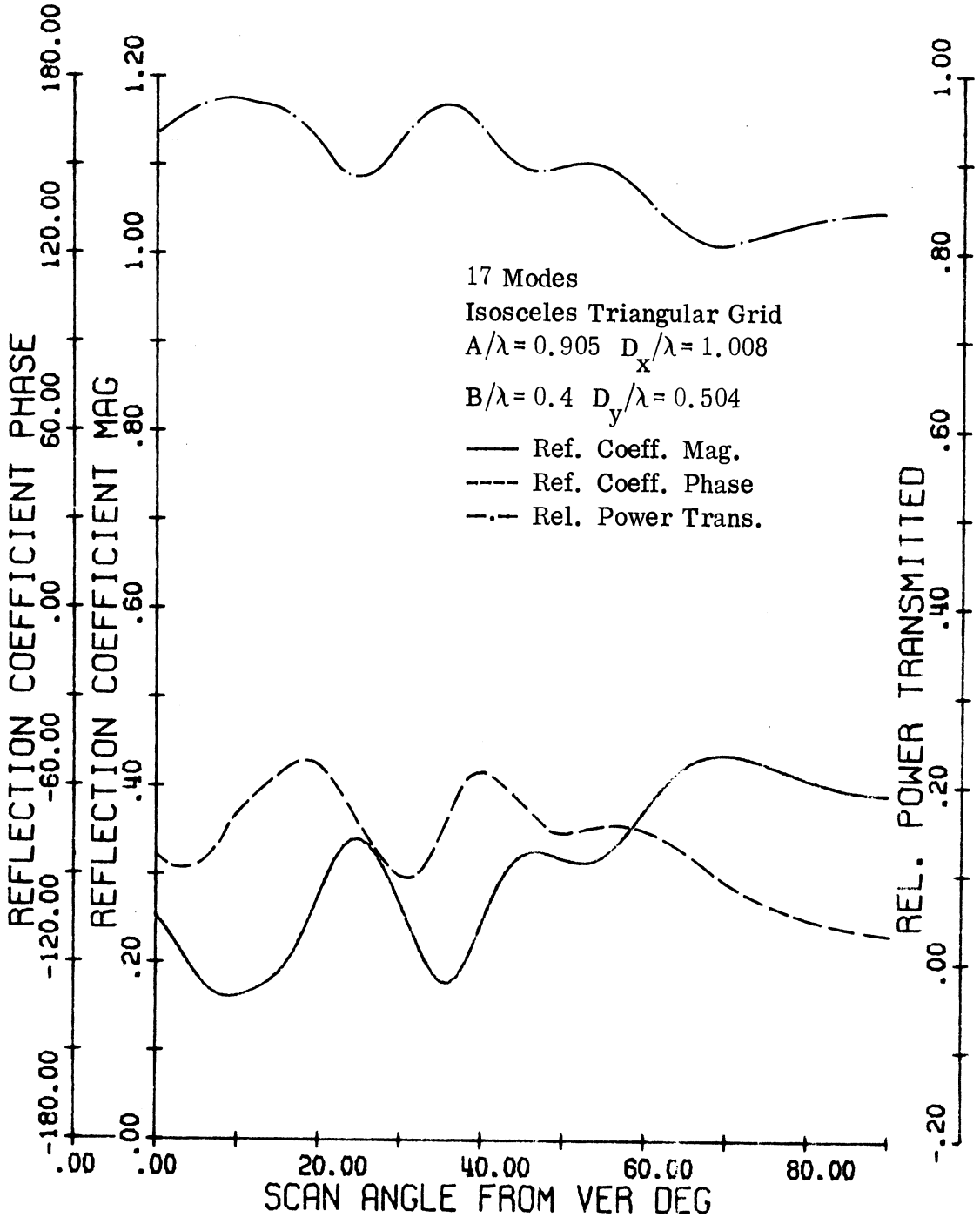

FIG. 3-30: 7-COLS. 7-ROWS ARRAY G=0.5 PHI= 75.00
F= 11900.000MHZ ELEMENT POS. (1, 1)

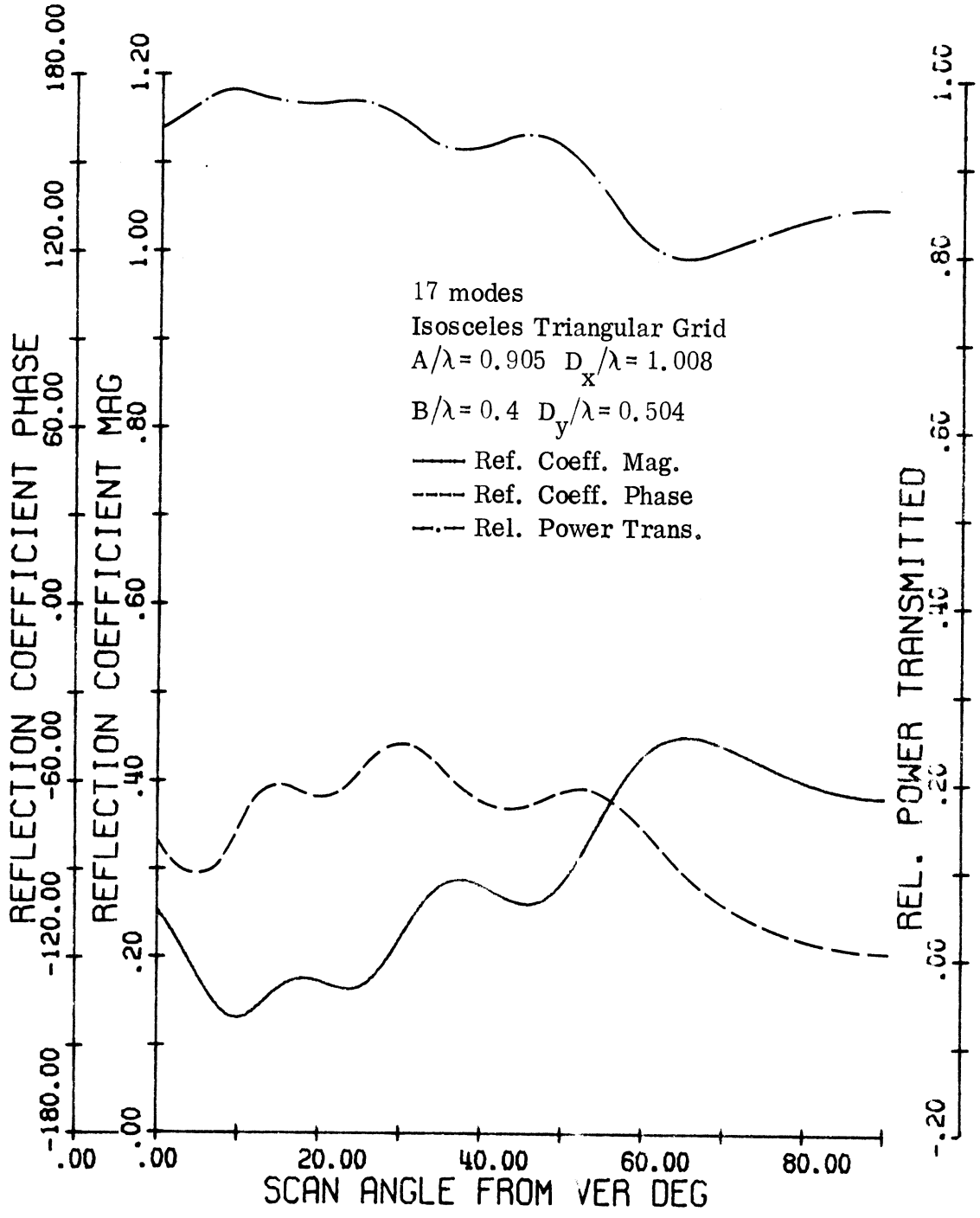

FIG. 3-31: 7-COLS. 7-ROWS ARRAY G=0.5 PHI= 90.00
F= 11900.000MHZ ELEMENT POS. (1, 1)

It is to be noted with the data obtained from the computations for the 7 x 7 slot array that the reflection factor coefficient has a negative phase corresponding to the position of the null. This corresponds to a capacitive input impedance.

Notice that no null was predicted in the E-plane scan for this array. This is in agreement with the experimental results and contrary to the infinite array analysis.

3.2.3 169-Element Rectangular Grid Array

The rectangular grid represents the simplest arrangement of elements for a planar array. The array considered here consists of 13 rows and each row has 13 slots. The elements are open-ended square waveguides as shown in the diagramatic sketch of the array in Fig. 3-32. The same array was analyzed by Farrell and Kuhn (7) using the infinite array approach. The analytical as well as the experimental results are shown in Fig. 1-2. Figures 3-33 to 3-36 show the reflection coefficient magnitude and phase and the relative power transmitted as obtained using the finite array analysis. These data were obtained using seven modes. The seven modes are all the possible TE_{MN} and TM_{MN} modes that have M as high as 1 and N as high as 2. The modes used are the most relevant for the E-plane scan (see Chapter IV). Experimentally, this array exhibited only an E-plane null (7).

Remarks similar to those mentioned for the 49-element array apply to the interpretation of the results for this array.

3.3 Discussion of the Results Obtained Using Finite Array Analysis

So far the methods used for computation provide data which indicate that a good check can be made on the input impedance behavior as a function of beam direction for finite arrays. It is to be observed that the location of the blind spot coincides with the maximum of the reflection coefficient magnitude. In the operation of an array, to have a blind spot suddenly occur as the beam is being scanned must be related to the unusual situation of no power being radiated by the antenna array as a transmitter (or correspond-

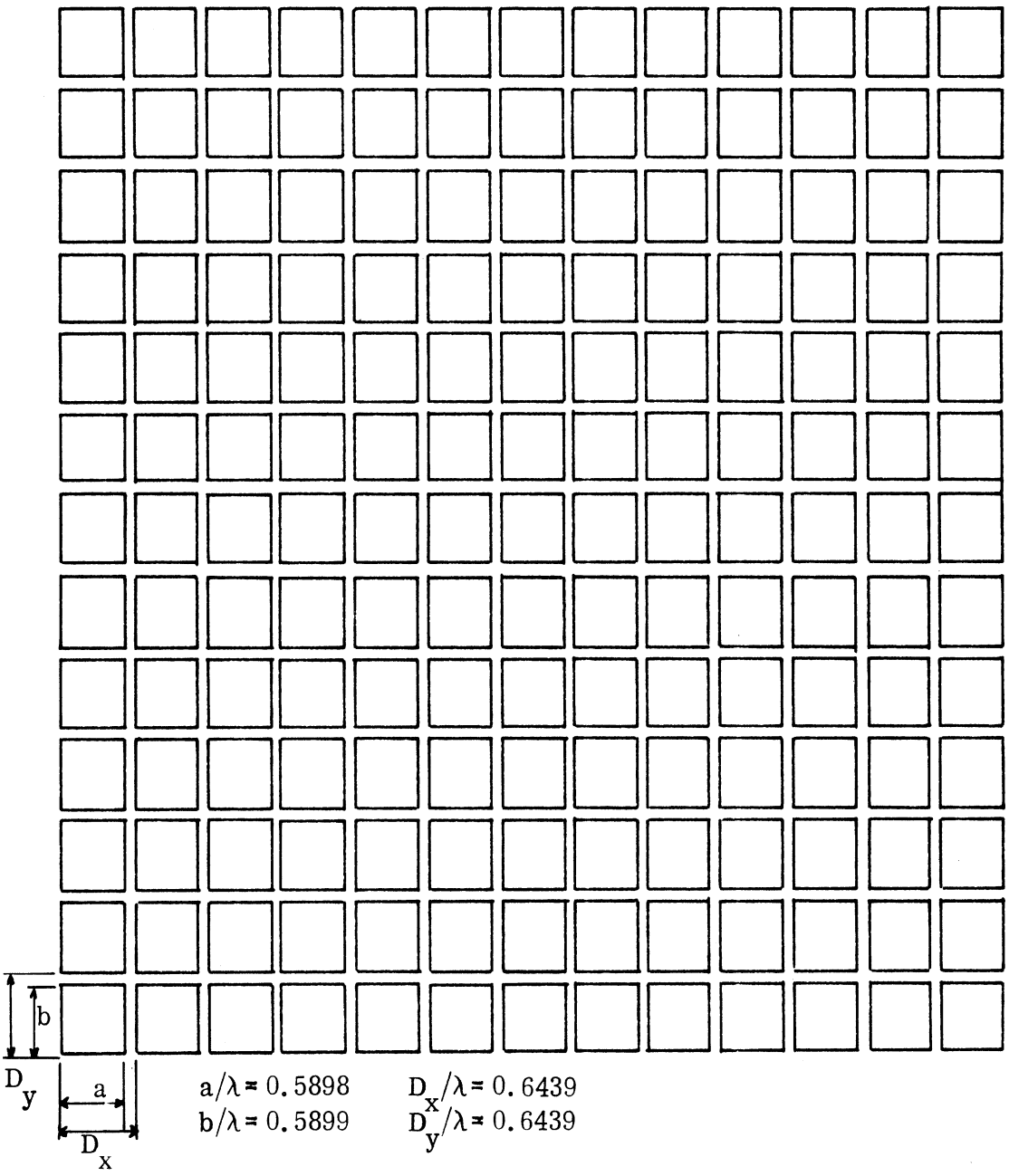

Fig. 3-32: 169-element rectangular grid array.

ingly no power being received by the array if the incident wave is from the direction of the blind spot). On the transmitting case the decrease in radiated power is due to a large mismatch in impedance where most of the power is reflected back to the generator. Evidently, this can happen if the power

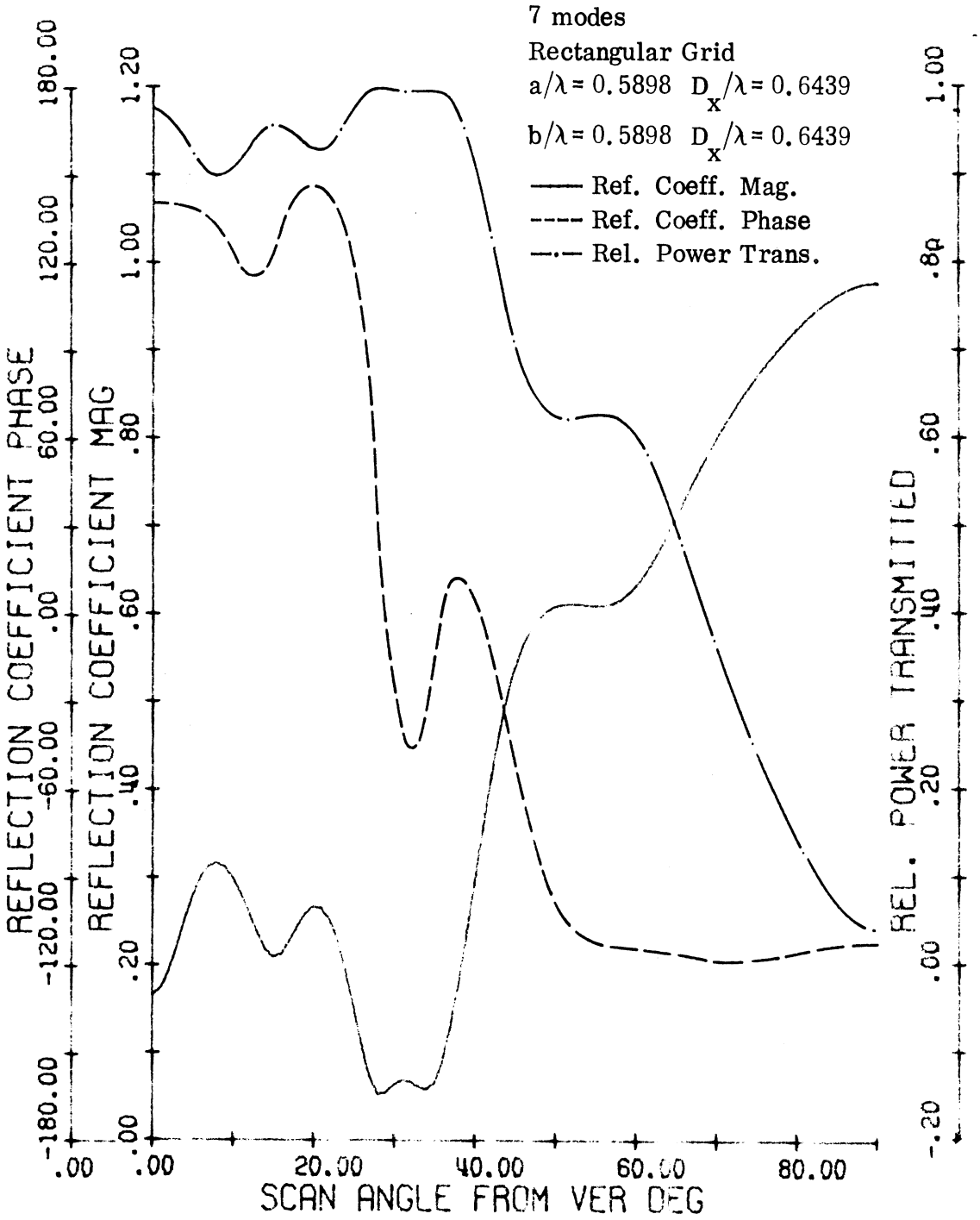

FIG. 3-33: 13-COLS. 13-ROWS ARRAY G=0.0 PHI= 45.00
F= 10000.000MHZ ELEMENT POS. (7, 7)

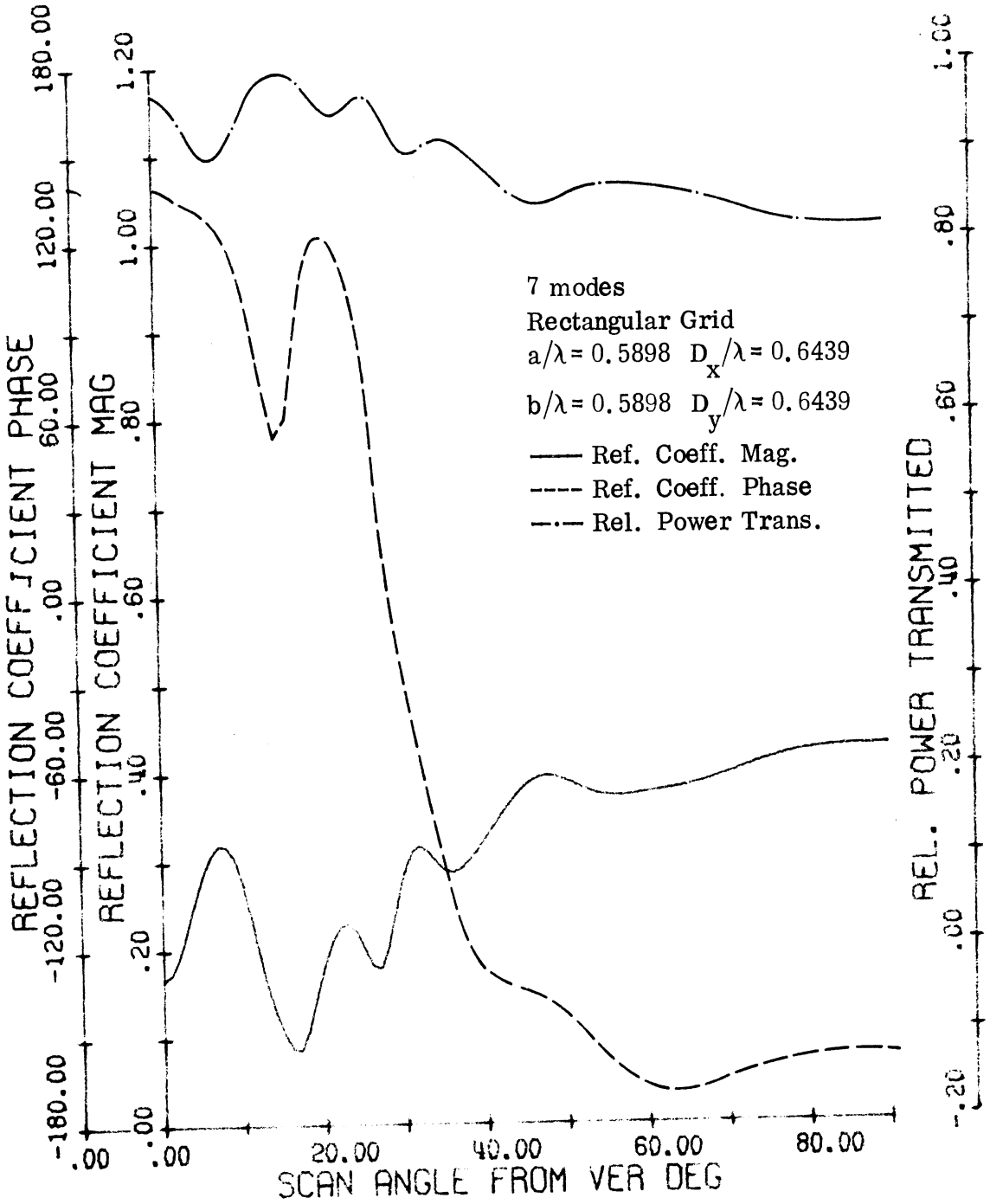

FIG. 3-34: 13-COLS. 13-ROWS ARRAY G=0.0 PHI= 60.00
F= 10000.000MHz ELEMENT POS. (7, 7)

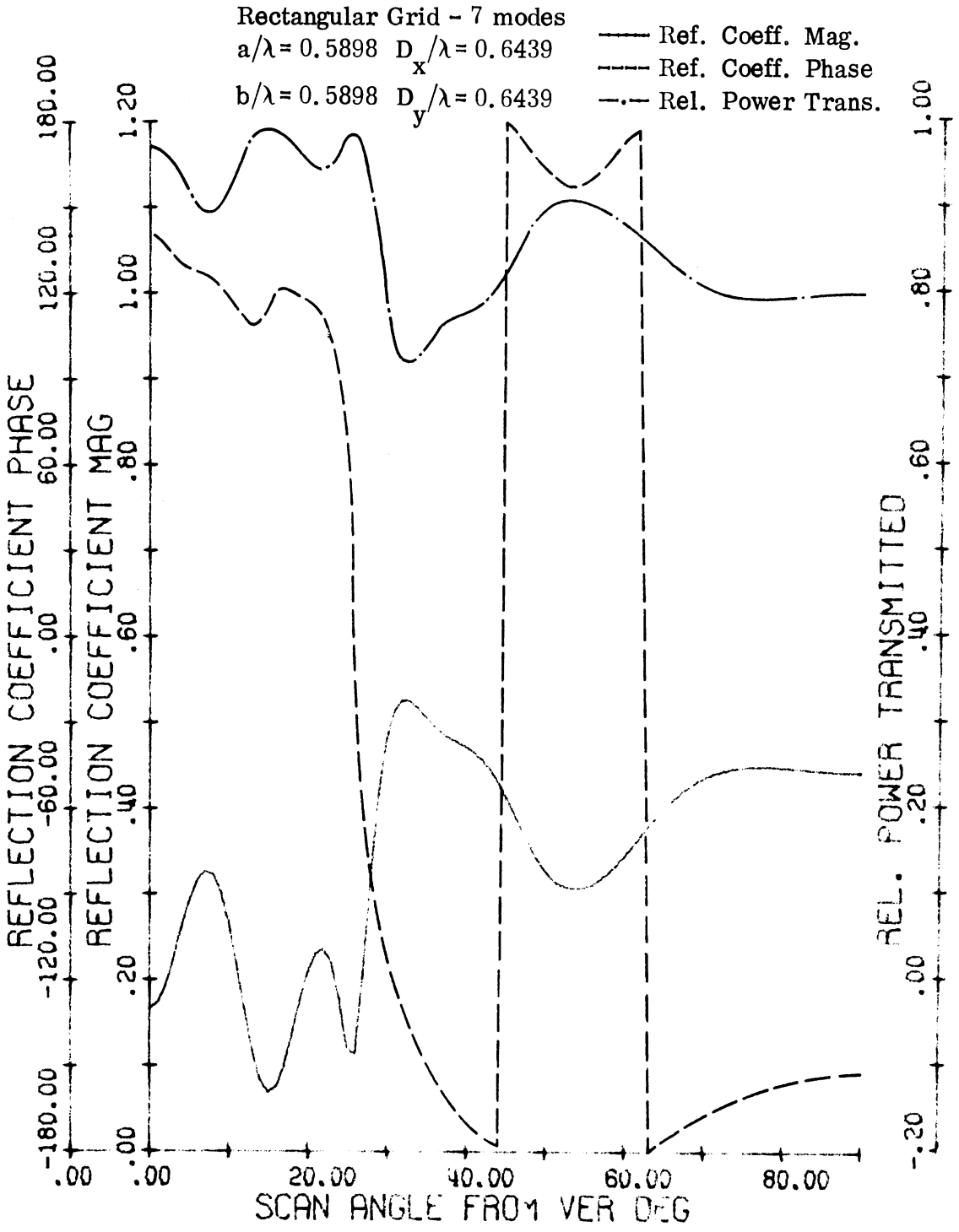

FIG. 3-35: 13-COLS. 13-ROWS ARRAY G=[illegible].0 PHI= 75.00
F= 10000.000MHZ ELEMENT POS. (7, 7)

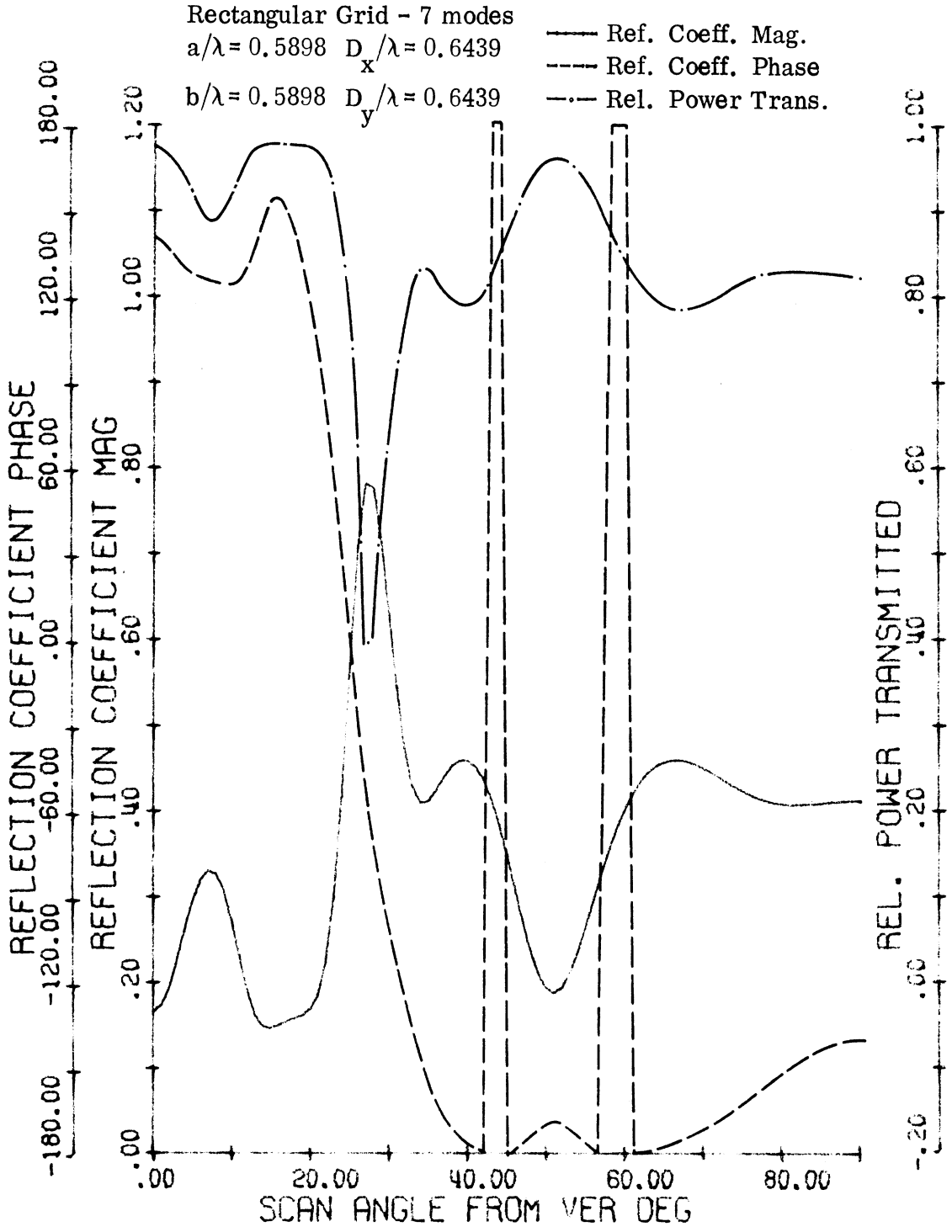

FIG. 3-36: 13-COLS. 13-ROWS ARRAY G=0.0 PHI= 90.00
F= 10000.000MHZ ELEMENT POS.: 7, 7)

coupled back into a typical element is nearly equal to the incident power to that element. This can occur if the other elements in the vicinity have their respective phases so adjusted that the coupled components add up to a large reflected component. A discussion of the details of this mechanism regarding the reasons for the transmission factor to become nearly zero is covered in detail in the next chapter.

The results obtained above are in close agreement with the experimental data available. Although the data on a complete array are not provided it is reasonable to deduce that the behavior of the complete array has characteristics somewhere between those for the center slot and a corner slot. Generally, the array characteristics would be closer to those of edge elements for a relatively small array and approach the characteristics for the center slot as the array becomes very large. Specific interpretations will depend on the particular array geometry.

It is important to notice that using TE_{10} and TE_{20} alone for the 49-element triangular array one can detect the occurrence of a blind spot in the H-plane scan. It is also important to notice that inclusion of TE_{11}, TM_{11}, TE_{12} and TM_{12} modes in the case of the 169-element rectangular grid array predicted the E-plane null. The significance of these modes for this latter scan was emphasized by Diamond (6).

The finite array analysis was able to provide information about any individual element in the finite arrays considered. The results were in closer agreement with the experiment than those obtained from the infinite array analysis. This was demonstrated by the finite behavior of the null and the accuracy of the position. It was also demonstrated in the case of the 49-element triangular grid array where the infinite array analysis predicted an E-plane null where such a null was not detected experimentally on the finite array nor predicted using the finite array analysis.

CHAPTER IV

DISCUSSIONS AND CONCLUSIONS

In this chapter an explanation of the "blind spot" phenomenon is presented. A comparative study of the method developed in this research with the previously established methods of analysis is used to substantiate the new method. The developed theoretical approximations and the computational methods are of a general nature and can be applied for other electromagnetic problems. Suggestions for future work in this area are presented.

4.1 Blind Spot

In order to gain an understanding of why "blind spots" occur, the behavior of the coupling between various modes at the aperture of a waveguide slot in an array environment should be studied. The so-called "blind spot" is characterized by the high reflection coefficient which occurs at a particular scan angle. The phenomenon referred to here is known as internal resonance (2). It corresponds to modes characterized by the dimensions of the waveguide rather than to modes due to structures outside the array surface, such as fences or dielectric layers. Lechtreck (27) has explained "blind spots" as resulting from accumulation of many coupling contributions at certain critical scan angles. This interpretation is pursued in more detail. Modes that are not excited by direct feed can still originate at the array surface by coupling from excited mode illuminations. These modes in turn couple back to the excited mode. In effect these unexcited modes act as additional couplers between excited modes.

Consider the problem of an array of rectangular waveguide slots uniformly spaced in a metal ground plane. Let TE_{10} be the only mode excited. The total reflected power in any one element is then the sum of all the coupling contributions from all of the elements of the array including the element itself. Thus one should be able to focus on the coupling from all modes in all slots to the TE_{10} mode in the slot under consideration. For

simplicity consider the presence of unexcited modes due only to coupling from the TE_{10} mode in all slots (see section 2.6). Now, keeping in mind the sign relationship discussed in section 2.4, one notices that the direct coupling between TE_{10} mode in any two slots does not change sign if the horizontal or the vertical positions of the two slots under consideration are interchanged. Further examination will reveal that the same statement is true for the indirect coupling between the TE_{10} modes in any two slots even via an intermediate mode in a third slot, if the third slot is also changed in position adequately. In other words, if one considers the images around any of the vertical or horizontal directions of any of the slots (source, field or intermediate), then the coupling for the original arrangement is the same as the coupling from the image arrangement. Hence for the slot in the middle of the array the reflected power is approximately four times that due to slots in one quadrant alone.

Consider the triangular grid arrangements of slots shown in Fig. 4-1.

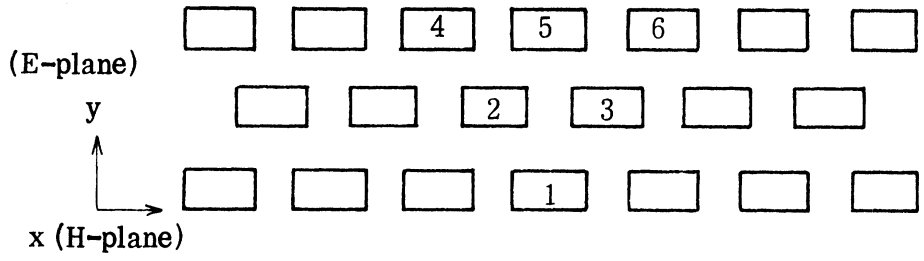

Fig. 4-1: Coupling accumulation in a triangular grid array H-plane scan.

At broadside the illuminations of all slots are in phase. The direct coupling between the TE_{10} modes in slots 4 and 6 and the TE_{10} mode in slot 1 add up, since both coupling coefficients are equal. In fact, because of symmetry, these couplings add up to double the value of just one of the slots. The same statement is true for the indirect coupling between TE_{10} modes in slots 4 and 6 to the TE_{10} mode in slot 1 resulting via the TE_{20} modes in slots 2 and 3, respectively. This is also true for direct coupling between the TE_{10} modes in slots 2 and 3 and the TE_{10} mode in slot 1. Generally, direct and indirect coupling from the TE_{10} mode in any two slots symmetrically positioned with respect to slot 1, will behave similarly as long as symmetric paths are considered. It is interesting to notice that the coupling from TE_{10} in slot 6 to TE_{10} in slot 1 via TE_{20} in slot 3 is neutralized by the coupling of TE_{10} mode in slot 5 to the TE_{10} mode in slot 1 via TE_{20} mode in slot 3 since both of these coupling coefficients are equal and are of opposite sign. Similarly, the coupling from TE_{10} in slot 4 to TE_{10} in slot 1 via TE_{20} in slot 2 is neutralized by the coupling from TE_{10} in slot 5 to TE_{10} in slot 1 via TE_{20} in slot 2.

Scanning the beam of the array in the H-plane requires progressive phase shift in the x-direction. Consider, for example, the situation of $\pi/2$ (90^{o}) phase shift between consecutive elements in the same row. The coupling of TE_{10} in slots 4 and 6 to TE_{10} in slot 1, both directly and indirectly, is going to cancel. In the meantime, direct coupling from TE_{10} in slot 5 and indirect coupling through TE_{20} in slots 2 and 3 are going to add up vectorially. The sum of the coupling from TE_{10} in slots 2 and 3 to TE_{10} in slot 1 will decrease to 0.707 its broadside value. Still a third example is the interesting situation when the phase shift between the illuminations of consecutive slots in the same row differs in phase by π (180^{o}). Direct and indirect coupling of TE_{10} in slots 4 and 6 are again going to add up. Indirect coupling of TE_{10} in slot 5 to TE_{10} in slot 1 via TE_{20} in slots 2 and 3 are going to add up in phase with the indirect coupling from TE_{10} in slots 4 and 6 via TE_{20} in slots 2 and 3, respectively. How-

ever, in this case coupling from TE_{10} in slots 2 and 3 to TE_{10} in slot 1 cancels out. Generally in the above discussion what is true for TE_{20} is true for any mode with even index along the direction of scan (H-plane). Emphasis has been directed to the TE_{20} mode because besides simplifying the description, the operating frequency for ordinary waveguides can frequently get very close to the TE_{20} cutoff frequency. Since there is the factor of $1/\sqrt{k^2-k_c^2}$ in the coupling coefficient normalization factor (see equations (2.33) and (2.34)) it should be evident that modes close to cutoff are especially important. Figure 4-2 shows the change in the coupling coefficient between TE_{10} in slots 5 and 6 and TE_{10} in slot 1 as the effect of higher order modes in these slots and other slots in between are considered.

Stating the above observations more compactly, the effects of modes with different parity along the direction of scan from that of the excited mode can become significantly large especially if these modes are close to cutoff. In the case of the 7x7 antenna array with a triangular grid arrangement of slots as analyzed in the previous chapter, Table 4-1 shows the values

Table 4-1 Coupling from TE_{10} illuminations in various slots to incident TE_{10} in slot 1 in Fig. 4-1.

Coupling from TE_{10} in slot no.	Via TE_{20} in slot No.	Magnitude	Phase
2	-	.0772	209.1^o
3	-	.0772	209.1^o
4	-	.0255	322.3^o
4	2	.068	30.5^o
5	-	.0926	76.2^o
5	2	.068	210.5^o
5	3	.068	210.5^o
6	-	.0255	322.3^o
6	3	.068	30.5^o

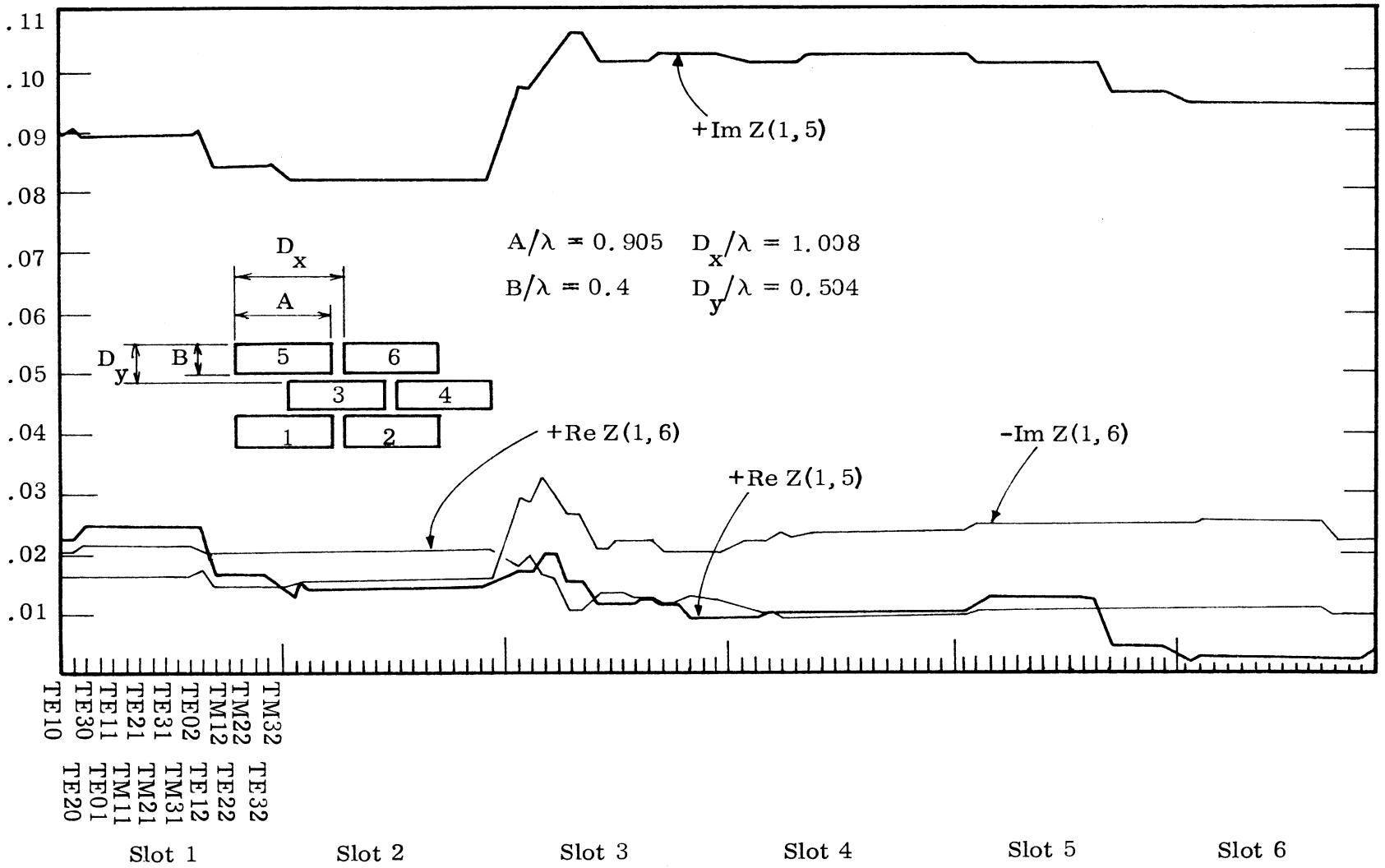

Fig. 4-2: Effect of unexcited modes on the coupling between two slots

of coupling coefficients from TE_{10} in the slots of Fig. 4-1 to the TE_{10} mode in slot 1. Bear in mind that the data shown in Table 4-1 apply to this particular array with the waveguide slots of a given size and with the particular spacings between slots used in this array. Also, of course, the data are dependent upon the frequency used.

On this basis, while the TE_{20} is most significant for H-plane scanning the TE_{11} and TM_{11} would be more significant with E-plane scanning. This is in agreement with the ordering of mode importance for different scan directions as presented by Farrell and Kuhn (7).

Several studies have indicated, in general, that analysis based on TE_{10} alone cannot predict blind spot behavior (5-7), and higher order modes are necessary if the blind spot behavior is to be revealed. In some cases of TE_{10} and TE_{20} alone (Diamond (6) and Farrell and Kuhn (5-7)) demonstrated blind spot behavior. Here it has been shown that, in fact, modes of different parity along the direction of scan contribute heavily to the occurrence of these blind spots. Indeed, a maximum of the reflected components of the excited mode occurs near scan angles where phasing between elements of the antenna array is such that the resultant reflected amplitude of the main mode due to all couplings in maximized.

4.2 Relation Between the Reflection Coefficient and Coupling Coefficients for an Infinite Array

Define C'_{jk} to be the total coupling coefficient representing the coupling between the TE_{10} illumination in one slot and reflected component of the same mode in another slot including the direct and indirect coupling due to other elements of the array. These slots are $j+(1-(-1)^K)\frac{G}{2}$ D_x apart in the x-direction, and kDy apart in the y-direction.

G is the grid parameter which equals 0.5 for isosceles triangular grid and equals 0.0 for rectangular grid.

Dx and Dy are grid dimensions as defined before.

Let

$$C_{jk} = \frac{4\,C'_{jk}}{(1+\delta_{oj})(1+\delta_{ok})} \tag{4.1}$$

where:

$$\delta_{oj} = \begin{cases} 1 & j = 0 \\ 0 & j \neq 0 \end{cases} \quad \text{and} \quad \delta_{ok} = \begin{cases} 1 & k = 0 \\ 0 & k \neq 0 \end{cases} .$$

For a uniformly excited array one can express the TE_{10} reflection coefficient in any slot of an infinite array of a uniformly spaced isosceles triangular grid as follows:

$$\begin{aligned} R = &\left[C_{oo} + C_{02}\cos 2\psi y + C_{04}\cos 4\psi y + \ldots\right] + \\ &+ \left[C_{11}\cos\psi y + C_{13}\cos 3\psi y + C_{15}\cos 5\psi y + \ldots\right]\cos\frac{\psi x}{2} + \\ &+ \left[C_{20} + C_{22}\cos\psi y + C_{24}\cos 4\psi y + \ldots\right]\cos\psi x + \\ &+ \left[C_{31}\cos\psi y + C_{33}\cos 3\psi y + C_{35}\cos 5\psi y + \ldots\right]\cos\frac{3\psi x}{2} \end{aligned} \tag{4.2}$$

where

ψx is the steering phase in the x-direction or the phase shift between two consecutive elements in the same row and equals $D_x k \sin\theta\cos\phi$,

ψy is the steering phase in the y-direction or the phase shift between two consecutive rows and equals $D_y k \sin\theta\sin\phi$,

or

$$\begin{aligned} R = &\sum_{\ell=0}^{\infty}\sum_{i=1}^{\infty} C_{2\ell,\ 2i}\cos 2i\psi y \cdot \cos 2\ell\frac{\psi x}{2} + \\ &+ C_{2\ell+1,\ 2i+1}\cos(2i+1)\psi y \cdot \cos(2\ell+1)\frac{\psi x}{2} . \end{aligned} \tag{4.3}$$

Similarly, for uniformly spaced, uniformly excited infinite rectangular grid

one can write:

$$R = \sum_{\ell=0}^{\infty} \sum_{i=0}^{\infty} C_{\ell i} \cos i\psi y \cos \ell\psi x \quad . \tag{4.4}$$

This means that the reflected power can be represented as a two-dimensional Fourier series in the harmonics of steering phases. The inverse operator yields the individual coupling coefficients between the excited TE_{10} mode components in an array environment in terms of the reflection coefficient as a function of the beam direction:

$$C'_{jk} = \frac{1}{4\pi^2} \int_0^{2\pi} \int_0^{2\pi} R(\psi x, \psi y) \cos i\psi y \cos(1-G)\, \ell\psi x \, d\psi x \, d\psi y \quad . \tag{4.5}$$

4.3 Advantages of Finite Array Analysis

The assumption of an infinite array has been frequently used to simplify the analysis for an element in the midst of a large array. On the basis of such an assumption all elements would behave similarly; hence, periodicity conditions can be used, which greatly reduces the cost of the calculations. Obviously, this type of analysis does not provide information concerning elements on the edge of large arrays. Wasylkiwskyj (17) used an extension of the Wiener-Hopf factorization procedure for solving an infinite order difference equation for the analysis of a semi-infinite array. The solution for mutual coupling coefficients as well as for active reflector coefficients in a phased semi-infinite array is expressed explicitly in terms of the active impedance in a phased infinite array. As Cha (18) indicates, in finite array analysis it is necessary to compute the interaction matrix and its inverse only once; then the unknown reflection coefficients and higher order modal coefficients for any scan angle can then be found. This is not possible in infinite array calculations where a different interaction matrix would have to be computed and inverted at each scan angle. This is true

because the matrix entries for an infinite array calculation describe the interaction between internal waveguide modes and modes exterior to the waveguides. Since the latter depend on the phase between elements the matrix elements in this case are dependent on the scan angle. In the case of finite array analysis the matrix entries represent coupling between internal modes in one slot to internal modes in the same or other slots, which are independent of the scan angle.

The assumption introduced in this work, which neglects the interaction between unexcited modes to other unexcited modes, greatly reduces the number of entries to be calculated. Moreover, it allows the generation of augmented coefficients representing the coupling between excited modes only to other excited modes, including direct coupling between those modes and indirect coupling through other unexcited modes at the surface of the antenna array. As in the examples solved in Chapter III, utilizing a matrix representing the relation between incident or reflected amplitudes of the excited modes and the illumination of those modes on the array surface the reflection coefficient corresponding to any scan angle can be obtained for any slot without the need to invert the matrix.

The finite array analysis has no restriction on the choice of the plane of the scan. In the infinite array analysis only H-plane scans or quasi-E-plane scans are considered if the problem is to be reduced to a scalar one-dimensional problem. For a true E-plane scan, the problem is essentially a two-dimensional vector one. No simplification is possible (1).

Finite array analysis is capable of describing the behavior of the center element as well as an edge element. Such results should be very useful in designing array feed networks. This type of analysis is essential for limited size arrays where the infinite array assumption would lead to intolerable errors. Finite array analysis also can be used economically for predicting behavior of large arrays. One can establish a criterion for the minimum array size around a centrally located element such that this element and all others could be considered in an infinite array environment. Any

array equal or larger than this minimum size array could be analyzed utilizing the same range of coupling coefficients. Such a criterion will depend, of course, on the shape and dimensions of the array elements and the lattice.

The method of finite array solution employed here can be extended to non-uniformly spaced arrays, but, of course, at more expense depending upon the amount of symmetry destroyed. On the other hand, non-uniformly spaced arrays are not suitable for phase scanning because of the randomness in element position. Instead non-uniformly filling or thinning of an otherwise uniformly spaced array is an attractive way of obtaining the same desirable characteristics of a non-uniformly spaced array. Such an array can easily be accommodated in this method simply by removing entries corresponding to thinned elements both in the matrix and column vectors. The effects of mode traps at the apertures of different elements could be included in a similar way.

4.4 Approximations and Computational Techniques

The main use of sparsity techniques is to reduce the size of the storage needed in core memory storage. Under conditions of sparsity there is still the problem of finding the most convenient way of solving the matrix equation involved. In the general consideration of a matrix it is important to recognize that it is possible to eliminate elements which are redundant within the matrix. Often this redundancy is associated with the electromagnetic problem at hand. Application of the well known principle of reciprocity together with geometric symmetry frequently is a useful means of ascertaining such redundancy. Element storage is minimized by eliminating or reducing redundancy. Such a procedure in many cases may prove a strong tool since it achieves the same objective as sparsity from the storage point of view.

It was shown in Chapter III for the cases of a slot array of rectangular grid or isosceles triangular grid arrangements that it was possible to reduce the storage size from $(\text{NOS} \times \text{NOM})^2$ to just $\text{NOS}\left(\frac{\text{NOM}^2+\text{NOM}}{2}\right)$ where NOS

is the number of slots and NOM is the number of modes. This reduced value in the storage requirement represents coupling from all modes in all slots to all modes in the corner slot of a uniformly spaced planar array. By neglecting the contributions from unexcited modes to other unexcited modes and assuming only one mode is excited it was possible to cut down the storage size needed to only NOS x NOM. This number corresponds to coupling from all modes in all slots to TE_{10} in the corner slot.

By careful computer programming it is possible to avoid storing even this reduced number of elements in the core all at one time. One way to do this is by properly sectionalizing the computer program, and storing coupling coefficients corresponding to one slot as soon as they are calculated. This procedure then means that the maximum core storage per array of the machine imposes a limit not on the product $(NOM \times NOS)^2$, but rather on the number of modes used (NOM). A separate subroutine can be written to generate any desired row or column of the original matrix.

Attention is now directed to the sign relations established in Section 2.4 for normalized coupling coefficients between modes. Besides the normal reciprocity and symmetry relations which they express, they also relate the integrals calculated for the normalized coupling coefficient between the M_1N_1 mode in slot A to M_2N_2 in slot B, to the normalized coupling coefficient between the M_2N_1 mode in slot A to the M_1N_2 mode in slot B. It is also imperative to notice that the integrals calculated for the coupling from one mode to a TE_{MN} or a TM_{MN} mode is the same as long as the modal indices are the same; only the multiplying coefficients are different.

It is believed that the methods mentioned in this Section could be used to advantage in many other electromagnetic problems.

4.5 Possible Means of Eliminating "Blind Spot" Phenomenon

As discussed in Section 4.2 modes of different parity along the direction of scan are shown to contribute heavily to the occurence of the so-called "blind spots". One method of elimination of "blind spots" described here is

based upon the suppression of certain modal components of unlike parity (compared with TE_{10}) from any slot illumination. For normal operation of open-ended waveguides only the lowest order mode is excited, and the higher order modes are excited only at the aperture due to coupling from dominant mode illumination at the array face. It is believed that selective mode traps for modes of different parity at the apertures can reduce the effects of those modes on couplings between illuminations of the dominant mode. An example of a simple scheme for such traps is one thin wire in the direction of the width placed at one-half the height of the slot and bends to two wires in the direction of the height placed at one-quarter of the width distance from each of the two side walls as shown in Fig. 4-3 for rectangular guides. It is expected that the voltage induced by the TE_{20} mode will circulate current in the loop formed by the trap wire and the bottom side of the waveguide, while the voltage induced by the TE_{10} mode will cancel out. The evaluation of the effects of

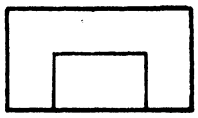

Fig. 4-3: Mode trap for TE_{20}.

these traps on the TE_{10} mode performance and/or the construction of more elaborate traps that would minimize the TE_{20} mode content without having adverse effects on the TE_{10} mode is left for future research. The possibility of extending this analysis to other types of apertures and arrays is also a good prospect for future work.

Figures 4-4 to 4-10 show the performance of the 49-element triangular grid array mentioned in Chapter III, if there were no TE_{20} mode present. These results were obtained by setting equal to zero all the coefficients

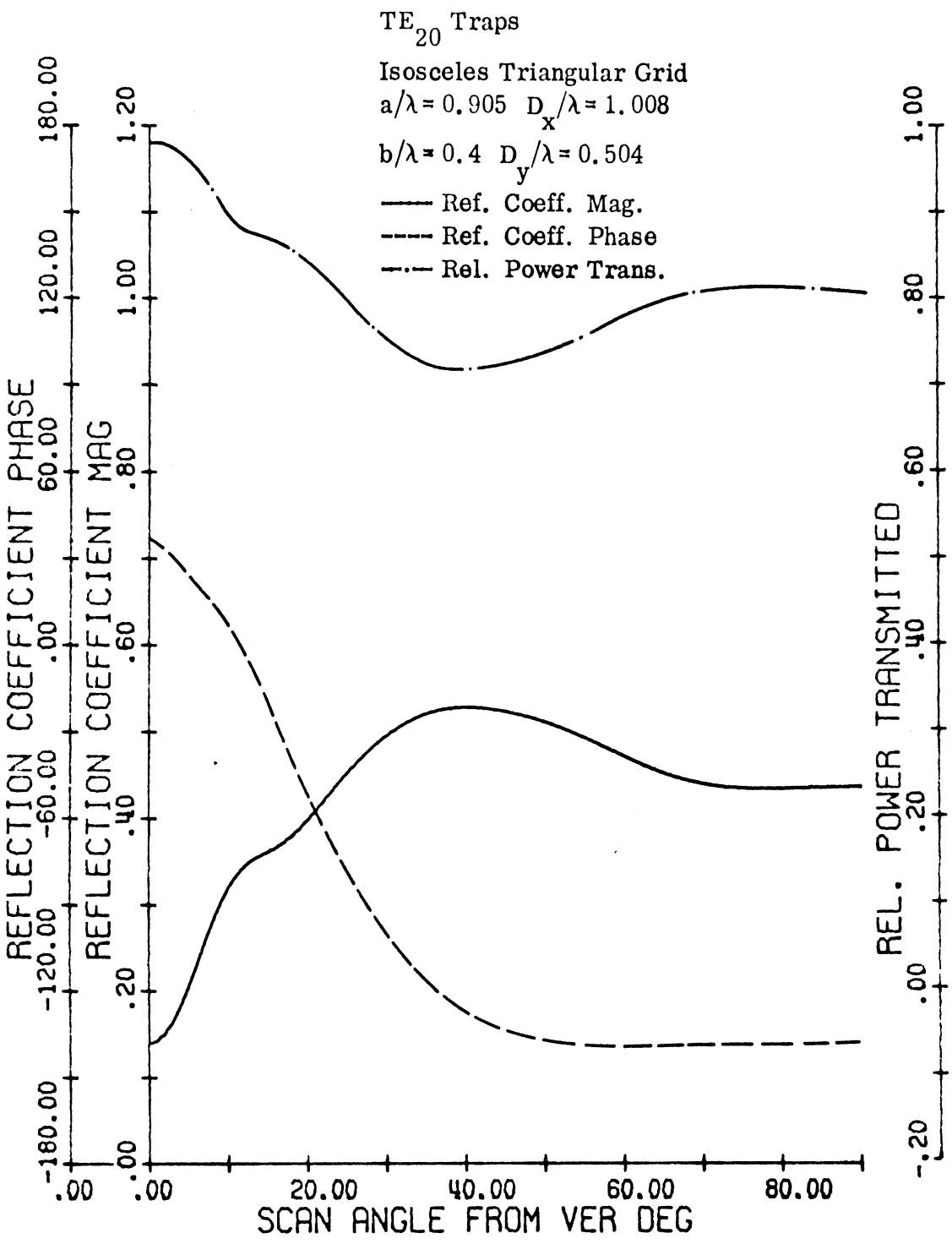

FIG. 4-4: 7-COLS. 7-ROWS ARRAY G=0.5 PHI= 0.0
F= 11900.000MHZ ELEMENT POS. (4, 4)

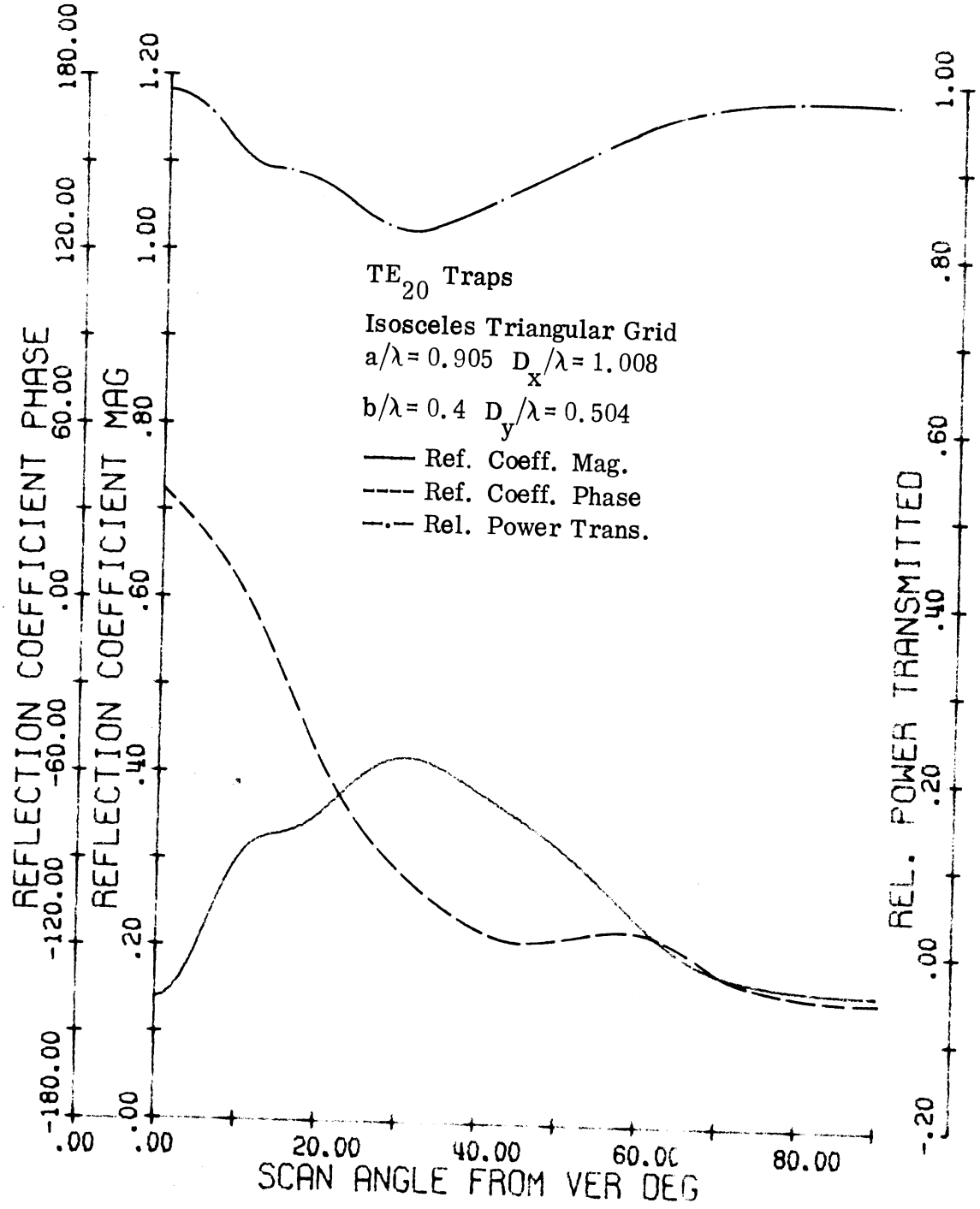

FIG. 4-5: 7-COLS. 7-ROWS ARRAY G=0.5 PHI= 15.00
F= 11900.000MHZ ELEMENT POS. (4, 4)

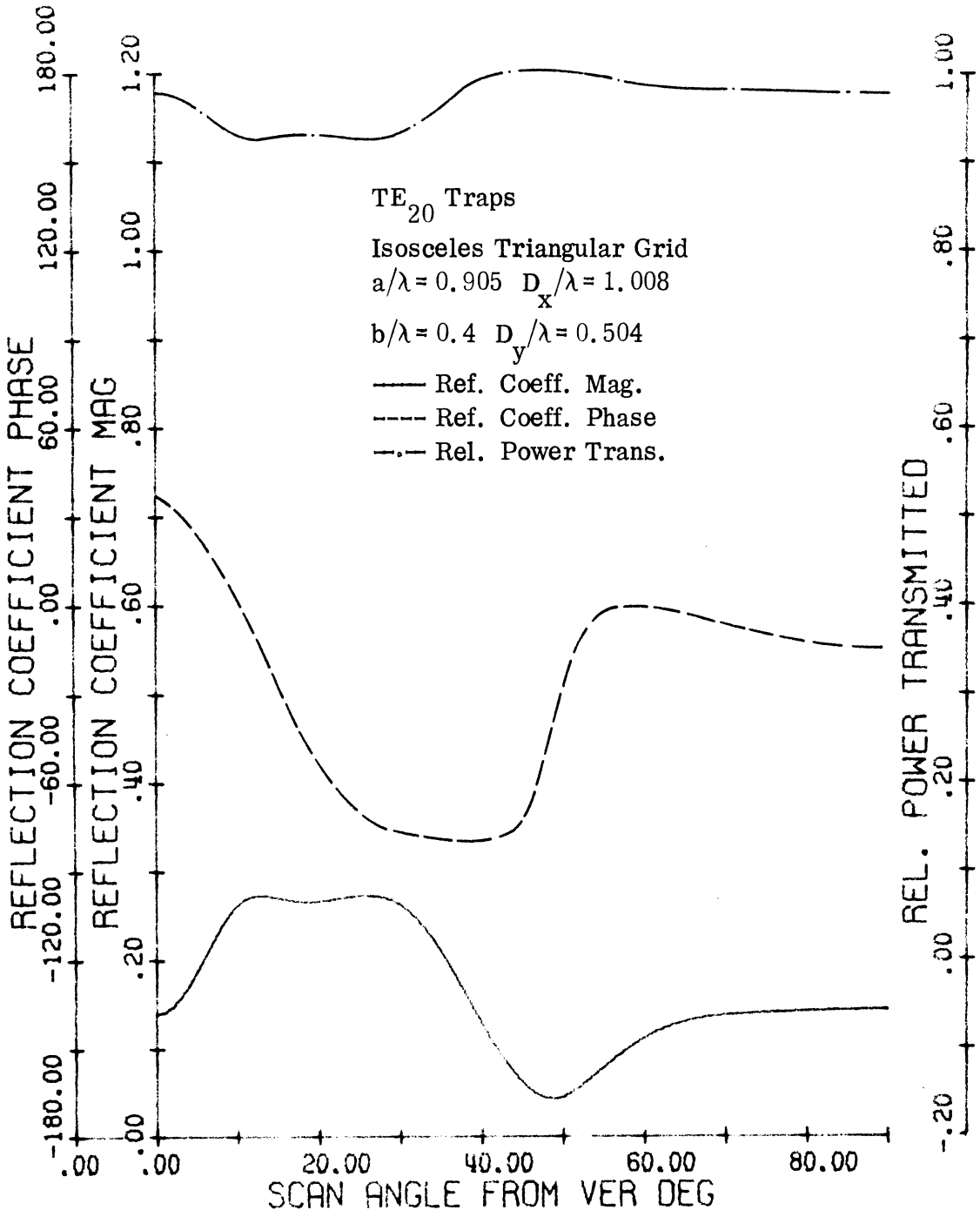

FIG. 4-6: 7-COLS. 7-ROWS ARRAY G=0.5 PHI= 30.00
F= 11900.000MHZ ELEMENT POS.(4, 4)

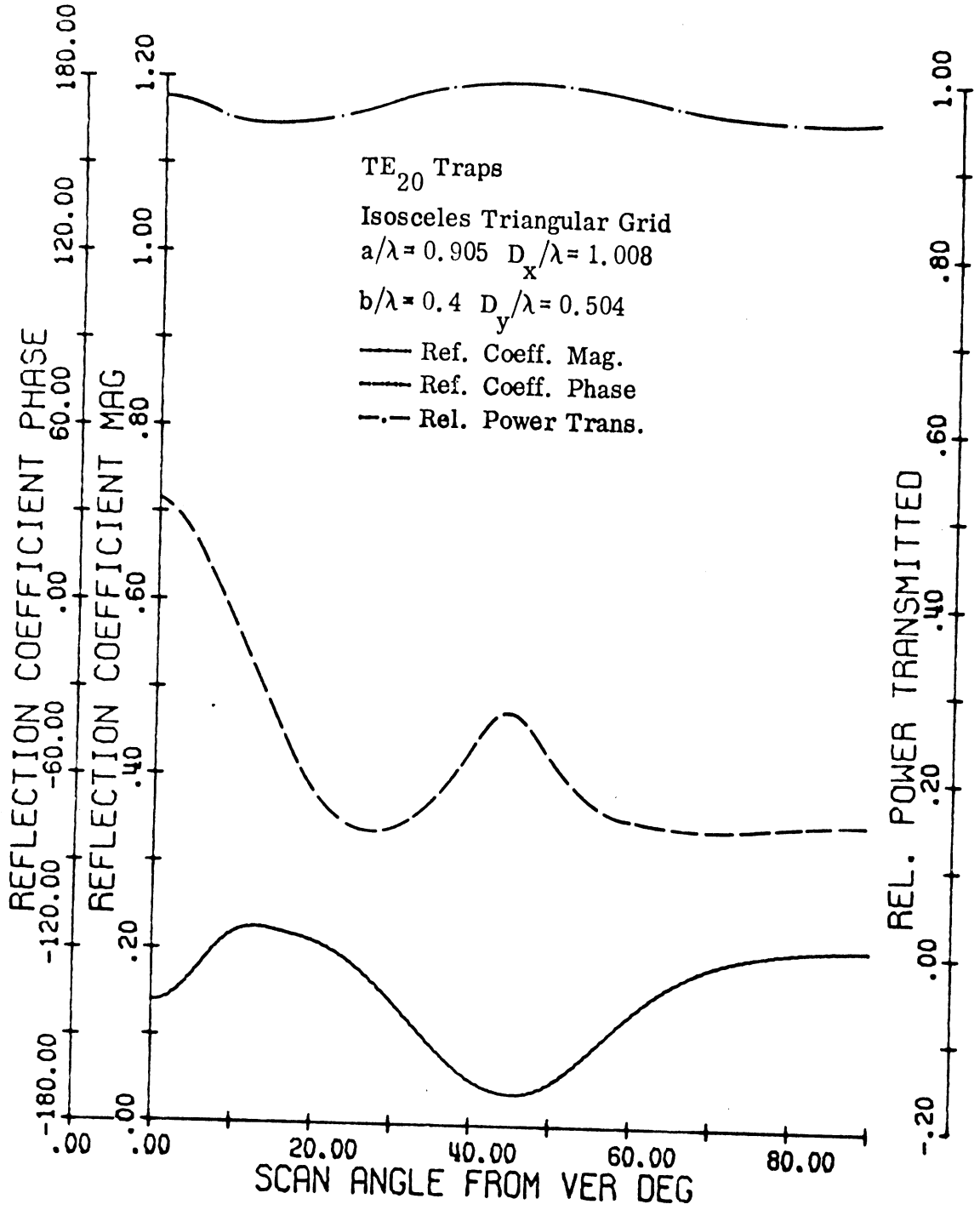

FIG. 4-7: 7-COLS. 7-ROWS ARRAY G=0.5 PHI= 45.00
F= 11900.000MHZ ELEMENT POS. (4, 4)

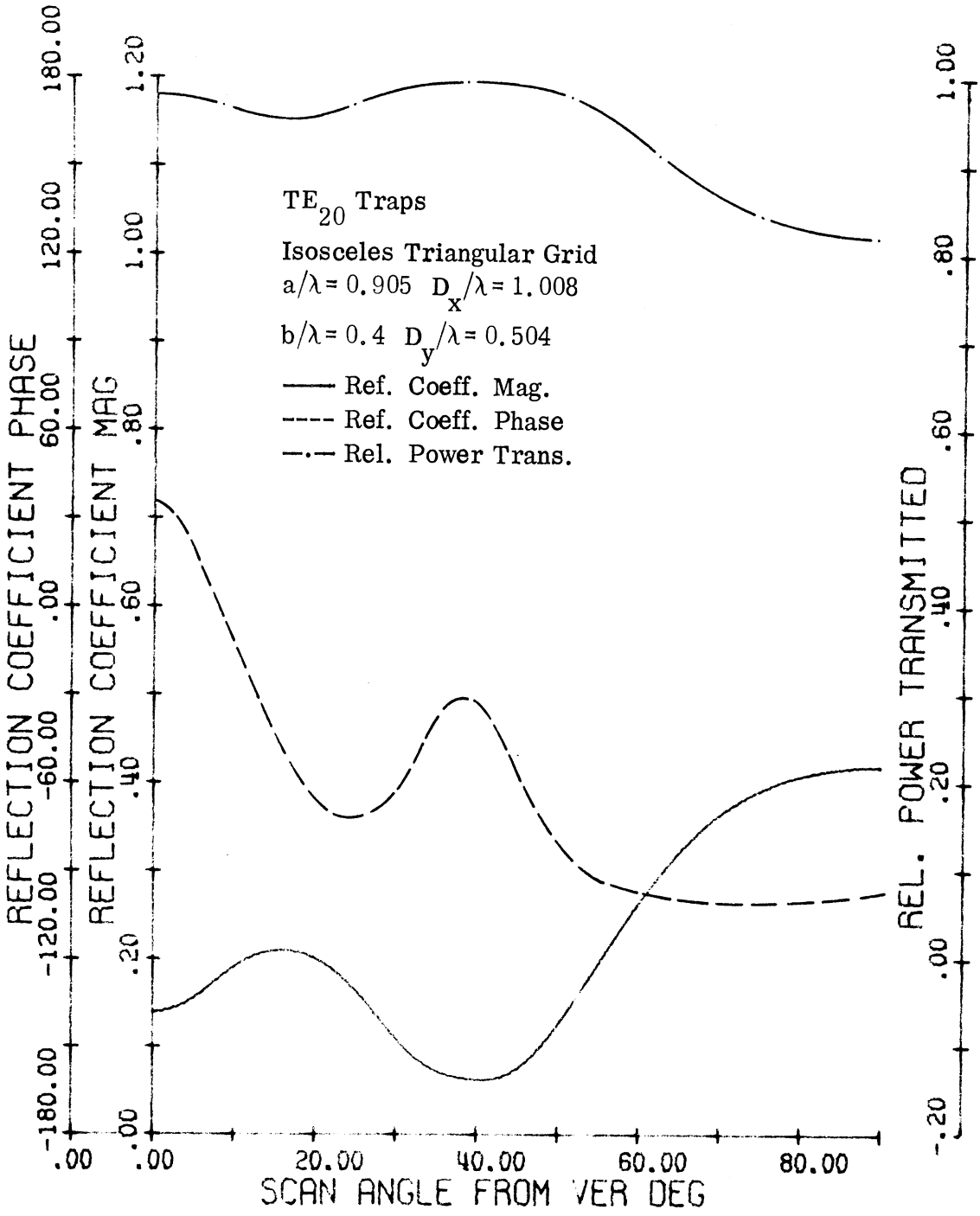

FIG. 4-8: 7-COLS. 7-ROWS ARRAY G=0.5 PHI= 60.00
F= 11900.000MHZ ELEMENT POS. (4, 4)

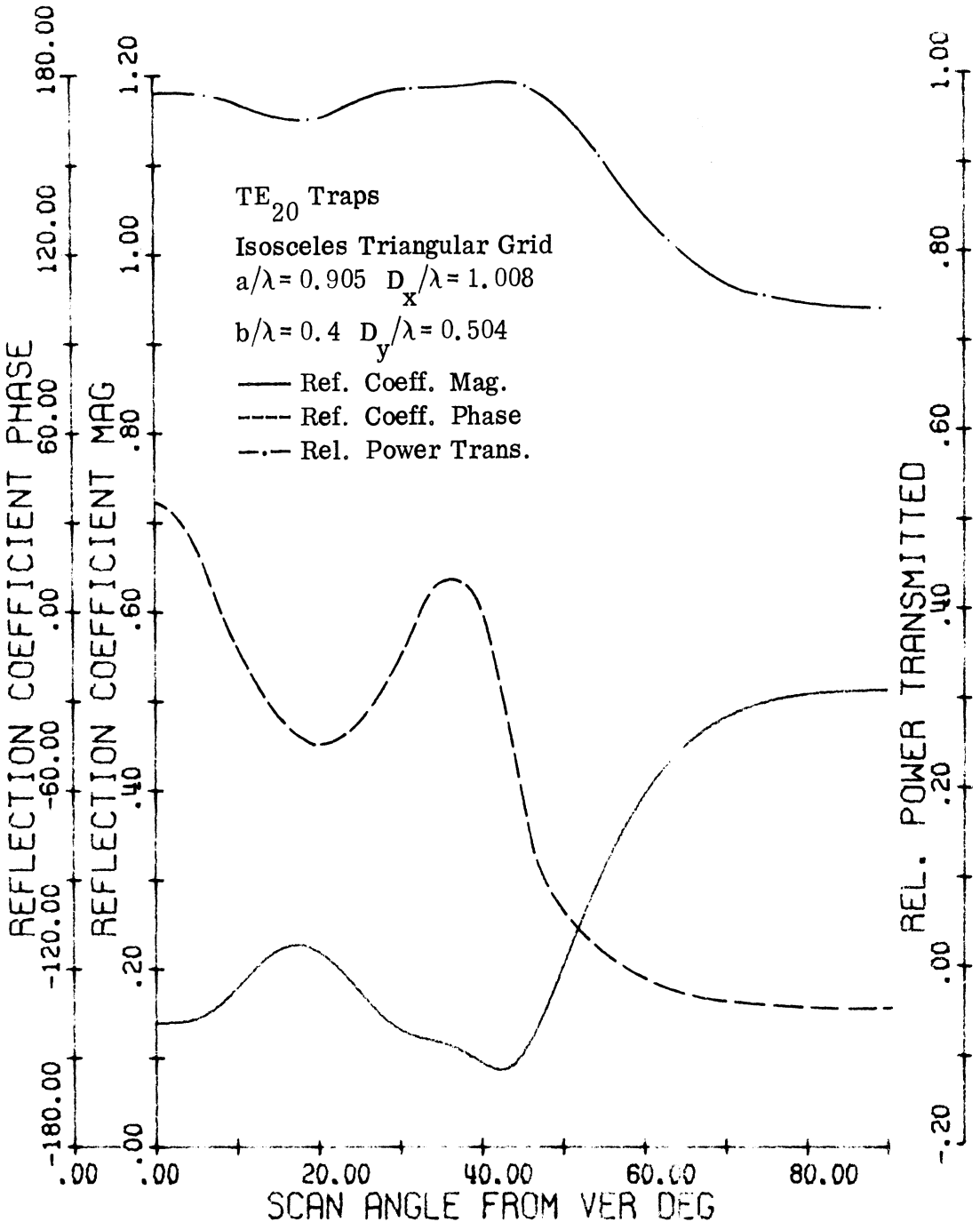

FIG. 4-9: 7-COLS. 7-ROWS ARRAY G=0.5 PHI= 75.00

F= 11900.000MHZ ELEMENT POS. (4, 4)

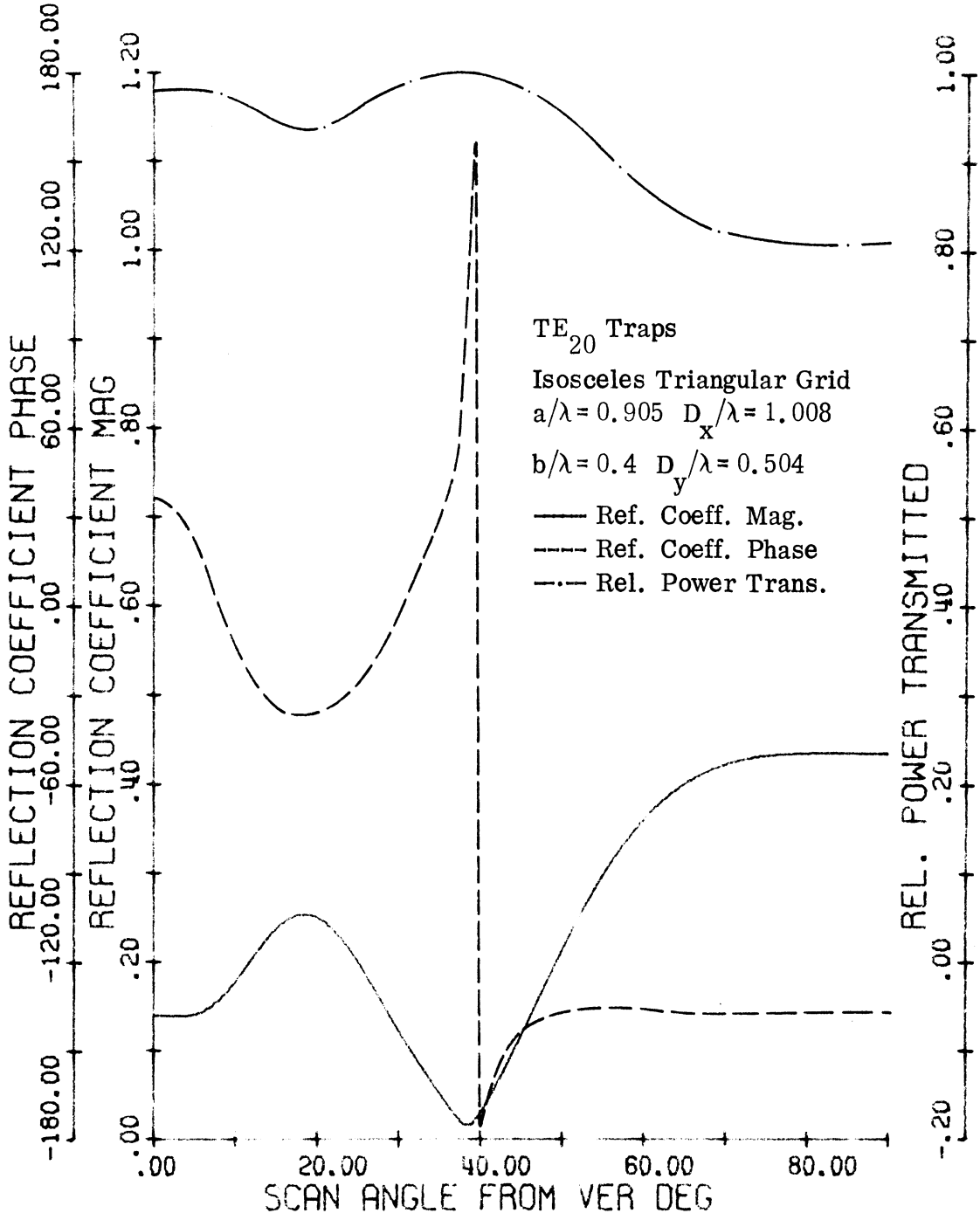

FIG. 4-10: 7-COL 3. 7-ROWS ARRAY G=0.5 PHI= 90.00

F= 11[illegible].000MHZ ELEMENT POS.(4, 4)

corresponding to TE_{20} in the basis matrix representing the arrays .

Another method for "blind spot" reduction was discussed by Argwal and Lo (16). The random spacing of the elements of an array can reduce the null introduced at certain scan directions due to severe mismatch. However, the randomness in the element position is associated with a feeding problem. Adjusting the phase of different elements for a given scan becomes a tougher task due to the lack of symmetry. On the other hand, non uniform filling of an otherwise uniformly spaced grid appears as an attractive means of realizing some of the advantages of a non uniformly spaced array. The finite array analysis can easily be used for non uniformly filled uniform grids. The rows and columns corresponding to the thinned elements can simply be removed from the basic matrix. Further investigation along these lines is left for future work.

4.6 Summary

1) A formulation of the finite array problem has been presented. Each mode in each slot of the physical array has been treated as a separate port. The coupling coefficients between ports can be evaluated in terms of double integrals. These double integrals contain a Green's function and can be evaluated numerically. The advantages of the finite array formulation over the infinite array formulation were discussed.

2) The infinite set of linear algebraic equations is then truncated to a finite set. The limitation on the size of that finite set of linear equations arises from the upper bound on the size of the largest array of numbers storable on the computer in use.

3) The use of symmetry and reciprocity characteristics for that type of formulation has been analyzed. A new relation beyond the usual symmetry and reciprocity has also been discussed. This relation relates the integrals involved in evaluating the coupling coefficient between the M_1N_1 mode in one slot and the M_2N_2 mode in another slot to the integrals involved in evaluating

the coupling coefficient between the M_1N_2 mode and the M_2N_1 mode in the same slots. A method to make use of the symmetry and reciprocity characteristics and the relation mentioned to reduce the calculation effort and the storage requirements has been described.

4) The use of symmetry and reciprocity characteristics reduced the number of coefficients to be calculated and stored for uniformly spaced rectangular or isosceles triangular grid arrays from $(NOS \times NOM)^2$ to

$$NOS \cdot \frac{NOM^2 + NOM}{2},$$

where NOS is the number of the physical elements in the array,

NOM is the number of modes to be considered in each element.

This can still require the handling of a fairly large number of coefficients.

5) A new approximation has been introduced. This approximation neglects the effect of coupling among unexcited modes in the calculation of input impedance of the excited modes. The couplings from excited modes to unexcited modes and thence back to excited modes are still included. The use of approximation cut the number of coefficients to be handled down to $NOS^2 \times NOM$ for non uniform grid arrays and to a mere $NOS \times NOM$ for rectangular or isosceles triangular grid arrays. This type of approximation is general in nature and can be extended to other electromagnetic problems.

6) The finite array analysis has been checked against experimental data on a seven slot linear array of slots arranged for weak coupling, a 49-slot triangular grid array and a 169-slot square grid array. Close agreement has been observed throughout.

7) The mechanism linking the modes of different parity along the direction of scan to the "blind spot" has been explained. A method for "blind spot" reduction has been suggested based on the suppression of such modes. Preliminary calculations indeed show the effectiveness of the suppression of such modes in reducing the "blind spot".

CHAPTER V

SCANNING OF A SLOT BY MODE CONTROL

5.0 Preliminary

The use of multiply-fed slot apertures corresponds to using the aperture with more than one mode. In the work of this group an experimental slot was arranged in a large metal ground plane. This slot was fed from a short section of waveguide having three coaxial inputs. One coaxial feed was used to provide excitation of the dominant TE_{10} mode and the other two were arranged at the proper positions across the guide to excite the TE_{20} mode. The latter two feeds were on the top side of the waveguide and were arranged to feed in 180^{o} phase opposition. This was necessary in order to establish the TE_{20} mode with best utilization of the power to the feeds.

5.1 Magnitude Ratio and Phase Control

An antenna slot excited by the TE_{10} and TE_{20} modes has the interesting properties that the radiation pattern can be controlled. Two ways of controlling the radiation pattern are available. One method which was tried and which proved most practical was to control the ratio of the magnitudes of the electric field of the TE_{20} mode to that of the TE_{10} mode. A second method of control, tried only briefly, was to utilize various phase differences between the TE_{20} and TE_{10} inputs. This phase control of the modes was utilized while keeping the ratio of the amplitude of the TE_{20} mode to the amplitude of the TE_{10} mode constant.

In scanning a slot by either of these methods certain distortions of the radiation pattern occur. For instance, with a slot in a large metal plane it was found that in scanning from the mid-position in the H-plane by increasing the relative amplitude of the TE_{20} mode over the TE_{10} the main beam would move off the broadside position in the direction that was due to one lobe of the TE_{20} mode augmenting the field of the TE_{10} mode. When the main beam

moved in this manner it was found that a minor lobe would occur in the other direction. This minor lobe increased in size as the angle of scan from broadside increased. Figure 5-1 shows a slot aperture with the usual field distributions of the two modes to be considered. With field distributions as in Figure 5-1 it is possible to predict the pattern to be produced in the scanning of the beam of this slot as the TE_{20} mode assumes various levels relative to the TE_{10} mode. The parameter τ is used to indicate the ratio of the amplitude of the E-field of the TE_{20} mode to the amplitude of the E-field of the TE_{10} mode. It will be found that when $\tau = 0$ corresponding to no TE_{20} mode present that the usual pattern corresponding to a magnetic dipole is observed. It is to be recognized that a rectangular slot in a metal plane has a pattern corresponding closely to that of a magnetic dipole provided the slot has a height dimension which is very small compared to the width dimension of the waveguide. Thus the magnetic dipole pattern is the most appropriate characterization for slots which approach the configuration of slits (small in E-direction).

Kitsuregawa and Tachikawa (29) showed that if the amplitude ratio $\tau = 1$ is maintained and the time phase angle, ψ, between the modes is varied then the direction of the beam is almost invariant and only the phase pattern changes significantly. The variation of the phase pattern means the position of the phase center of the radiated wave varies. Such a control system with $\tau = 1$ constant and ψ varying could be used for a feed horn of a beam scanning parabolic antenna. Since scanning with phase control was considered to be outside of the scope of this research effort no additional time was expended on this approach.

5.2 Analysis for Radiation Pattern

Using the general method of Kitsuregawa and Tachikawa (29) the following analysis may be made. For a rectangular aperture "a" wide by "b" high

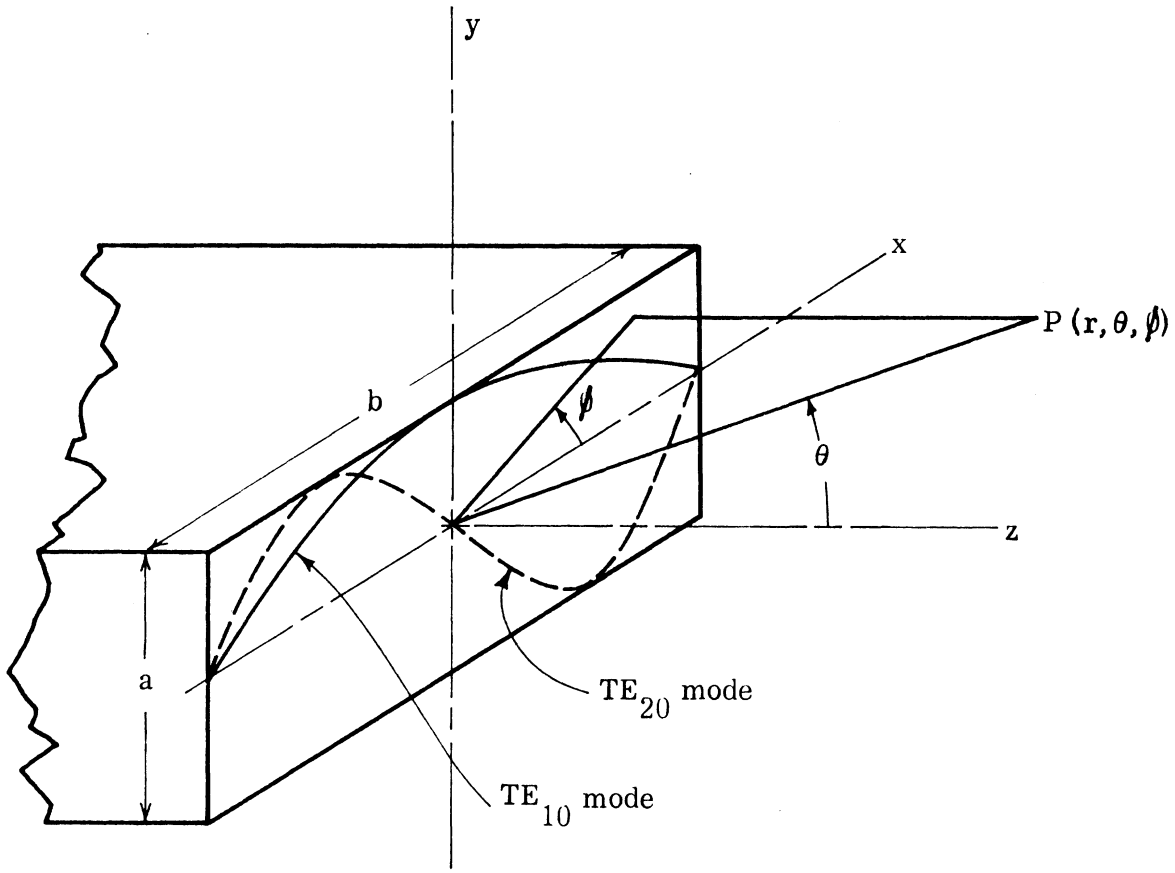

Fig. 5-1: Rectangular aperture with two lowest modes.

as shown in Figure 5-1, the radiation intensity is given by:

$$\Phi(\theta, \phi) = S^2 \Phi_0 \tag{5.1}$$

where Φ_0 is the radiation intensity of unit moment source and

$$\Phi_0 = \frac{(1 + \cos\theta)^2}{960\,\pi\,\lambda^2} \quad . \tag{5.2}$$

See equation 4.72 of reference by Wolff (30) for the above expression. S is the designation for a space factor and is given by

$$S = |F| = \int_{-\frac{a}{2}}^{\frac{a}{2}} \int_{-\frac{b}{2}}^{\frac{b}{2}} E(x,y)\, e^{+jk(x \sin\theta \cdot \cos\phi + y \sin\theta \cdot \sin\phi)}\, dx\, dy, \tag{5.3}$$

where, λ is the wavelength in surrounding space, $k = \frac{2\pi}{\lambda}$ = phase parameter in surrounding space, and $E(x,y)$ = electric field distribution over the slot aperture. If only the TE_{10} and TE_{20} modes in the aperture are to be considered then

$$E(x,y) = E_0 \left(\cos\frac{\pi}{a} x + \tau e^{j\psi} \sin\frac{2\pi}{a} x \right) \tag{5.4}$$

where the ratio τ is given by:

$$\tau = \frac{\text{amplitude of } TE_{20} \text{ mode electric field}}{\text{amplitude of } TE_{10} \text{ mode electric field}} \quad .$$

ψ is the phase difference and is given by: ψ = phase difference between TE_{20} and TE_{10} modes at aperture. The factor F may now be written:

$$F = E_0 \frac{2a\lambda \sin\left(\frac{\pi b}{\lambda} \sin\theta \cdot \sin\phi\right)}{\sin\theta \cdot \sin\phi} \left[\frac{\cos\left(\frac{\pi a}{\lambda} \sin\theta \cdot \cos\phi\right)}{\pi^2 - (ka)^2 \sin^2\theta \cos^2\phi} \right.$$

$$\left. - 2\tau \frac{\sin\left(\frac{\pi a}{\lambda} \sin\theta \cdot \cos\phi\right)}{(2\pi)^2 - (ka)^2 \sin^2\theta \cos^2\phi} \left\{ \sin\psi - j\cos\psi \right\} \right]. \qquad (5.5)$$

The power directivity function of the radiator is:

$$d(\theta, \phi) = \frac{\Phi(\theta, \phi)}{\Phi_{av}} \qquad (5.6)$$

where $\Phi_{av} = \frac{W}{4\pi}$ and (5.7)

$$W = \iint \frac{1}{2\eta} R\,(E \cdot E^*)\, d\,x\, dy = \text{total radiated power}, \qquad (5.8)$$

and η is the impedance of free space ($\eta = \sqrt{\frac{\mu_0}{\epsilon_0}}$).

For the slot radiator having both TE_{10} and TE_{20} modes the gain function in the H-plane (the x-z plane) is:

$$d(\theta) = \frac{8ab(1+\cos\theta)^2}{(1+\tau^2)\,\pi\,\lambda^2} \left[\left\{ \frac{\cos u}{1 - (2u/\pi)^2} - \frac{\tau}{2} \sin\psi \left[\frac{\sin u}{1 - (u/\pi)^2} \right] \right\}^2 \right.$$

$$\left. + \left\{ \frac{\tau}{2} \cos\psi \left[\frac{\sin u}{1 - (u/\pi)^2} \right] \right\}^2 \right] \qquad (5.9)$$

where $u = \frac{\pi a}{\lambda} \sin\theta$. (5.10)

Introducing the normalized directivity function D_A by:

$$D_A(\theta, \phi) = \frac{d(\theta, \phi)}{N} \qquad (5.11)$$

where $$N = \frac{32}{\pi} \frac{ab}{\lambda^2} \,, \qquad (5.12)$$

N is a normalizing factor for a rectangular horn. Then D_A in the H-plane (x - z plane) is given by:

$$D_A(\theta, 0) = \frac{(1+\cos\theta)^2}{4(1+\tau)^2} \left[\left\{ \frac{\cos u}{1 - (2u/\pi)^2} - \frac{\tau}{2} \sin\psi \left[\frac{\sin u}{1 - (u/\pi)^2} \right] \right\}^2 + \left\{ \frac{\tau}{2} \cos\psi \left[\frac{\sin u}{1 - (u/\pi)^2} \right] \right\}^2 \right] \qquad (5.12)$$

The above expression simplifies if $\psi = \pm 90^o$ as is desirable for amplitude ratio control. With ψ set equal to $+ 90^o$ the expression for D_A gives the directivity for various ratios of modal excitation as shown in Figure 5-2. For every chosen value of "τ" and with ψ set at $+ 90^o$ equation (5.12) gives D_A or the relative power versus u.

5.3 Results

The curves shown in Figure 5-2 are theoretically based curves utilizing the methods of Kitsuregawa, et al (1962) as used in the analysis of the previous section. Experimental tests were made using a slot formed by S-band waveguide terminated in an aperture in a large metal plane. Waveguide WR 284 (RG-48/u) was used and in order for this waveguide to support the TE_{20} mode, it is, of course, necessary to operate it at a frequency higher than S-band. The experimental results obtained in the project were somewhat erratic but in general confirmed the radiation pattern behavior as calculated for Figure 5-2. Much difficulty was experienced in maintaining the desired phase between the TE_{10} and TE_{20} modes.

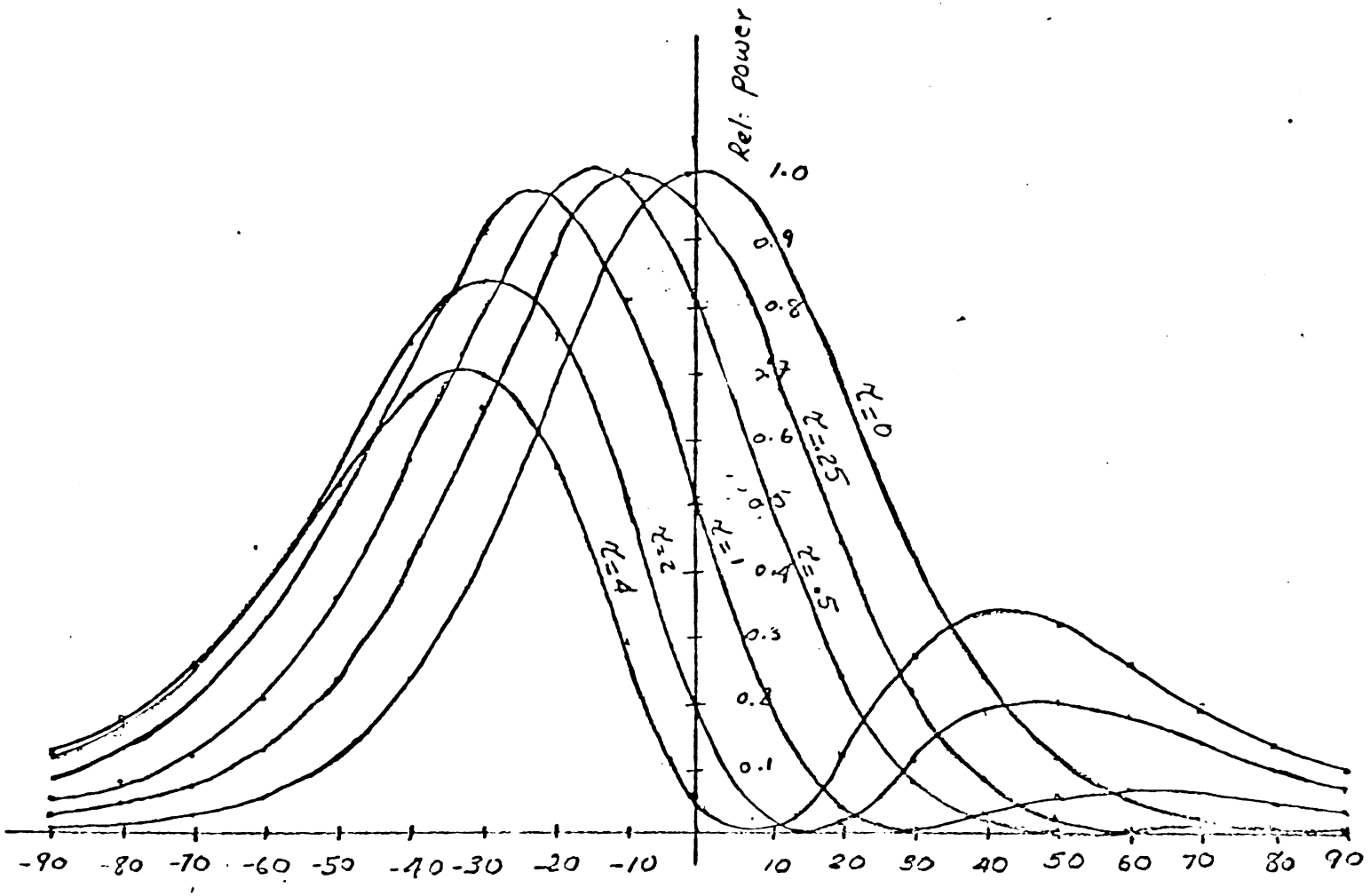

Fig. 5-2: Radiation power pattern for rectangular slot TE_{10} and TE_{20} modes in phase quadrature at the aperture $a/\lambda = 1.2$.

Some study was made of the use of the TE_{30} mode combined with the TE_{10} and also when combined with both the TE_{10} and TE_{20} modes. No appreciable advantage could be observed in the utilization of this third mode. Furthermore the use of still higher modes requires the use of still larger waveguide.

The use of additional modes to scan in the E-plane direction appeared to hold very little promise. The narrow dimension of the waveguide slot in that direction makes it difficult from the array standpoint to consider increasing the size of that dimension in order to accommodate the transmission of the higher modes. In addition, the wider slots add significantly to the potential for cross polarization problems.

In using Figure 5-2 to relate to the actual scan angle, it is necessary to consider the ratio a/λ. For two mode operations this could be typically 1.2 for illustration purposes. Then if the TE_{20} mode is set at the same amplitude as the TE_{10} mode the main beam will be positioned approximately 24^{o} from the broadside position. Furthermore the main beam in this scan position will be very nearly 95 percent of the strength of the main beam in the broadside position with only the TE_{10} mode excited. If while maintaining the phase angle $\psi = 90^{o}$ the ratio of the amplitudes of the TE_{20} to TE_{10} is increased to the ratio 2:1 the main beam will then be scanned still further to approximately 30^{o}. However, under this condition the power in the main beam will be down to approximately 84 percent of the main beam at broadside. Furthermore, the secondary beam which develops on the other side of broadside will have increased to almost 23 percent of the main beam in relative power. It appears that for amplitude ratios greater than $\tau = 1$ undesirable effects commence. Thus scanning from broadside position of approximately 30^{o} represents a reasonable limit for scanning of a single slot in the H-plane direction through the use of the two modes TE_{10} and TE_{20}.

As can be observed from equation (5.12) and Figure 5-2 changing from $\psi = +90^{o}$ to $\psi = -90^{o}$ results in the changing the signs of the abscissa angles or alternately revolving the pattern about the ordinate axis. In actual usage this means the scanning will occur in the opposite direction from broadside.

5.4 Appraisal of Results

The use of the TE_{10} and TE_{20} modes as described in the previous sections appears to have a very limited potential for obtaining the H-plane scan in large arrays. A major disadvantage is the early occurrence of a large side lobe as the beam is scanned off broadside. Also the dual mode of operation greatly increases the impedance matching problems for the slots together with the associated feed networks.

Additional modes can be used as shown in reference (31). However, still greater slot width is then required. This latter reference considers some of the effects of amplitude errors. Also some coverage is given there to the details of feeding multimode slots. With the limitations observed for modal slot scanning no attempts were made to incorporate the multi-terminal slot into the study of planar arrays. However, the planar array analysis as given in earlier chapters can accommodate such use.

REFERENCES

(1) Amitay, N., V. Galindo and C. P. Wu, Theory and Analysis of Phased Array Antennas, Wiley-Interscience, New York (1972).

(2) Gregorwich, W. S., A. Hessel, G.H. Knittel, and A.A. Oliner, "A waveguide simulator for the determination of a phased-array resonance", IEEE G-AP Internat'l Symp. Digest, pp. 134-141 (1968).

(3) Lechtreck, L.W., "Effects of coupling accumulation in antenna arrays", IEEE G-AP Internat'l Symp. Digest, pp. 144-149 (1965).

(4) Oliner, A.A., "Surface-wave effects and blindness in phased-array antennas", Phased-Array Symp. Digest, Polytechnic Institute of Brooklyn, Long Island Graduate Center, Farmingdale, New York (1970).

(5) Farrell, G.F. Jr., and D.H. Kuhn, "Mutual coupling effects of triangular-grid arrays by modal analysis", IEEE Trans. AP (Communications), Vol. AP-14, No. 5, pp. 652-654 (1966).

(6) Diamond, B.L., "Resonance phenomena in waveguide arrays", IEEE G-AP Internat'l Symp. Digest, pp. 110-115 (1967).

(7) Farrell, G.F. Jr., and D.H. Kuhn, "Mutual coupling in infinite planar arrays of rectangular waveguide horns", IEEE Trans. AP, Vol. AP-16, No. 4, pp. 405-414 (1968).

(8) Borgiotti, G.V., "A novel expression for the mutual admittance of planar radiating elements", IEEE Trans. AP, Vol. AP-16, No. 3, pp. 329-333 (1968).

(9) Borgiotti, G.V., "Modal analysis of periodic planar phased arrays of apertures", Proc. IEEE, Vol. 56, No. 11, pp. 1881-1892 (1968).

(10) Knittel, G.H., A. Hessel, and A.A. Oliner, "Element pattern nulls in phased arrays and their relation to guided waves", Proc. IEEE, Vol. 56, No. 11, 1822-1836 (1968).

(11) Galindo, V. and C.P.Wu, "On the asymptotic decay of coupling for infinite phased arrays", Proc. IEEE, Vol. 56, No. 11, pp. 1873-1880 (1968).

(12) Mailloux, R.J., "Radiation and near-field coupling between two collinear open-ended waveguides", IEEE Trans. AP, Vol. AP-17, No. 1, pp. 49-55 (1969).

(13) Mailloux, R.J., "First-order solutions for mutual coupling between waveguides which propagate two orthogonal modes", IEEE Trans. AP, Vol. AP-17, No. 6, pp. 740-746 (1969).

(14) Lyon, J.A.M., R.M. Kalafus, Y.K. Kwon, C. Digenis, M.A.H. Ibrahim, and C.C. Chen, "Derivation of aerospace antenna coupling factor interference prediction techniques", Tech. Rep. AFAL-TR-66-57, The University of Michigan Radiation Laboratory, Ann Arbor (1966).

(15) Wu, C.P., "Characteristics of coupling between parallel-plate waveguides with and without dielectric plugs", IEEE Trans. AP, Vol. AP-18, No. 2, pp. 188-191 (1970).

(16) Argwal, V.D. and Y.T. Lo, "Mutual coupling in phased arrays of randomly spaced antennas", IEEE Trans. AP, Vol. AP-20, No. 3, pp. 288-295 (1972).

(17) Wasylkiwskyj, W., "Mutual coupling effects in semi-infinite arrays", IEEE Trans. AP, Vol. AP-21, No. 3, pp. 277-285 (1973).

(18) Cha, A. G.T., "The analysis of finite planar antenna arrays", NRL Memorandum Report 2568, Naval Research Laboratory, Washington, D.C. (1973).

(19) Adams, A.T., "The rectangular cavity slot antenna with homogeneous isotropic loading", Ph.D. Thesis, The University of Michigan, Ann Arbor (1964).

(20) Mentzer, J.R., Scattering and Diffraction of Radio Waves, Pergamon Press, London and New York (1955).

(21) Tai, C.T. "The induced MMF method", IEEE Trans. AP, Vol. AP-15, No. 4, pp. 527-530 (1967).

(22) Rektorys, K. (Ed.), Survey of Applicable Mathematics, The MIT Press, Cambridge Massachusetts (1969).

(23) Collins, R.E., Foundations for Microwave Engineering, McGraw-Hill Book Company, New York (1966).

(24) Collins, R.E., Field Theory of Guided Waves, McGraw-Hill Book Company, New York (1960).

(25) Jones, D.S., The Theory of Electromagnetism, (Pergamon) Macmillan, New York (1964).

(26) Klein, C. and R. Mittra, "Stability of matrix equations arising in electromagnetics", IEEE Trans. (Communications) Vol. AP-21, No. 6, pp. 902 (1973).

(27) Lecktreck, L.W., "Effects of coupling accumulation in antenna arrays", IEEE Trans. AP, Vol. AP-16, No. 1, pp. 31-36 (1968).

(28) Girrardi, P.G., "A study of mutual coupling reduction in phased array antennas by the use of a time sharing technique", Ph.D. Thesis, The University of Michigan, Ann Arbor (1972).

(29) Kitsuregawa, T. and S. Tachikawa, "Antenna Beam Shifting By Dual Modes", Wescon, Los Angeles, California, August 21-24, 1962.

(30) Wolff, E.A., Antenna Analysis, John Wiley and Sons, Inc., New York, 1965.

(31) Thiele, G.A., L. Wagner, and C. H. Walter, "Multimode Antennas", Technical Report AFAL-TR-72-86, The Ohio State University Electroscience Laboratory, Columbus, March, 1972.

APPENDIX A

Since G is a function of $x-x'$, and $y-y'$, a simple change of variable will allow direct integration with respect to two of the four variables involved where G is independent of the integration variables. Use of this simplification permits one to find the integrals I_1, I_2, I_3 and I_4, as introduced in Chapter II.

For any m, M, n, N

$$I_1^{\ell imn}{}_{LIMN} = \int_{(I-1)D_y}^{(I-1)D_y+b} dy \int_{(L-1)D_x}^{(L-1)D_x+a} dx \int_{(i-1)D_y}^{(i-1)D_y+b} dy' \int_{(\ell-1)D_x}^{(\ell-1)D_x+a} dx' \cdot$$

$$\left[\cos\left[\frac{N\pi}{b}(y-(I-1)D_y)+\frac{n\pi}{b}(y'-(i-1)D_y)\right]\cdot\right.$$

$$\left.\cos\left[\frac{M\pi}{a}(x-(L-1)D_x)+\frac{m\pi}{a}(x'-(\ell-1)D_x)\right]G(x-x',\ y-y')\right] \qquad (A.1)$$

using the substitutions: (refer to Figs. A-1 through A-3)

$$x-x' = \frac{a}{\pi}\lambda+(L-\ell)D_x \qquad x = \frac{\frac{a}{\pi}\mu_1 \mp m\frac{a}{\pi}\lambda+(M\mp m)(L-1)D_x}{M\mp m}$$

$$M(x-(L-1)D_x)\mp m(x'-(\ell-1)D_x) = \frac{a}{\pi}\mu \qquad x' = \frac{\frac{a}{\pi}\mu - M\frac{a}{\pi}\lambda+(M\mp m)(\ell-1)D_x}{M\mp m}$$

$$y-y' = \frac{b}{\pi}\sigma+(I-i)D_y \qquad y = \frac{\frac{b}{\pi}\nu+n\frac{b}{\pi}\sigma+(N\mp n)(I-1)D_y}{N\mp n}$$

$$N(y-(I-1)D_y)\mp n(y'-(i-1)D_y) = \frac{b}{\pi}\nu \qquad y' = \frac{\frac{b}{\pi}\nu - N\frac{b}{\pi}\sigma+(N\mp n)(i-1)D_y}{N\mp n}$$

The Jacobian for this transformation of coordinates is:

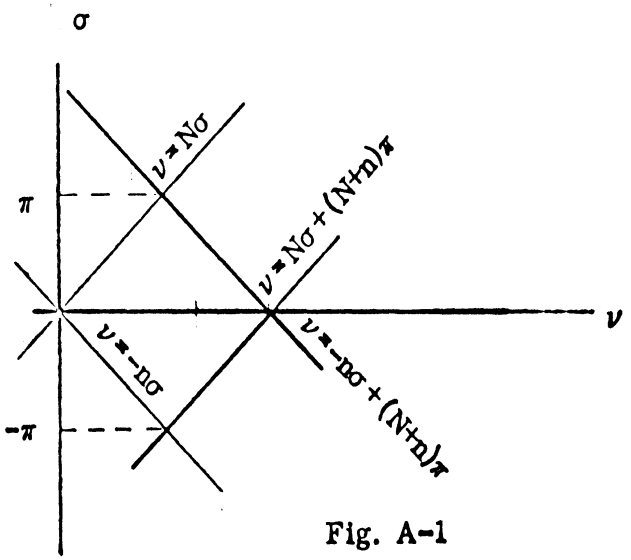

Fig. A-1

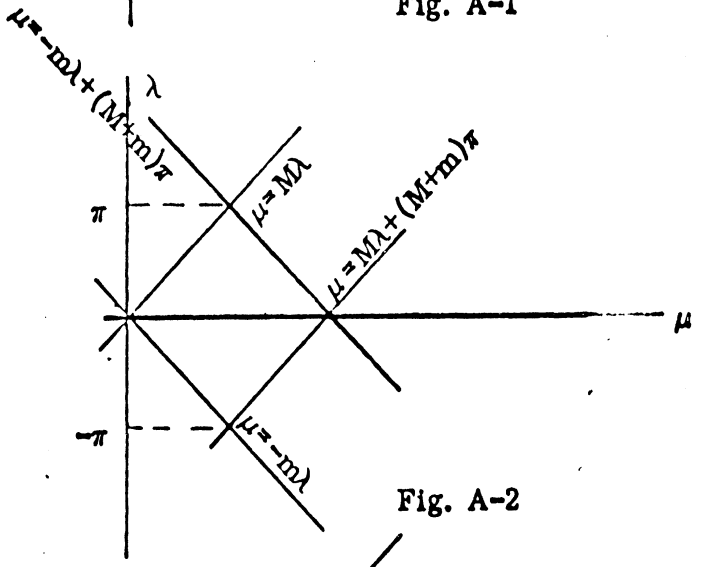

Fig. A-2

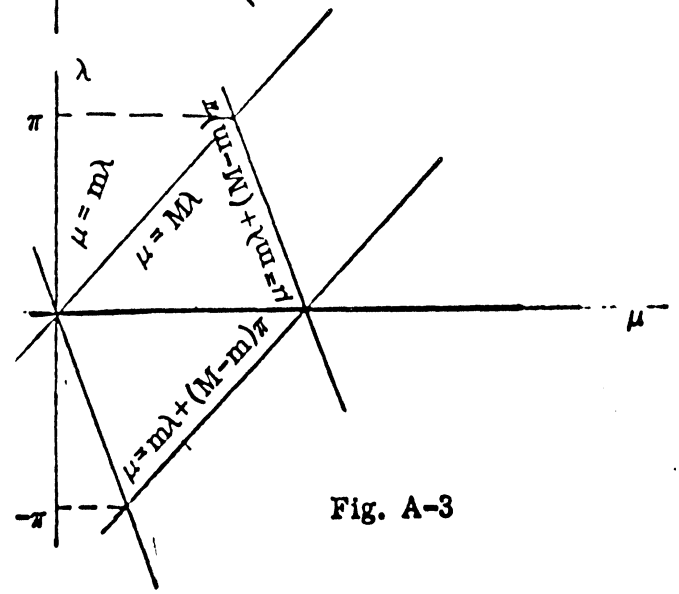

Fig. A-3

$$J = \frac{\partial(x, x', y, y')}{\partial(\lambda, \mu, \sigma, \nu)} = \begin{vmatrix} \frac{ma}{\pi(M+m)} & \frac{a}{\pi(M+m)} & 0 & 0 \\ \frac{-Ma}{\pi(M+m)} & \frac{a}{\pi(M+m)} & 0 & 0 \\ 0 & 0 & \frac{bn}{\pi(N+n)} & \frac{b}{\pi(N+n)} \\ 0 & 0 & \frac{1}{\pi(N+n)} & \frac{-bN}{\pi(N+n)} \end{vmatrix} = \left(\frac{ab}{\pi^2}\right)^2 \frac{1}{(M+m)(N+n)}$$

$$\underset{\ell imn}{LIMN} I_1 = \int_{-\pi}^{0} d\sigma \int_{-n\sigma}^{N\sigma+(N+n)\pi} d\nu \left\{ \int_{-\pi}^{0} d\lambda \int_{-m\lambda}^{M\lambda+(M+m)\pi} d\mu \left[\cos\nu \cos\mu G\left(\frac{a}{\pi}\lambda+(L-\ell)D_x, \frac{b}{\pi}\sigma+(I-i)D_y\right)\right] \right.$$

$$\left. + \int_{0}^{\pi} d\lambda \int_{M\lambda}^{-m\lambda+(M+m)\pi} d\sigma \left[\cos\nu \cos\mu G\left(\frac{a}{\pi}\lambda+(L-\ell)D_x, \frac{b}{\pi}\sigma+(I-i)D_y\right)\right] \right\} J$$

$$= \int_{0}^{\pi} d\sigma \int_{N\sigma}^{-n\sigma+(N+n)\pi} d\nu \left\{ \int_{-\pi}^{0} d\lambda \int_{-m\pi}^{M\lambda+(M+m)\pi} d\mu \left[\cos\nu \cos\mu G\left(\frac{a}{\pi}\lambda+(L-\ell)D_x, \frac{b}{\pi}\sigma+(I-i)D_y\right)\right] \right.$$

$$\left. + \int_{0}^{\pi} d\lambda \int_{M\lambda}^{-m\lambda+(M+m)\pi} d\sigma \left[\cos\nu \cos\mu G\left(\frac{a}{\pi}\lambda+(L-\ell)D_x, \frac{b}{\pi}\sigma+(I-i)D_y\right)\right] \right\} J$$

$$= \int_{-\pi}^{0} d\sigma \int_{-n\sigma}^{N\sigma+(N+n)\pi} d\nu \left\{ \int_{-\pi}^{0} \left[(-)^{M+m}\sin M\lambda + \sin m\lambda \right] \cos\nu\, G\left(\frac{a}{\pi}\lambda+(L-\ell)D_x, \frac{b}{\pi}\sigma+(I-i)D_y\right) d\lambda \right.$$

$$\left. - \int_{0}^{\pi} \left[\sin M\lambda + (-)^{M+m}\sin m\lambda \right] \cos\nu\, G\left(\frac{a}{\pi}\lambda+(L-\ell)D_x, \frac{b}{\pi}\sigma+(I-i)D_y\right) d\lambda \right\} J$$

$$+ \int_{0}^{\pi} d\sigma \int_{N\sigma}^{-n+(N+n)\pi} d\nu \left\{ \int_{-\pi}^{0} \left[(-)^{M+m}\sin M\lambda + \sin m\lambda \right] \cos\nu\, G\left(\frac{a}{\pi}\lambda+(L-\ell)D_x, \frac{b}{\pi}\sigma+(I-i)D_y\right) d\lambda \right.$$

$$-\int_0^{\pi}\left[\sin M\lambda+(-)^{M+m}\sin m\lambda\right]\cos\nu\, G\left(\frac{a}{\pi}\lambda+(L-\ell)D_x,\ \frac{b}{\pi}\sigma+(I-i)D_y\right)d\lambda\Bigg\}J$$

$$=\int_{-\pi}^{0}d\sigma\int_{-n\sigma}^{N\sigma+(N+n)\pi}d\nu\left\{-\int_0^{\pi}\left[\left[(-)^{M+m}\sin M\lambda+\sin m\lambda\right]\cos\nu\, G\left(-\frac{a}{\pi}\lambda+(L-\ell)D_x,\frac{b}{\pi}\sigma+(I-i)D_y\right)\right.\right.$$

$$\left.\left.+\left[\sin M\lambda+(-)^{M+m}\sin m\lambda\right]\cos\nu\ G\left(\frac{a}{\pi}\lambda+(L-\ell)D_x,\frac{b}{\pi}\sigma+(I-i)D_y\right)\right]d\lambda\right\}$$

$$+\int_0^{\pi}d\sigma\int_{N\sigma}^{-n+(N+n)\pi}d\nu\left\{-\int_0^{\pi}\left[\left[(-)^{M+m}\sin M\lambda+\sin m\lambda\right]\cos\nu\, G\left(-\frac{a}{\pi}\lambda+(L-\ell)D_x,\frac{b}{\pi}\sigma+(I-i)D_y\right)\right.\right.$$

$$\left.\left.+\left[\sin M\lambda+(-)^{M+m}\sin m\lambda\right]\cos\nu\ G\left(\frac{a}{\pi}\lambda+(L-\ell)D_x,\frac{b}{\pi}\sigma+(I-i)D_y\right)\right]d\lambda\right\}$$

We then treat the integral w.r.t. $d\sigma$, $d\nu$ in an identical manner to get:

$$\underset{\ell\,\mathrm{imn}}{\mathrm{LIMN}}\ I_1=\frac{\left(\frac{ab}{\pi^2}\right)^2}{(M+m)(N+n)}\int_0^{\pi}\int_0^{\pi}\left[(-)^{M+m}\sin M\lambda+\sin m\lambda\right]\left[(-)^{N+n}\sin N\sigma+\sin n\sigma\right]\cdot$$

$$G\left(-\frac{a}{\pi}\lambda+(L-\ell)D_x,\ -\frac{b}{\pi}\sigma+(I-i)D_y\right)$$

$$+\left[(-)^{M+m}\sin M\lambda+\sin m\lambda\right]\left[\sin N\sigma+(-)^{N+n}\sin n\sigma\right]G\left(-\frac{a}{\pi}\lambda+(L-\ell)D_x,\frac{b}{\pi}\sigma+(I-i)D_y\right)$$

$$+\left[\sin M\lambda+(-)^{M+m}\sin m\lambda\right]\left[(-)^{N+n}\sin N\sigma+\sin n\sigma\right]G\left(\frac{a}{\pi}\lambda+(L-\ell)D_x,\frac{-b}{\pi}\sigma+(I-i)D_y\right)$$

$$+\left[\sin M\lambda+(-)^{M+m}\sin m\lambda\right]\left[\sin N\sigma+(-)^{N+n}\sin n\sigma\right]G\left(\frac{a}{\pi}\lambda+(L-\ell)D_x,\frac{b}{\pi}\sigma+(I-i)D_y\right)d\lambda d\sigma \tag{A.2}$$

Similarly for: $m \neq M$:

$$\underset{\ell\,\mathrm{imn}}{\mathrm{LIMN}}\ I_2=\int_{(I-1)D_y}^{(I-1)D_y+b}dy\int_{(L-1)D_x}^{(L-1)D_x+a}dx\int_{(i-1)D_y}^{(i-1)D_y+b}dy'\int_{(\ell-1)D_x}^{(\ell-1)D_x+a}dx'\ \cdot$$

$$\left[\cos\left[\frac{N\pi}{b}(y-(I-1)D_y)+\frac{n\pi}{b}(y-(i-1)D_y)\right]\cos\left[\frac{M\pi}{a}(x-(L-1)D_x-\frac{m\pi}{a}(x'-(\ell-1)D_x)\right]G(x-x';y-y')\right] \tag{A.3}$$

$$I_2^{LIMN}{}_{\ell imn} = \frac{\left(\frac{ab}{\pi^2}\right)^2}{(M-m)(N+n)}\int_0^{\pi}\int_0^{\pi}\left[(-)^{M-m}\sin M\lambda-\sin m\lambda\right]\left[(-)^{N+n}\sin N\sigma+\sin n\sigma\right]\cdot$$

$$\cdot\, G(-\frac{a}{\pi}\lambda+(L-\ell)D_x,\ -\frac{b}{\pi}\sigma+(I-i)D_y)\cdot$$

$$\left[(-)^{M-m}\sin M\lambda-\sin m\lambda\right]\left[\sin N\sigma+(-)^{N+n}\sin n\sigma\right]G(-\frac{a}{\pi}\lambda+(L-\ell)D_x,\ \frac{b}{\pi}\sigma+(I-1)D_y)\cdot$$

$$\left[\sin M\lambda-(-)^{M-m}\sin m\lambda\right]\left[(-)^{N+n}\sin N\sigma+\sin n\sigma\right]G(\frac{a}{\pi}\lambda+(L-\ell)D_x,\ -\frac{b}{\pi}\sigma+(I-i)D_y)\cdot$$

$$\left[\sin M\lambda-(-)^{M-m}\sin m\lambda\right]\left[\sin N\sigma+(-)^{N+n}\sin n\sigma\right]G(\frac{a}{\pi}\lambda+(L-\ell)D_x,\ \frac{b}{\pi}\sigma+(I-i)D_y)\,dy\,d\sigma\ . \tag{A.4}$$

For m = M, use substitutions (refer to Fig. A-4)

$$x-x' = \frac{a}{\pi}\lambda+(L-\ell)D_x$$

$$x+x' = \frac{a}{\pi}\mu-(L-\ell)D_x$$

$$J = -\frac{1}{2}\left(\frac{a}{\pi}\right)^2$$

$$2x = (\mu+\lambda)\frac{a}{\pi}$$

$$2x' = \frac{a}{\pi}(\mu-\lambda)-2(L-\ell)D_x$$

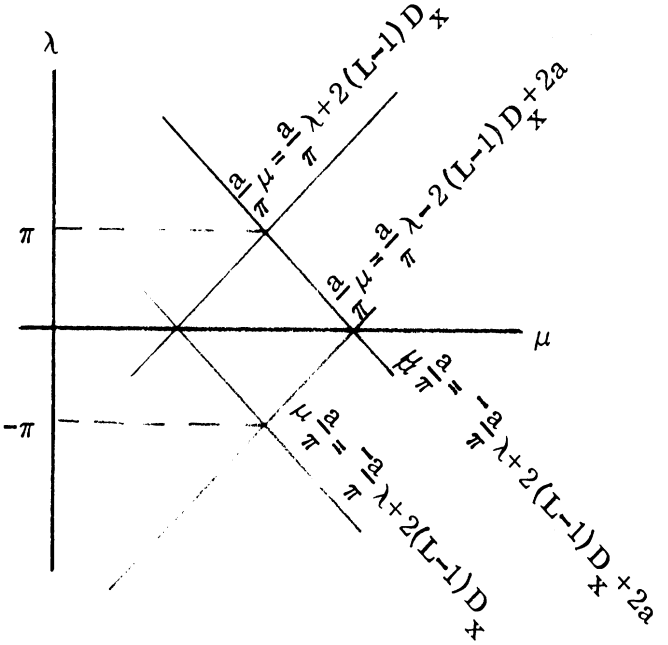

Fig. A-4:

For m = M:

$$I_2^{LIPQ}{}_{\ell imn} = \frac{\left(\frac{ab}{\pi^2}\right)^2}{(N+n)}\int_0^{\pi}\int_0^{\pi}(\lambda-\pi)\cos M\lambda\left\{\left[(-)^{N+n}\sin N\sigma+\sin n\sigma\right]G(-\frac{a}{\pi}\lambda+(L-\ell)D_x,\ -\frac{b}{\pi}\sigma+(I-i)D_y)\right.$$

$$+\left[\sin N\sigma+(-)^{N+n}\sin n\sigma\right]G\left(-\frac{a}{\pi}\lambda+(L-\ell)D_x,\ \frac{b}{\pi}\sigma+(I-i)D_y\right)$$

$$+\left[(-)^{N+n}\sin N\sigma+\sin n\sigma\right]G\left(\frac{a}{\pi}\lambda+(L-\ell)D_x,\ -\frac{b}{\pi}\sigma+(I-i)D_y\right)$$

$$+\left[\sin N\sigma+(-)^{N+n}\sin n\sigma\right]G\left(\frac{a}{\pi}\lambda+)L-\ell)D_x,\ \frac{b}{\pi}\sigma+(I-i)D_y\right)\Bigg\}d\lambda d\sigma\ .\qquad (A.5)$$

By going through a similar procedure for I_3 and I_4 we get:

$$I_3^{LIMN}{}_{\ell imn} = \int_{(I-1)D_y}^{(I-1)D_y+b} dy \int_{(L-1)D_x}^{(L-1)D_x+a} dx \int_{(i-1)D_y}^{(I-1)D_y+b} dy' \int_{(\ell-1)D_x}^{(\ell-1)D_x+a} dx' \cdot$$

$$\left[\cos\left[\frac{N\pi}{b}(y-(I-1)D_y)-\frac{n\pi}{b}(y'-(i-1)D_y)\right]\cos\left[\frac{M\pi}{a}(x-(\ell-1)D_x)+\frac{m\pi}{a}(x'-(\ell-1)D_x\right]G(x-x',y-y')\right]$$

(A.6)

For $n \neq N$:

$$I_3^{LIMN}{}_{\ell imn} = \frac{\left(\frac{ab}{\pi^2}\right)^2}{(M+m)(N-n)}\int_0^{\pi}\int_0^{\pi}\left[(-)^{M+m}\sin M\lambda+\sin m\lambda\right]\left[(-)^{N-n}\sin N\sigma-\sin n\sigma\right]\cdot$$

$$G\left[-\frac{a}{\pi}\lambda+(L-\ell)D_x,\ -\frac{b}{\pi}\sigma+(I-i)D_y\right]\cdot$$

$$\left[(-)^{M+m}\sin M\lambda+\sin m\lambda\right]\left[\sin N\sigma-(-)^{N-n}\sin n\sigma\right]G\left[-\frac{a}{\pi}\lambda+(L-\ell)D_x,\ \frac{b}{\pi}\sigma+(I-i)D_y\right]\cdot$$

$$\left[\sin M\lambda+(-)^{M+m}\sin m\lambda\right]\left[(-)^{N-n}\sin N\sigma-\sin n\sigma\right]G\left[\frac{a}{\pi}\lambda+(L-\ell)D_x,\ -\frac{b}{\pi}\sigma+(I-i)D_y\right]\cdot$$

$$\left[\sin M\lambda+(-)^{M+m}\sin m\lambda\right]\left[\sin N\sigma-(-)^{N-n}\sin n\sigma\right]G\left[\frac{a}{\pi}\lambda+(L-\ell)D_x,\ \frac{b}{\pi}\sigma+(I-i)D_y\right]d\lambda d\sigma\ .$$

(A.7)

If $n = N$ then:

$$I_3^{LIMN}{}_{\ell imn} = \frac{\left(\frac{ab}{\pi^2}\right)^2}{(M+m)}\int_0^{\pi}\int_0^{\pi}(\sigma-\pi)\cos N\sigma\left\{\left[(-)^{M+m}\sin M\lambda+\sin m\lambda\right]\cdot\right.$$

$$\cdot\, G\left(-\frac{a}{\pi}\lambda+(L-\ell)D_x,\ -\frac{b}{\pi}\sigma+(I-i)D_y\right)+$$

$$+\left[(-)^{M+m}\sin M\lambda+\sin m\lambda\right]G\left(-\frac{a}{\pi}\lambda+(L-\ell)D_x,\ \frac{b}{\pi}\sigma+(I-i)D_y\right)$$

$$+\left[\sin M\lambda+(-)^{M+m}\sin m\lambda\right]G\left(\frac{a}{\pi}\lambda+(L-\ell)D_x,\ -\frac{b}{\pi}\sigma+(I-i)D_y\right)$$

$$+\left[\sin M\lambda+(-)^{M+m}\sin m\lambda\right]G\left(\frac{a}{\pi}\lambda+(L-\ell)D_x,\ \frac{b}{\pi}\sigma+(I-i)D_y\right)\Bigg\}\,d\lambda\,d\sigma \qquad (A.8)$$

Also:

$$I_4^{\ell imn}{}_{LIMN} = \int_{(I-1)D_y}^{(I-1)D_y+b} dy \int_{(L-1)D_x}^{(L-1)D_x+a} dx \int_{(i-1)D_y}^{(i-1)D_y+b} dy' \int_{(\ell-1)D_x}^{(\ell-1)D_x+a} dx' \cdot$$

$$\left[\cos\left[\frac{M\pi}{a}(x-(L-1)D_x)-\frac{m\pi}{a}(x'-(i-1)D_x\right]\cos\left[\frac{N\pi}{b}(y-(I-1)D_y-\frac{n\pi}{b}(y'-(i-1)D_y)\right]\cdot\right.$$

$$\left.G(x-x',\ y-y')\right] \quad . \qquad (A.9)$$

For $m \neq M$ and $n \neq N$:

$$I_4^{\ell imn}{}_{LIMN} = \frac{\left(\frac{ab}{2}\right)^2}{(M-m)(N-n)\pi^2}\int_0^{\pi}\int_0^{\pi}\left[(-)^{M-m}\sin M\lambda-\sin m\lambda\right]\left[(-)^{N-n}\sin N\sigma-\sin n\sigma\right]\cdot$$

$$G\left(-\lambda+(L-\ell)D_x,\ -\sigma+(I-i)D_y\right)$$

$$+\left[(-)^{M-m}\sin M\lambda-\sin m\lambda\right]\left[\sin N\sigma-(-)^{N-n}\sin n\sigma\right]G\left(-\lambda+(L-\ell)D_x,\ \sigma+(I-i)D_y\right)$$

$$+\left[\sin M\lambda-(-)^{M-m}\sin m\lambda\right]\left[(-)^{N-n}\sin N\sigma-\sin n\sigma\right]G\left(\lambda+(L-\ell)D_x,\ -\sigma+(I-i)D_y\right)$$

$$+\left[\sin M\lambda-(-)^{M-m}\sin m\lambda\right]\left[\sin N\sigma-(-)^{N-n}\sin n\sigma\right]G\left(\lambda+(L-\ell)D_x,\ \sigma+(I-i)D_y\right)\,d\lambda\,d\sigma \qquad (A.10)$$

For $m = M$ and $n \neq N$:

$$I_4^{\substack{LIMN\\ \ell imn}} = \frac{\left(\frac{ab}{2}\right)^2}{(N-n)\pi}\int_0^{\pi}\int_0^{\pi}(\lambda-\pi)\cos M\lambda\left\{\left[(-)^{N-n}\sin N\sigma-\sin n\sigma\right]\cdot\right.$$

$$\cdot\left[G(-\lambda+(L-\ell)D_x,\ -\sigma+(I-i)D_y)+G(\lambda+(L-\ell)D_x,\ -\sigma+(I-i)D_y)\right]+$$

$$\left.+\left[\sin N\sigma-(-)^{N-n}\sin n\sigma\right]\left[G(-\lambda+(L-\ell)D_x,\ \sigma+(I-i)D_y)+G(\lambda+(L-\ell)D_x,\ \sigma+(I-i)D_y\right]\right\}d\lambda\,d\sigma \qquad (A.11)$$

For $m \neq M$ and $n = N$:

$$I_4^{\substack{LIMN\\ \ell imn}} = \frac{\left(\frac{ab}{2}\right)^2}{(M-m)\pi}\int_0^{\pi}\int_0^{\pi}\left\{\left[(-)^{M-m}\sin M\lambda-\sin m\lambda\right]G(-\frac{a}{\pi}\lambda+(L-\ell)D_x,\ -\sigma+(I-i)D_y)+\right.$$

$$+G(-\frac{a}{\pi}\lambda+(L-\ell)D_x,\ \frac{b}{\pi}\sigma+(I-i)D_y)$$

$$+\left[\sin M\lambda-(-)^{M-m}\sin m\lambda\right]G(\frac{a}{\pi}\lambda+(L-\ell)D_x,\ -\sigma+(I-i)D_y)$$

$$\left.+G(\frac{a}{\pi}\lambda+(L-\ell)D_x,\ \frac{b}{\pi}\sigma+(I-i)D_y)\right\}(\sigma-\pi)\cos N\sigma\,d\lambda\,d\sigma \qquad (A.12)$$

For $m = M$ and $n = N$:

$$I_4^{\substack{LIMN\\ \ell imn}} = \left(\frac{ab}{2}\right)^2\int_0^{\pi}\int_0^{\pi}(\lambda-\pi)\cos M\lambda\,(\sigma-\pi)\cos N\sigma\left[G(-\frac{a}{\pi}\lambda+(L-\ell)D_x,\ -\frac{b}{\pi}\sigma+(I-i)D_y)+\right.$$

$$+G(-\frac{a}{\pi}\lambda+(L-\ell)D_x,\ \frac{b}{\pi}\sigma+(I-i)D_y)$$

$$\left.+G(\frac{a}{\pi}\lambda+(L-\ell)D_x,\ -\frac{b}{\pi}\sigma+(I-i)D_y)+G(\frac{a}{\pi}\lambda+(L-\ell)D_x,\ \frac{b}{\pi}\sigma+(I-i)D_y)\right]d\lambda\,d\sigma\ . \qquad (A.13)$$

UNCLASSIFIED

Security Classification

DOCUMENT CONTROL DATA - R & D

(Security classification of title, body of abstract and indexing annotation must be entered when the overall report is classified)

1. ORIGINATING ACTIVITY (Corporate author)

The University of Michigan Radiation Laboratory
2216 Space Research Bldg., North Campus
Ann Arbor, Michigan 48105

2a. REPORT SECURITY CLASSIFICATION

UNCLASSIFIED

2b. GROUP

N/A

3. REPORT TITLE

VHF-UHF PHASED ARRAY TECHNIQUES
PART II: MUTUAL EFFECTS IN FINITE ARRAYS OF SLOTS

4. DESCRIPTIVE NOTES (Type of report and inclusive dates)

Technical Report, Scientific, Interim

5. AUTHOR(S) (First name, middle initial, last name)

Mohamed A. Hidayet, John A. M. Lyon and Charles B. Loftis, Jr.

6. REPORT DATE	7a. TOTAL NO. OF PAGES	7b. NO. OF REFS
December 1973	126	31

8a. CONTRACT OR GRANT NO.	9a. ORIGINATOR'S REPORT NUMBER(S)
F33615-71-C-1495	
b. PROJECT NO. 6099	004970-2-T
c. Task 05	9b. OTHER REPORT NO(S) (Any other numbers that may be assigned this report)
d.	AFAL-TR-73-399, Part II

10. DISTRIBUTION STATEMENT

Distribution limited to U.S. Government Agencies only; Test and Evaluation Data; December, 1973. Other requests for this document must be referred to AFAL-TEM.

11. SUPPLEMENTARY NOTES	12. SPONSORING MILITARY ACTIVITY
	Air Force Avionics Laboratory Air Force Systems Command Wright-Patterson Air Force Base, Ohio

13. ABSTRACT

The analysis of finite planar arrays of slots is developed. This analysis includes as special cases the linear array of slots with weak coupling and the linear array with strong coupling. This strong coupling case has not been available heretofore in the literature. Likewise the analysis of the finite planar array is presented for the first time in this report. The degenerate or special case of the linear array with the weak coupling of slots is presented with experimental confirmation of results. The experiments of others were used to verify the finite planar array analysis. A complete and error free program has been written in Fortran IV language during this study. This program will enable the sponsor to fully utilize the advanced methods of calculation of array performance without the necessity of making expensive experimental models of planar arrays. This type of early design calculation also makes it possible to avoid "blind spots" in the projected array performance. The analysis may be adapted to arrays using other than slot elements through the use of the same basic approximation methods as well as with full use of reciprocity and symmetry.

The report includes a detailed analysis of mutual coupling effects in linear and planar finite phased arrays of rectangular slots in a perfectly conducting ground plane. Internal TE and TM waveguide modes with unknown coefficients are assumed inside the waveguide. The electromagnetic field outside is evaluated in terms of the waveguide illuminations at the array aperture. The resulting infinite set of linear equations relating the illumination to the incident amplitudes in the guides is then truncated. The finite set of equations is further simplified by neglecting the contribution among modes not directly excited by waveguide feeds. This new approximation

(continued)

DD FORM 1 NOV 65 1473

UNCLASSIFIED

Security Classification

14. KEY WORDS	LINK A		LINK B		LINK C	
	ROLE	WT	ROLE	WT	ROLE	WT
Antenna Array Analysis						
Mutual Effects in Arrays						
Blind Spots in Arrays						
Finite Array Analysis						
Mutual Coupling Slot Arrays						

ABSTRACT (continued)

greatly reduces the size of the resulting matrix and one is left with an augmented matrix equation which directly relates the main mode illuminations to the main mode excitations. The entries in this augmented matrix include the effects of unexcited modes implicitly. The importance of such a matrix in practical applications cannot be overemphasized. Deep insight was given to the mechanism giving rise to the so-called "blind spot" phenomenon. Computer programs were developed which accommodated linear as well as planar arrays of both rectangular grid arrangement and isosceles triangular grid arrangement.

The study presented here, besides having the advantage of being adaptable to finite arrays at reasonable costs, would give information related to the center element as well as any other elements including edge elements. Another advantage is that the matrix thus calculated is scan-independent. These features should be contrasted to what is available for a study based upon the infinite array assumption around a center element. Thus the matrix here represents information about the physical dimensions of the array and the geometry of the array grid; such information would be particularly useful in designing array feed networks and computer controlled phased arrays. Although the basic analysis can accommodate non-uniformly spaced arrays, great savings in the computations cost is realized with uniformly spaced arrays. This includes nonuniformly filled arrays of uniform grids.

A means for "blind spot" control is suggested, based on the suppression of modes of different parity along the direction of scan from that of the excited mode. Preliminary calculation did show the plausibility of this suggestion.

Studies of multi-terminal, multi-mode slot elements were made. It is shown that a limited amount of scan in the H-plane can be obtained through the proper proportioning of the amount of TE_{10} and TE_{20} excitation. A means is required for keeping the time phase between the two modes constant at 90^{o}. To propagate the higher mode a larger slot is required. Also the amount of scan possible is extremely limited. Scanning in this manner is also characterized by the build-up of a large unwanted side lobe which for large scan angles from broadside may approach the same magnitude as the main lobe but is located on the opposite side. It is possible to scan a slot even less effectively by varying the relative time phase of the two modes. It was concluded that scanning in the H-plane through the use of additional modes is not justified within the objectives of the present study. No great saving of space would be accomplished and much complication would be added. Mode scanning in the E-plane appears even less feasible. However, it should be mentioned that the planar array analysis described can be adapted to the slot excitation of more than one mode.